NOTE TO USERS

Calcium-dependent ion channels of retinal Müller glial cells

By

Nicole Cheryl Welch

Submitted to the Faculty of Graduate Studies in partial fulfillment of
the requirements for the degree of Doctor of Philosophy
at
Dalhousie University
Halifax, Nova Scotia
Canada

(December, 2004)

Your file Votre référence
ISBN: 0-494-00959-4
Our file Notre référence
ISBN: 0-494-00959-4

DALHOUSIE UNIVERSITY

To comply with the Canadian Privacy Act the National Library of Canada has requested that the following pages be removed from this copy of the thesis:

Preliminary Pages

Examiners Signature Page (pii)

Dalhousie Library Copyright Agreement (piii)

Appendices

Copyright Releases (if applicable)

For my Nanny

Table of Contents

List of Figures

List of Tables

Abstract

Müller cells are the principal glial cells of the vertebrate retina and perform a number of functions vital to retinal integrity, some of which require electrical activity. In this study, ion channels in freshly isolated salamander Müller cells were identified and studied using electrophysiological, immunocytochemical and fluorescent imaging techniques.

High-voltage-activated (HVA) Ca channel currents were found to activate positive to –30 mV in acutely isolated Müller cells. These currents were partially sensitive to L-type Ca channel blockers. Imaging techniques showed that L-type Ca channels were localized broadly over the Müller cell membrane and not segregated to individual regions. HVA Ca channel currents were highly sensitive to the N-type Ca channel blocker, ω-conotoxin GVIA, but were only modestly blocked by ω-agatoxin IVA, a P/Q-type Ca channel blocker. Immunochemistry revealed that while N-type Ca channels were widely distributed throughout all regions of the Müller cell, P/Q-type Ca channels were found only in the apical processes. The observations suggest the presence of either a mixed population of Ca channel subtypes or a single, unconventional HVA Ca channel subtype sharing several Ca channel characteristics.

A calcium-activated potassium (K_{Ca}) channel current recorded in Müller cells was enhanced by the application of A23187, a Ca^{2+} ionophore, and blocked by iberiotoxin, a specific blocker of large-conductance K_{Ca} channels. TEA also reduced this current. Cd^{2+} had only a small blocking effect on K_{Ca} channel currents suggesting that Ca^{2+} influx through voltage-gated Ca channels is not the principal means of activation. K_{Ca} channel activation was sensitive to release of Ca^{2+} from intracellular stores.

Ionomycin, a Ca^{2+} ionophore, activated a Ca^{2+}-activated Cl (Cl_{Ca}) channel current. Cl_{Ca} channel currents were abolished by Cd^{2+} and enhanced by depolarization indicating that channel activation was sensitive to Ca^{2+} influx through voltage-dependent Ca channels. ClC-3 channels, which are reportedly Ca^{2+} sensitive, are also expressed in Müller cells. Using antibody dialysis, ClC-3 was shown not to contribute to Cl_{Ca} channel currents. Immunochemistry revealed that ClC-3 was localized to intracellular organelles and was not at the plasma membrane of Müller cells.

These studies identified voltage-dependent Ca and Ca-dependent ion channels that contribute to Müller cell electrogenic processes. Knowledge of the biophysical properties and regulation of these ion channels increases our understanding of the function of Müller cells in the retina.

List of Abbreviations

a	ionic specific activity
ACPD	(1S,3R)-1-aminocyclopentane-1,3-dicarboxylic acid
4-AP	4-aminopryidine
ATP	adenosine triphosphate
AVOVA	analysis of variance
Ba	barium
Ba^{2+}	barium ion
bFGF	basic fibroblast growth factor
Ca	calcium
Ca^{2+}	calcium ion
$[Ca^{2+}]_i$	intracellular calcium concentration
CaM	calmodulin
cAMP	cyclic adenosine monophosphate
Cd	cadmium
Cl	chloride
Cl^-	chloride ion
Cl_{Ca}	calcium-activated chloride
Cl_{vol}	volume-sensitive chloide
cm	centimeter
CNS	central nervous system

Cs	cesium
DIDS	4,4`-diisothiocyanostilbene-2,2`-disulfonic acid
DM-BODIPY	[(-)-1,4-dihydro-2,6-dimethyl-4-(2-trifluromethylphenyl)-3,5-pyridinedicarboxylic acid 2-[4,4-difluoro-5,7-dimethyl-4-bora-3a,4a-diaza-3- (s-indacene)propionylamino] ethylethyl ester)]
DMSO	dimethylsulfoxide
DNA	deoxyribonucleic acid
DTT	dithiothreitol
EGTA	[ethyleneglycol-bis(aminoethyl)-N,N,N`,N`-tetraacetic acid]
E_K	equilibrium potential of potassium
exp	exponential of base e (2.713)
F	Faraday's constant = 9.6485 x 10^4 C/mol
GABA	gamma-aminobutyric acid
GPCR	G-protein coupled receptor
GTP	guanosine 5` triphosphate
GΩ	gigaohm
^{3}H-2-DG	^{3}H-2-deoxyglucose
HCl	hydrochloric acid
HEPES	N-(2-hydroxyethyl-piperazine-N`-(2-ethanesuphonic acid))
Hz	hertz
I	current
i	ionic species
ibTX	iberiotoxin

inl	inner nuclear layer
ipl	inner plexiform layer
IP_3	inositol triphosphate
K	potassium
K^+	potassium ion
K_A	A-type potassium channel
K_{Ca}	calcium-activated potassium
K_{DR}	delayed-rectifying potassium channel
K_{IR}	inward-rectifying potassium channel
LJP	liquid junction potential(s)
LVA	low-voltage-activated
m	slope factor
min	minutes
mg	milligrams
Mg	magnesium
Mg^{2+}	magnesium ion
ml	milliliters
mm	millimeters
mV	millivolts
MΩ	megaohms
Na	sodium
Na^+	sodium ion
nA	nanoamperes

nm	nanometer
nM	nanomolar
nS	nanosiemens
NMDA	N-methyl-D-aspartate
NOS	nitric oxide synthase
OH	hydroxide
onl	outer nuclear layer
opl	outer plexiform layer
PBS	phosphate buffered saline
PLC	phospholipase C
pF	picofarads
PKA	protein kinase A
PKC	protein kinase C
PNS	peripheral nervous system
PVR	proliferative vitreoretinopathy
R	universal gas constant = 8.3145 V C/mol K
rpm	revolutions per minute
RSS	retinal saline solution
SDS	sodium dodecyl sulfate
s.e.m.	standard error of the mean
T	temperature
TEA	tetraethylammonium
TTX	tetrodotoxin

u	ionic mobility
µg	micrograms
µl	microlitres
µm	micrometers
µM	micromolar
V	voltage
$V_{½}$	midpoint voltage
V^B	potential of the bath solution
V_c	command voltage
V_m	membrane potential
V^P	potential of the pipette solution
V_{rm}	resting membrane potential
z	ionic valency
~	approximately
°C	degrees Celcius
>/<	greater than/less than
Ω	Ohms
%	percentage
±	plus or minus

Acknowledgements

This thesis presents a collection of work that could not have been accomplished without the help and support of many people. I first must acknowledge Mel Kelly, my supervisor and mentor, whose wealth of ideas were an unlimited source of inspiration. A big thanks must also be extended to Steve Barnes for the countless discussions about the mysterious world of ion channels. A special thanks also goes out to Bill Baldridge for his assistance with all things relating to imaging techniques. Thank you to the lab's fabulous technicians, Michele Archibald, Terry Levatte, Kelly Stevens, and especially Christine Jollimore, for all their help and patience at being my sounding board for ideas and frustrations as both scientists and friends. I would also like to thank some of my fellow students who were instrumental in the success of this thesis: Chanjuan Shi taught me how to patch clamp, Anna-Maria Szczesniak has been a pillar of support, Stephanie Wood has been a great friend and colleague, and Mélanie Lalonde has been there for the last five years always ready to talk about ion channels, or life, as the case may be. It has been a crazy journey sometimes, thank you for riding it out with me.

On a more personal note, many close friends deserve special recognition, and I would like to thank Julie Dingwell, Laura Cole, Laura Stark, Kathleen Verner, and Nyassa Navidzedeh. Thank you to Chris Lee for his never-ending confidence in my intelligence and my ultimate success. Thanks to my little ones, my precious Cocoa, Suzie, Sam, Lily and Pokey. I don't know how to begin to express all the thanks that are owed my family for their support and encouragement. Regardless of age or circumstance, it takes a mother to calm an emotionally distraught child; thank you Mom. Thank you to Mary for always being there with a hug, a caring smile, and an always-needed "I love you". I would also like to thank Wayne for joining our crazy family and making it complete. Thank you to my Dad and Audrey for all of the support and understanding over the years. I must give a special thanks to Scott Pottie for his love, support, and ability to make me laugh while stressed and frantic.

Finally, how do I thank the biggest influence in my life whose love for me and confidence in my success was unwavering for 28 years? I cannot. But I know that my grandmother, my Nanny, is smiling today.

Publications

Parts of this thesis have been previously published:

Welch NC, Wood S, Jollimore C, Stevens K, Kelly MEM, and Barnes S (2004) High-voltage-activated calcium channels in Müller cells acutely isolated from tiger salamander retina. Glia (in press).

Welch NC, Wood S, Jollimore C, Stevens K, Kelly MEM, and Barnes S (2004) Characterization of HVA calcium channels in Müller cells isolated from tiger salamander retina. FASEB J S11525-0056.

Welch NC, Barnes S, and Kelly MEM (2003) Uniformly Distributed Calcium Channels in Retinal Müller Cells Exhibit Currents With a Distinctive Pharmacology. Invest. Ophthalmol. Vis. Sci. 44: E-Abstract 4138

Welch NC, Barnes S, and MEM Kelly (2002) Calcium and Calcium-Activated Potassium Currents in Müller Cells Isolated From Tiger Salamander Retina. Invest. Ophthalmol. Vis. Sci. 43: E-Abstract 4757.

Chapter 1

General Introduction

1. Glial cell function

In the human brain, glial cells outnumber neurons by a factor of 10 to 1. Several different types of glial cells exist including oligodendrocytes in the central nervous system (CNS) and Schwann cells in the peripheral nervous system (PNS). These two types of glia are the producers of nerve cell axon insulation; myelin (Bunge, 1968). Astrocytes, another type of glia, help to form the protective blood brain barrier in addition to performing "housekeeping" chores to promote efficient signaling between neurons such as neurotransmitter and ionic clearance from the synaptic cleft (Janzer and Raff, 1987; Bergles and Jahr, 1998). Glia are also involved in CNS development by providing structural framework as well as metabolic and trophic support for migrating neurons and axonal outgrowth (Hidalgo and Booth, 2000).

However, recent evidence suggests that glial cells may have a more dynamic role than their traditional neurosupportive roles in the CNS (Kuronsinski, 2002; Stevens, 2003). Although glial cells are inexcitable, they are capable of communicating with other glia as well as with neurons. Glia to glia communication involves intercellular calcium waves and chemical messengers, while neuron to glia communication uses signals such as ion fluxes, neurotransmitters and cell adhesion molecules (Fields and Stevens-Graham, 2002). Many neurotransmitter receptors are expressed on glial membranes and extracellular stimuli, such as glutamate or adenosine triphosphate (ATP), can signal an increase in glial intracellular calcium concentration ($[Ca^{2+}]_i$) (Cornell-Bell et al., 1990; Fam et al., 2000). For example, a localized elevation in $[Ca^{2+}]_i$

in one part of an astrocyte may propagate throughout the entire cell and is dependent on the concentration of intracellular inositol triphosphate (IP_3) (Strahonja-Packard and Sanderson, 1999). IP_3 is a second messenger that leads to the release of Ca^{2+} from intracellular stores. Ca^{2+} waves are also transmitted between glial cells, via IP_3, through gap junctions (Boitano et al., 1992) or via adenosine triphosphate (ATP)-activation of P2Y purinoceptors (Fam et al., 2000).

2. Glial cells in the retina

Müller cells are the principal glial cells of the vertebrate retina. Müller cells are radially oriented cells that traverse the entire depth of the retina from its inner vitreal border to almost the distal end of the photoreceptors (Figure 1.1). In vertebrates, the retina is organized into an alternating series of three layers of nerve cell bodies and two synaptic layers. The outer nuclear layer (*onl*) is comprised of the cell bodies of the rod and cone photoreceptors; the light-sensitive cells of the retina. The inner nuclear layer (*inl*) contains the cell bodies of bipolar, horizontal, and amacrine cells. The ganglion cell layer is made up of ganglion cells and displaced amacrine cells. Light must first travel through the thickness of the retina before striking and activating the photoreceptors. The phototransduction cascade begins with the photoreceptors which synapse onto bipolar cells in the outer plexiform layer (*opl*). Bipolar cells, in turn, synapse onto ganglion cells in the inner plexiform layer (*ipl*), and ganglion cell axons make up the optic nerve and carry the visual signal to the brain.

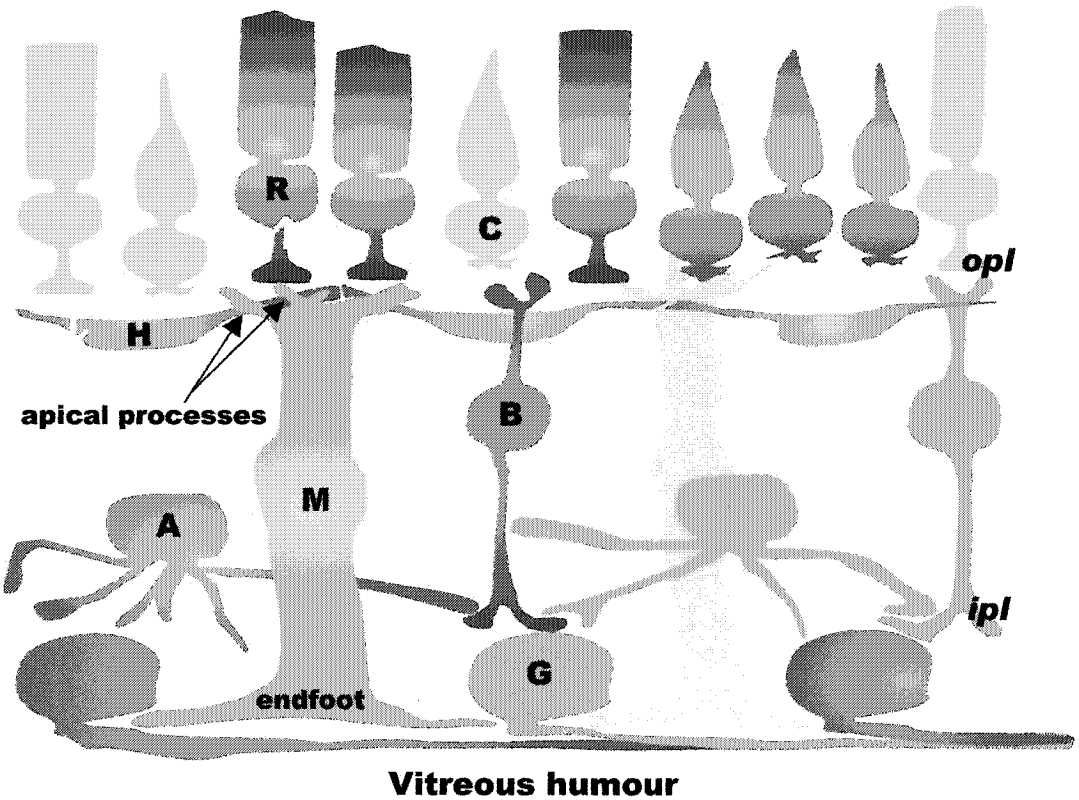

Figure 1.1. Schematic representation of retinal organization.
The photoreceptors, rods (R) and cones (C), synapse in the outer plexiform layer (*opl*) onto bipolar cells (B) and horizontal cells (H). Bipolar cells synapse on ganglion cells (G) in the inner plexiform layer (*ipl*). Ganglion cells axons make up the optic nerve. Amacrine cells (A) interact with bipolar cells. Müller cells (M) interact with all retinal neurons and span the entire depth of the retina from the photoreceptors through to the ganglion cells adjacent to the vitreous humour.

The endfoot is the specialized region of the Müller cell and terminates in the ganglion cell layer adjacent to the vitreous body. Müller cells extend branches throughout the retina which surround or come in contact with every class of retinal neurons, as well as with other glia, and with the blood vessels of vascularized retinas. Branches in the outer retina, some of which ensheath the photoreceptor inner segments, are known as Müller cell apical processes (Sarantis and Mobbs, 1992). Müller cells are found in all regions of the retina, except for the optic nerve head. The mammalian retina has between 10^6 and 10^7 Müller cells (Distler and Dreher, 1996).

Müller cells are the only glial cells in vertebrate species having avascular retinas, such as lizards, amphibians, birds and some mammals; and are the predominant glia of vascularized retinal species (Ramussen, 1974). In addition to Müller cells, astrocytes, microglia, and, to a lesser extent, oligodendrocytes are also present in vascular retinas. Astrocytes are confined to the innermost layers of the retina where they ensheath retinal vessels and form a close association with ganglion cell axons. These interactions may provide a potential communication link between ganglion cell axons, retinal vasculature, and the vitreous body, contributing to the regulation of extracellular potassium (K^+) in the inner retina (Rungger-Brändle et al., 1993). Furthermore, astrocytes produce vascular endothelial growth factor and may be involved in the retinal vasculature development (Stone et al., 1995). In the retina, microglia are associated primarily with vasculature and are found in all layers from the inner border to the *opl*. Microglia distribution changes with age reflecting various stages, i.e. patterns of

cell death, of retinal development. The debris of the dying neurons is engulfed and phagocytosed by microglia and disposed of via the vascular system (Hume et al., 1983). Oligodendrocytes are the fourth type of glia and are rarely observed in the retina. The presence of oligodendrocytes in the retina is noted only when myelinated ganglion cell axons are found in the nerve fiber layer such as the medullary rays of the rabbit retina (Ehinger et al., 1994).

3. Müller cell-neuron support interactions

3.1 Energy coupling

The energy demands of the retina support such processes as phototransduction, maintenance of ionic gradients, and synaptic activity. Energy is supplied through the uptake of glucose and oxygen from the choroidal or retinal circulation. Autoradiographic studies using ^{3}H-2-deoxyglucose (^{3}H-2-DG), a nonmetabolizable analog of glucose, showed that while ^{3}H-2-DG could be taken up directly by photoreceptors (Witkovsky and Yang, 1982), exogenous glucose is avidly taken up by the Müller cells (Poitry-Yamate and Tsacopoulos, 1991). It has been suggested that glucose uptake by the Müller cells, via glucose transporters located on the apical processes (Watanabe et al., 1994), is mediated by the actions of synaptically released glutamate (Sarthy and Ripps, 2001). Müller cells synthesize and release large amounts of lactate, a metabolite of glucose, which is transferred to photoreceptors (Poitry-Yamate et al., 1995). The same study also found lactate was the preferred substrate, compared to glucose, for oxidative metabolism in photoreceptors. This suggests that Müller cells serve

as an intermediary for transferring energy from the glucose carried in blood vessels to the neurons (Figure 1.2).

3.2 Neurotransmitter clearance and metabolism

Glutamate is the primary excitatory neurotransmitter released during visual processing in the retina and is involved in synaptic transmission from photoreceptors to bipolar cells and from bipolar cells to ganglion cells. Termination of glutamate synaptic transmission and prevention of glutamate excitotoxicity requires the removal of glutamate from the synapse. Overstimulation of glutamate receptors, such as ionotropic NMDA receptors, has been linked to neuronal cell death (Demaurex and Distelhorst, 2003). Retinal ganglion cells are particularly sensitive to prolonged activation of NMDA receptors (Sucher et al., 1991). In purified retinal ganglion cell cultures, glutamate caused a dose-dependent increase in cell death, whereas co-culture of ganglion cells and Müller cells was neuroprotective against glutamate challenge (Kawasaki et al., 2000).

In the retina, glutamate is removed from the extracellular space primarily by high affinity glutamate transporters on Müller cells. The presence of four glutamate transporter subtypes was found in Müller cells (Eliasof et al., 1998). The L-glutamate/L-aspartate transporter (GLAST) was specifically located to Müller cells (Eliasof et al., 1998). GLAST is a high affinity, Na^+-dependent, electrogenic glutamate transporter and is primarily responsible for re-uptake of glutamate in the retina. The GLAST activity of Müller cells is essential for

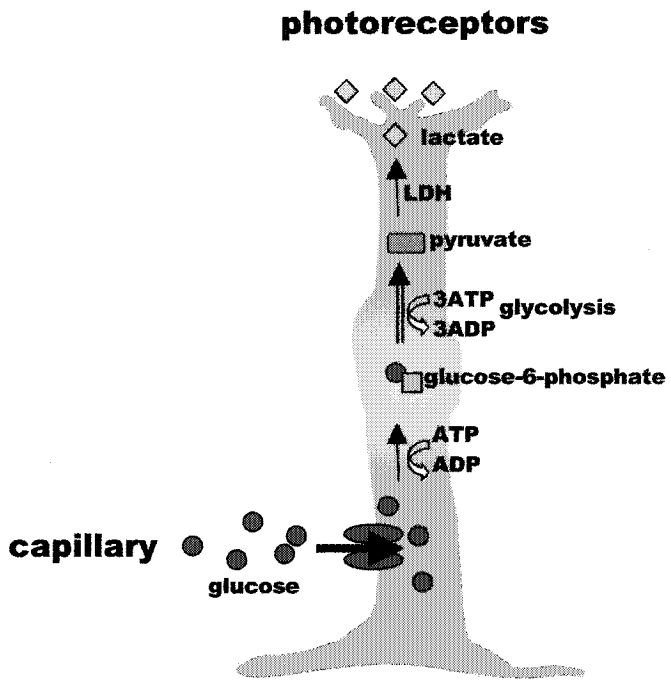

Figure 1.2. Proposed schematic of energy coupling.
Glucose (●) released from the capillaries is taken up by glucose transporters (●●) on the Müller cell and converted to glucose-6-phosphate (●□) before entering glycolysis. The product of glycolysis is pyruvate which can be converted to lactate (◇) by the enzyme lactate dehydrogenase (LDH). Lactate is released by Müller cells and taken up by the photoreceptors.

normal retinal synaptic activity since GLAST-deficient mutant mice did not exhibit normal signal transmission between photoreceptors and bipolar cells. Furthermore, retinal damage after ischemia in GLAST-deficient mice was intensified compared to wild-type mice (Harada et al., 1998). The presence of Müller cells is necessary to protect retinal neurons against glutamate excitotoxicity *in vitro* (Heidinger et al., 1999). Glaucoma, a group of progressive optic neuropathies, is characterized by degeneration of ganglion cells and their axons. The result is a distinct appearance of the optic disc and a concomitant pattern of visual loss (Weinreb and Khaw, 2004). In a rat model of glaucoma, glutamate homeostasis was shown to be compromised (Woldemuisse et al., 2004). Since Müller cells are instrumental in retinal glutamate uptake, this suggests that alterations in Müller cell function may contribute to glaucoma.

Müller cell neuroprotection of ganglion cells was dependent upon activity of a glial-specific enzyme, glutamine synthetase, which required the presence of both glial cells and neurons. Pure retinal neuron cultures were destroyed by glutamate challenge while Müller cell-only cultures did not exhibit any glutamine synthetase activity, suggesting that a neuron-glia interaction was required for neuroprotection. Glial cells are the only retinal cells which express glutamine synthetase, an enzyme catalyzing the conversion of glutamate, ammonia and ATP into glutamine (Rieppe and Norenberg, 1977). Therefore, glutamate must be taken up by the Müller cell to be metabolized by glutamine synthetase (Figure 1.3).

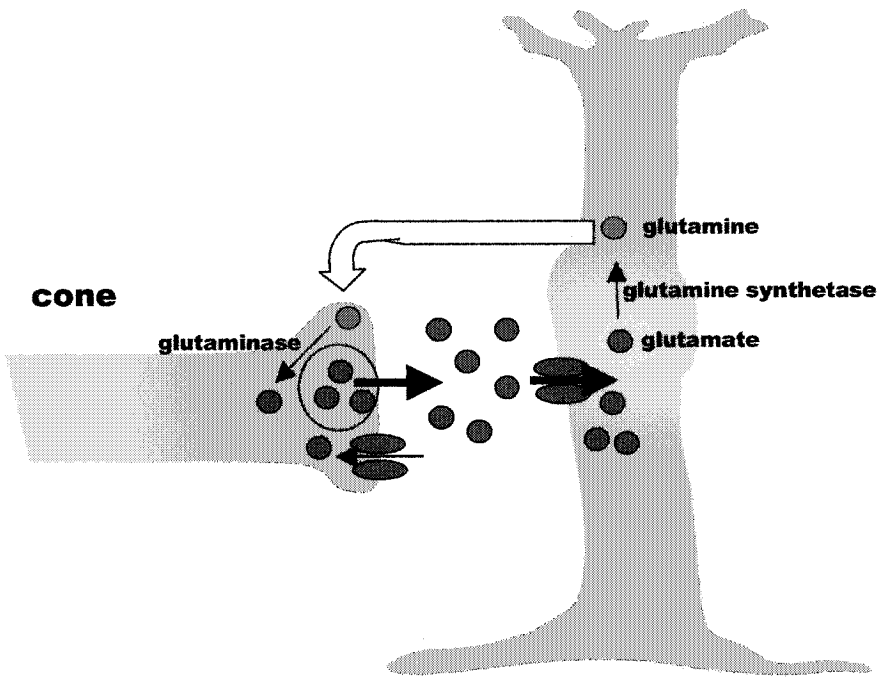

Figure 1.3. Schematic for recycling of glutamate between photoreceptors and Müller cells.
Glutamate transporters ( ) on Müller cells are the dominant mechanism of removal of glutamate ( ) from the synapse. In the Müller cell, glutamate is inactivated by conversion to glutamine by glutamaine synthetase. Glutamine is transported to the neuron where it can be converted back into glutamate by glutaminase (or to GABA in inhibitory neurons).

The inactivation of glutamate by glutamine synthetase produces glutamine, which is transferred back to retinal neurons. Glutamine is a precursor for the synthesis of glutamate and, subsequently, gamma-aminobutyric acid (GABA) (Hamberger et al., 1979). Müller cells lack the enzyme which converts glutamate to GABA, glutamic acid decarboxylase, and thus, GABA is synthesized almost exclusively in GABAergic neurons. In the retina, GABA, the primary inhibitory neurotransmitter, is released by horizontal cells and amacrine cells. Müller cells do posess high affinity, Na^+-dependent, electrogenic GABA transporters, GAT-1 and GAT-3 (Honda et al., 1995; Biedermann et al., 2002). The GABA transporters are expressed in the membrane of the apical processes, which are localized in the outer retina where GABA uptake is performed exclusively by Müller cells (Biedermann et al., 2002). The two mitochondrial enzymes responsible for degradation of GABA, GABA-transaminase and succinic acid semialdehyde dehydrogenase, are present in the Müller cell (Hyde and Robinson, 1974).

3.3 K^+ siphoning

Light-evoked neuronal stimulation in the retina produces increases in $[K^+]_o$ in the *opl* and *ipl*. Müller cells rapidly clear the elevated $[K^+]_o$ to ensure minimal fluctuations in neuronal excitability. K^+ can be taken up by the Müller cell passively or actively via a (Na^+, K^+)-ATPase pump. Müller cells regulate $[K^+]_o$ by a spatial buffering mechanism (Newman et al., 1984). Spatial buffering currents, via inward-rectifying K^+ channels (K_{IR}), redistribute extracelluar K^+ from regions of high $[K^+]_o$ to low $[K^+]_o$ (Figure 1.4). The density of K_{IR} channels

is higher on the Müller cell endfoot, a region of the cell adjacent to the vitreous humour (Newman, 1993). This is a specialized form of spatial buffering, known as K^+ siphoning, whereby most of the neuronally released excess K^+ is transferred to the vitreous humor, which acts as a K^+ sink, or to the subretinal space where $[K^+]_o$ is low (Karwoski et al., 1989).

4. Müller cell-neuron signaling interactions

4.1 Glutamate and GABA

In addition to maintaining a proper neuronal environment, Müller cells, like all glia in the CNS, have recently emerged as a more dynamic player in retinal signaling. Human Müller cells express functional ionotropic NMDA glutamate receptors (Puro et al., 1996b), but only metabotropic glutamate receptors (mGluRs) are expressed on salamander Müller cells (Schwartz, 1993). Activation of NMDA receptors, an ionotropic glutamate receptor, inhibited K_{IR} currents in human Müller cells (Puro et al., 1996b). Although salamander Müller cells do not express ionotropic glutamate receptors, metabotropic glutamate receptor activation also inhibited K_{IR} currents (Schwartz, 1993). K_{IR} channels on Müller cells dominate the cell's K^+ conductance and are important in the removal of excess K^+. Glutamate inhibition of K_{IR} channels might allow localized depolarization with subsequent activation of other K channels which, under these conditions, could contribute to K^+ siphoning. In certain pathologies, such as glaucoma, when glutamate concentrations are believed to be elevated, K^+

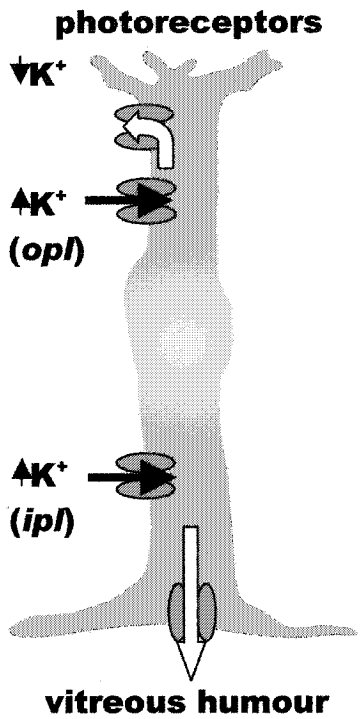

Figure 1.4. Schematic representation of K^+ siphoning in Müller cells. Light-evoked increases in $[K^+]_o$ within the *opl* and *ipl* are removed from the synapse by influx through K channels ( ) and redistributed to regions where $[K^+]_o$ is unchanged (vitreous humour) or reduced by neuronal activity (subretinal space).

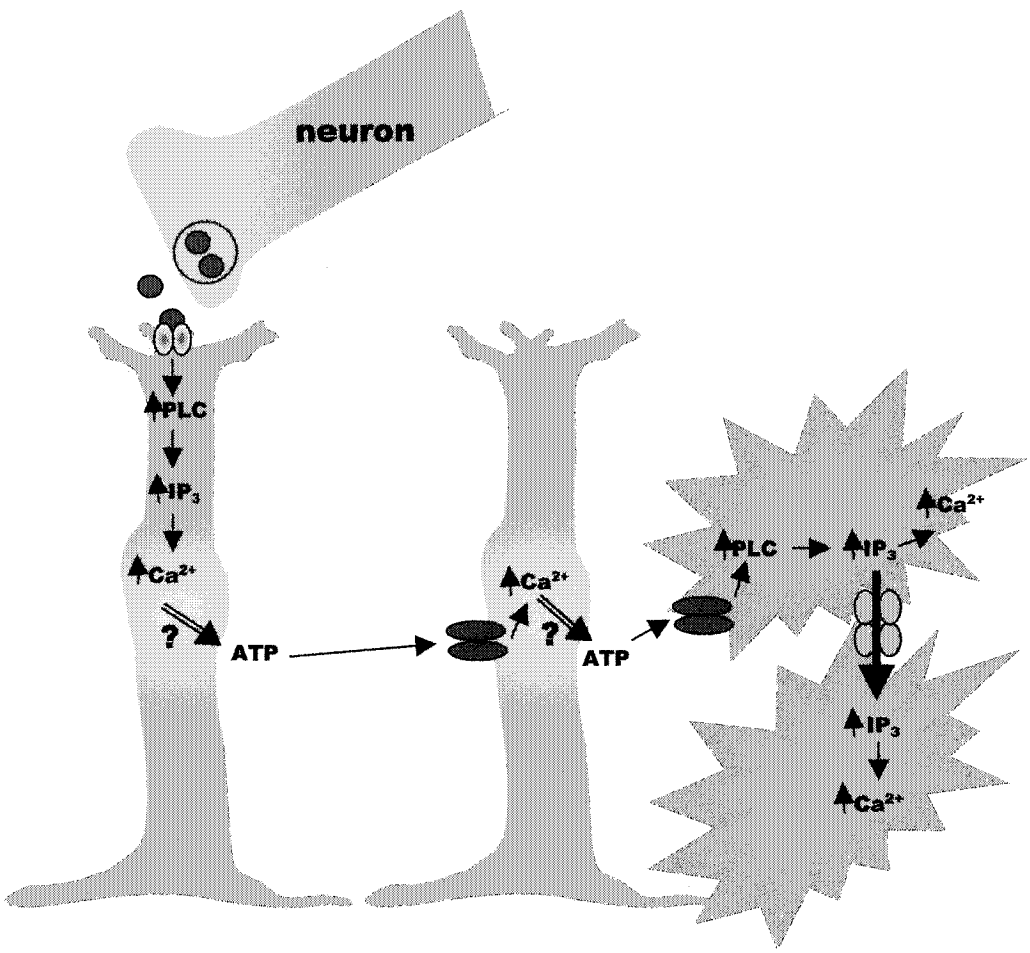

Figure 1.5. Schematic representation of intercellular glial Ca^{2+} wave propagation in the retina.
Glutamate (●) released from neurons activates an mGluR (◎)on Müller cells which initiates a G-protein signaling cascade involving activation of phospholipase C (PLC). PLC-catalyzed the production of inositol triphosphate (IP_3) induces Ca^{2+} release from stores and elevated $[Ca^{2+}]_i$. Increased $[Ca^{2+}]_i$ causes adenosine triphosphate (ATP) to be released into the extracellular space by an undefined mechanism. ATP acts as an messenger between Müller cells by binding to purinergic receptors (●●) on adjacent Müller cells to cause an elevation in $[Ca^{2+}]_i$, continuting the cycle of ATP release. Thus, the Ca^{2+} wave is propagated from Müller cell to Müller cell and from Müller cell to astrocyte. Ca^{2+} wave propagation between astrocytes is via diffusion of an intracellular messenger, IP_3, through gap junctions (◎◎).

channel to open and hyperpolarize the ganglion cell to inhibit firing (Newman, 2003).

The communication between Müller cells and neurons, in particular ganglion cells, is not simply unidirectional. Elevations in Müller cell $[Ca^{2+}]_i$, most prominent in the endfoot, are observed when the retina is stimulated with repetitive light flashes or when ganglion cell axons are stimulated electrically. The increase in glial $[Ca^{2+}]_i$ is blocked in the presence of tetrodotoxin (TTX) suggesting a direct involvement of ganglion cells (Newman, 2004).

The consequences of increased $[Ca^{2+}]_i$, and the ubiquitous nature of Ca^{2+} as an intracellular messenger, indicates that the role of Müller cells may be varied and wide ranging. Besides the studies described above, which detail Müller cell-induced inhibition of ganglion cell excitability, Müller cell Ca^{2+} waves can also increase alterations in ganglion cell excitability (Newman and Zahs, 1998). The identity of an excitation mechanism is still unknown and has been suggested to involve glial release of glutamate (Newman and Zahs, 1998) in a manner similar to that observed in the hippocampus (Araque et al., 1998). This mechanism proposes that elevated intracellular Ca^{2+} might induce glutamate release from Müller cells which could act on retinal ganglion cell NMDA receptors. Activation of NMDA receptors could enhance ganglion cell excitability and increase the retinal signals to the brain.

Müller cell influences on signaling in the outer retina, such as the *opl*, also remain unclear. Müller cells do contain the Ca^{2+}-sensitive enzyme, nitric oxide synthase (NOS) (Kurenny et al., 1995). Elevations in Müller cell $[Ca^{2+}]$ may

activate NOS and stimulate the production of nitric oxide (NO). NO has been shown to increase Ca channel currents in rod photoreceptors which may increase the glutamate released in the *opl* (Kurenny et al., 1994; Kourennyi et al., 2004). Studies in cone photoreceptors suggest NO tightly modulates Ca^{2+} influx, and therefore, glutamate release. NO can increase Ca^{2+} influx into cone photoreceptors by modulating cyclic nucleotide–gated channels (Savchenko et al., 1997), but cone photoreceptor Ca channel activity is suppressed by NO (Kourennyi et al., 2004). The opposing actions of NO on rod and cone Ca channel activity, and hence, glutamate release, alter the balance of rod and cone synaptic strength and the input to retinal neurons of the *inl*. Alterations in the relative strength of rod and cone input to second-order neurons have been shown to occur during changes in illumination (Yang and Wu, 1996). Müller cell production of NO in the outer retina might contribute to the light- and dark-adaptation response of retinal signaling.

Elevations in $[Ca^{2+}]_i$ may directly, or indirectly via a host of second messenger pathways, modulate Ca^{2+}-dependent processes. Ca^{2+}-activated K channels (K_{Ca}) are expressed in Müller cells (Newman, 1985b). Increased $[Ca^{2+}]_i$ may directly act on K_{Ca} channels to transiently shift the channel activation to more negative membrane potentials and facilitate the opening of these channels. Alternatively, Ca^{2+} might activate protein kinase C (PKC) which has been shown to suppress K_{Ca} channel activity (Schopf et al., 1999). Therefore, Ca^{2+} waves in Müller cells may regulate these large-conductance K_{Ca} channels as well as other Ca^{2+}-dependent ion channels such as Ca^{2+}-activated Cl (Cl_{Ca}) channels. The role

of Müller cell large conductance K_{Ca} channels and Cl_{Ca} channels in the retina is discussed below.

5. Müller cell ion channels

5.1 K channels

One of the key roles of Müller cells in the retina is to maintain $[K^+]_o$ through K^+ siphoning, a process dependent on K_{IR} channels. The resting membrane potential of Müller cells is set by K^+ conductance, which is dominated by the K_{IR} channel (Newman, 1993). The conductances of inwardly rectifying ion channels, such as K_{IR}, are increased with hyperpolarization. The gating producing inward rectification arises from the plugging of the channel during outward current flow by either internal magnesium (Mg^{2+}) or cytoplasmic polyvalent ions. Thus, K_{IR} channel rectification is not a voltage-dependent gating mechanism intrinsic to the protein itself (Matsuda et al., 1987). K_{IR} channels are typically open at or near the equilibrium potential of K^+ (E_K) with maximal conductance arising at potentials below E_K. The driving force on the current through K_{IR} channels is due to the electrochemical gradient of K^+, thus, K_{IR} channels are highly sensitive to $[K^+]_o$. When $[K^+]_o$ in most regions of the retina is low, ~ 3 mM, the Nernst equation (equation 2.5; Chapter 2, General Methods; section 5) predicts E_K to be ~ -90 mV (assuming Müller cell $[K^+]_i$ is ~ 100 mM). Current flow through K_{IR} channels is outward at membrane potentials positive to E_K. Therefore, if Müller cell membrane potential is ~ -80 mV, then K_{IR} channels mediate K^+ efflux.

Illumination produces a localized rise in $[K^+]_o$, at both the *opl* and *ipl*, while $[K^+]_o$ in other regions of the retina decreases or remains the same (Sarthy and Ripps, 2001). K^+ siphoning redistributes K^+ from regions of high $[K^+]$, such as the plexiform layers, to regions of low $[K^+]$ such as the vitreous humour. K^+ siphoning is likely made possible by the distinct shape and the large size of the Müller cell, which may allow for variations in membrane potential at different regions of the cell. The localized rise in extracellular K^+ shifts E_K to more positive potentials only in the regions of Müller cell membrane adjacent to the plexiform layers. For example, light-induced elevations in $[K^+]_o$ to ~20 mM would shift E_K to ~ -40 mV. The resting membrane potential of the entire Müller cell remains clamped at –80 mV since only a small fraction of the membrane is near the plexiform layers and thus, the majority of the glial membrane is not experiencing any changes in $[K^+]_o$. Therefore, in the localized regions of the Müller cell where the membrane potential is negative to E_K, K^+ flows passively into the Müller cell. In regions where $[K^+]_o$ is unchanged by neuronal activity, such as the vitreous humour, the resting potential is positive to E_K and K^+ flows out of the Müller cell, allowing a gradient of K^+ movement throughout the Müller cell.

Other K channel subtypes have been described in Müller cells including a delayed rectifier K channel (K_{DR}), an A-type K channel (K_A), and a K_{Ca} channel (Chao et al., 1994; Newman, 1985b). K_{DR} channel activation is slow and requires prolonged depolarization to about -30 mV. In Müller cells, currents through K_{DR} channels could be blocked by external application of 4-aminopyridine (4-AP) or

tetraethylammonium (TEA) (Chao et al., 1994). Rapidly inactivating K^+ currents decayed within 1 s and could be blocked by 4-AP but not by TEA (Newman, 1985b). The Newman study (1985b) also found a K^+ current that was blocked by TEA and cadmium (Cd).

The functional significance of K_{DR}, K_A, and K_{Ca} channel expression in Müller cells is unknown since these channels are typically inactive at the Müller cell resting potential. In early postnatal days, K_{DR}, K_A, and K_{Ca} channels dominate the current-voltage relation of rabbit Müller cells. Resting membrane potential of postnatal day 1-6 rabbit Müller cells was always positive to –50 mV. In rabbit Müller cells, the density of K_{IR} channels was very low in early postnatal day retinas. With maturation, the activity of K_{DR}, K_A, and K_{Ca} channels is strongly down-regulated, while K_{IR} channel activity increased. The shift in K channel expression was accompanied by a hyperpolarization of the resting membrane potential, which was negative to –80 mV after postnatal day 9. The differential expression of voltage-sensitive K channels in immature glia suggests specific roles for these during retinal maturation (Bringmann et al., 1999a).

Changes in Müller cell K channels have also been noted in retinal pathologies. For example, differences in K channel activity were observed in Müller cells from healthy human donors compared to that of patients with proliferative retinopathy (PVR) with K_{IR} channel activity sharply reduced and K_{Ca} channel activity increased in Müller cells from diseased retinas. These changes in K_{IR} and K_{Ca} channel activity could be correlated to the less negative mean membrane potential (-52.8 mV) of Müller cells from diseased retinas compared to

that of cells from healthy donors (-80.6 mV) (Bringmann et al., 1999b). Furthermore, the proliferative activity of cultured Müller cells can be enhanced by exposure to elevated $[K^+]_o$, and this effect is prevented by a blockade of K_{Ca} channels with TEA (Reichenbach et al., 1997).

The physiological regulation of K_{Ca} channels is highly controlled within the Müller cell. Phosphorylation modulates the sensitivity of K_{Ca} channels to Ca^{2+} and to voltage with protein kinase A (PKA)-induced enhancement and PKC-induced suppression of K_{Ca} channel activity (Bringmann et al., 1997; Schopf et al., 1999). Glutamate has been shown to increase the open channel probability of K_{Ca} channels (Bringmann et al., 1997). Activation of metabotropic glutamate receptors on Müller cells has been shown to elevate intracellular Ca^{2+} levels (Kierstead and Miller, 1997), which, in turn, can activate K_{Ca} channel activity. An alternative source of increased $[Ca^{2+}]_i$ in Müller cells might include Ca^{2+} influx through voltage-gated Ca channels. Co-localization of K_{Ca} channels with Ca channels on Müller cell membranes might be an important mechanism of activation of K_{Ca} channels. For example, hippocampal neurons express K_{Ca} channels in close proximity to voltage-gated Ca channels, and Ca^{2+} influx through Ca channels has been shown to selectively activate K_{Ca} channels (Marrion and Tavalin, 1998).

5.2 Ca channels

The presence of voltage-gated Ca channels was originally confirmed by recording long-lasting, voltage-dependent barium (Ba^{2+})-mediated inward currents in isolated Müller cells (Newman, 1985b). With TEA included in the

bath solution, the Ca channel current could be blocked by Cd and verapamil but not by TTX. The current-voltage relation was consistent with the presence of a high-voltage-activated Ca channel with activation positive to -20 mV and peak current at 0 mV (Newman, 1985b).

The functional significance of Ca channels in Müller cells has not been clearly established. The expression of low-voltage-activated (LVA) and HVA Ca channel currents in freshly isolated Müller cells from postnatal rabbits appear to be developmentally regulated. A current activating at potentials positive to -80 mV and peaking at -40 mV was prominently expressed within the first three postnatal weeks, maximal at postnatal days 2 and 5, and decreased after postnatal day 18. The decrease in LVA Ca channel activity with maturation was accompanied by an increased in HVA Ca and K_{Ca} channel activity (Bringmann et al., 2000b; Bringmann et al., 1999a).

The physiological significance of the presence of voltage-gated Ca channels in Müller cells of the mature retina has yet to be fully established. Furthermore, in Müller cells, the physiological conditions that govern activation of Ca channels and K_{Ca} channels are unclear. Ca and K_{Ca} channel activation requires considerable membrane depolarization. However, the Müller cell membrane potential is highly dependent on $[K^+]_o$ and remains steadily hyper-olarized under physiological conditions. This would suggest that glial voltage-gated ion channels are normally inactive, in the absence of external stimuli capable of depolarizing the Müller cell membrane potential by at least 50 mV.

The morphology of the Müller cell may provide insight into potential mechanisms which might activate voltage-dependent ion channels. The thin processes in the apical and endfoot regions of the Müller cell may provide electrically "isolated" areas of the cell. That is, there may be large changes in membrane potential across local regions of the Müller cell, which do not affect the membrane potential of the entire cell. For example, the presence of a small population of voltage-gated sodium (Na) channels have been reported in some mammalian species and are postulated to be located on the thin, finger-like processes of the Müller cell endfoot, which project to inner membrane. The endfoot region of the Müller cell is surrounding spiking neurons, for example ganglion cells, and may therefore sense the depolarization of ganglion cells firing an action potential. This could result in an ephaptic depolarization of the Müller cell endfoot and the opening of Na channels (Reichenbach et al., 1997). The notion of localized depolarizations caused by current flow through an area of restricted extracellular space is not without precedent. In the *opl*, a theory of ephaptic depolarization is proposed to mediate the feedback mechanism between horizontal cells and cones (Byzov and Shura-Bura, 1986). A potential drop along the intercellular gap between the cone and the horizontal cell characterizes the phenomenon of ephaptic depolarization. The intercellular gap between the cone and the horizontal cell is restricted, and an influx of positive charge into the horizontal cell creates a current sink in the synapse. Cone Ca channels respond to the current sink by opening, thus the cone "senses" the current sink as a depolarization. Open hemichannels on the horizontal cell are postulated to

mediate the influx of charge that forms the current sink near the Ca channels of the presynaptic cone (Kamermans et al., 2001).

A similar mechanism of ephaptic depolarization might occur in the apical processes and endfoot regions of the Müller cell. In the salamander, Müller cell apical processes wrap around the synaptic terminals of both rods and cones and are within 1-3 microns of the site of glutamate release (Sarantis and Mobbs, 1992). The close proximity of Müller cell membranes with the depolarizing photoreceptors might facilitate ephaptic depolarization of the Müller cell apical processes, without affecting the overall membrane potential of the glial cell. The depolarization of an electrically isolated region of the Müller cell could activate any voltage-gated ion channels which are expressed in the vicinity.

5.3 Cl channels

There are not currently any descriptions of voltage-dependent anion channels in retinal glial cells. However, an ionotropic $GABA_A$ receptor-mediated Cl^- current has recently been reported in human Müller cells (Biedermann et al., 2004). Voltage-dependent Cl channels are expressed on the plasma membranes of astrocytes (Walz, 2002, for review). Cl channels have been described in cultured rat astrocytes which exhibited both outward rectification (Gray and Ritchie, 1986) and inward rectification (Fava et al., 2001). Plasma membrane Cl channels are important in the maintenance of cellular excitability, cell volume regulation, transepithelial transport, and synaptic inhibition (Jentsch et al., 1999). Cl channels are also expressed on the membranes of intracellular organelles, such as endosomes, lysosomes, synaptic vesicles, and mitochrondria. The opening of

mitochondrial voltage-dependent anion channels is believed to influence the assembly of the mitochondrial permeability transition pore, and Ca^{2+} overload, leading to mitochrondrial dysfunction (Crompton, 1999). This mechanism of mitochondrial dysfunction is theorized to underlie photoreceptor apoptosis in certain retinal degeneration conditions (Fox et al., 1999). Immunocytochemical evidence for mitochondrial Cl channels was found throughout the retina including the apical processes of the Müller cell (Gincel et al., 2002).

The ClC family of voltage-gated ion channels consists of nine members (Jentsch et al., 1999). These channels, including expression in both the plasma membrane and intracellular organelle membranes, are widely distributed throughout a variety of tissues. The physiological function of ClC channels is equally diverse and includes cell volume regulation, acidification of intracellular organelles and regulation of cellular excitability and transepithelial transport (Jentsch et al., 1999). The physiological importance of ClC channel expression is evident upon examining the wide range of diseases and deficiencies which result from mutations in these channels (Jentsch et al., 1999). Furthermore, studies of knockout mice, lacking the ability to express particular genes for members of the ClC channel family, such as ClC-2 and ClC-3, have demonstrated the necessity of these channels for appropriate CNS development (Bösl et al., 2001; Stobrawa et al., 2001).

There is strong evidence that the presence of ClC channels is required for normal retinal development. Two separate studies disrupted either the *Clcn2* or *Clcn3* gene and created blind mice (Bösl et al., 2001; Stobrawa et al., 2001).

Behavioural tests revealed that mice lacking ClC-2 were blind (Bösl et al., 2001) and ClC-3 deficient mice lacked an electrical response to electroretinogram testing (Strobrawa et al., 2001). The *Clcn2* gene encodes a ClC-2 Cl channel protein, which is a plasma membrane channel that is ubiquitously expressed and activated upon hyperpolarization (Thiemann et al., 1992). *Clcn2*$^{-/-}$ mice showed a dramatic loss of photoreceptors beginning at postnatal day 15 and progressively decreasing until few nuclei remained at postnatal day 65 (Bösl et al., 2001).

The ClC-3 Cl channel is controversial in its function and location. In particular, conflicting evidence both supports (Duan et al., 1997; Wang et al., 2003) and negates (Strobrawa et al., 2001; Li et al., 2002; Weylandt et al., 2001) the involvement of ClC-3 in cell volume regulation as the cell swelling–activated plasma membrane Cl channel. Functional expression of a cardiac clone of ClC-3 in NIH/3T3 cells resulted in an outwardly rectifying Cl^- conductance which was strongly enhanced by cell swelling (Duan et al., 1997). Similar results were found in native cells as well. Intracellular dialysis of anti-ClC-3 antibodies into canine pulmonary artery smooth muscle cells and guinea pig cardiac myocytes functionally inhibited the cell swelling-activated Cl channel (Wang et al., 2003). In contrast, other studies have described ClC-3 as an intracellular membrane Cl channel, involved in promoting acidification of synaptic vesicles (Strobrawa et al., 2001; Li et al., 2002). In fact, the Stobrawa study (2001) reported that there was no difference in the cell swelling-activated Cl^- current in the *Clcn3*$^{-/-}$ mice versus the wild-type mice.

While the identity of ClC-3 as the cell swelling-activated Cl channel remains unresolved, the developmental importance of the expression of ClC-3 is undisputed. *Clcn3*$^{-/-}$ mice experience severe postnatal degeneration in the hippocampus and retina. In the retina, there was a complete loss of photoreceptors and nuclei that formed the *opl* by postnatal day 28 (Stobrawa et al., 2001). Furthermore, glutamate uptake in the *Clcn3*$^{-/-}$ mice was decreased compared to wild-type mice. It has been suggested that there is a tight association between the glutamate transporter and a chloride channel in Müller cells, but the identity of such a channel is not known (Eliasof and Jahr, 1996). Glutamate activates an outward, anionic current at positive potentials, which may be important for preventing a large depolarization associated with the electrogenic uptake of glutamate (Eliasof and Jahr, 1996). Müller cells are responsible for maintaining proper glutamate concentrations in the retina. However, if Müller cell glutamate transporters are coupled to an anionic conductance through ClC-2 or ClC-3 channels, then removal of glutamate might be compromised in the ClC-2 and ClC-3 knockout mice. Glutamate could, therefore, accumulate at toxic levels in these mice to result in the photoreceptor degeneration that is seen in these animals.

Photoreceptors are the most metabolically active cells in the retina, relying heavily on the support of Müller cells. Disruption of Müller cell metabolic function, such as decreased glutamine synthetase activity, resulted in photoreceptor abnormal development (Jablonski and Iannaccone, 2000). A homozygous recessive mutation in zebrafish resulted in Müller cell degeneration

and development of fewer photoreceptors than wild-type zebrafish (Kainz et al., 2003). The arrest in photoreceptor development in the mutated fish was followed by degeneration of retinal neurons in both the *onl* and *inl* (Kainz et al., 2003). The pattern of degeneration of retinal cells in the mutated zebrafish, which was induced by Müller cell dysfunction, paralleled the retinal degeneration observed in the *Clcn3*$^{-/-}$ mice suggesting that voltage-dependent Cl channel expression is crucial for proper Müller cell functioning, retinal development, and maintenance of retinal neurons.

5.4 Rationale for studying Müller cell ion channels

Müller cells are the principal glial cells of the retina and are responsible for maintaining retinal integrity through mechanisms of K^+ siphoning and glutamate uptake. While K_{IR} channels are primarily responsible for regulating Müller cell membrane potential, many of the supportive functions of Müller cells are electrogenic and are sensitive to changes in membrane potential which may involve contributions from voltage-dependent ion channels, including voltage-gated Ca channels and other Ca^{2+}-dependent channels such as K_{Ca} and Cl channels. To date, relatively little is known about these channels; compared to K_{IR} channels, in Müller cells or how their activation affects Müller cell physiology. The objectives of this study are:

1) **To identify voltage-gated Ca channel subtype expression and membrane localization in salamander Müller cells.**
2) **To determine if the voltage-gated Ca channel(s) present on Müller cells can contribute to the activation of Ca^{2+}-activated K and Cl channels.**

Chapter 2

General Methods

1. Cell isolation

Müller cells were isolated from larval tiger salamanders, *Ambystoma tigrinum*, (Kons Scientific, Germantown, WI, USA). Salamanders were typically 10 – 20 cm in length and kept on a 12 hour light/dark cycle at 4 °C. All animals were treated in accordance with the guidelines set forth by the Canadian Council on Animal Care (www.ccac.ca). On the day of experimentation, animals were killed by decapitation and both eyes enucleated. One eye was place in a retinal saline solution (solution A, Table 2.1), and the other eye was stored at 4 °C in solution A for use within 24 hours. The retina was then carefully dissected from the posterior eyecup at room temperature, and the extracted retina was incubated for 15 minutes at ~30 °C in Ca^{2+}-free retinal saline solution (solution B, Table 2.1) containing 7 units/ml papain (Sigma Chemical Company, St. Louis, MO, USA). The papain-treated retina was removed from the enzymatic solution, washed in ~ 5 ml solution A, and mechanically triturated with a fire-polished Pasteur pipette in a final volume of 500 µl of solution A. The resulting cell suspension was aliquoted into plastic dishes (Becton Dickinson Labware, Lincoln Park, NJ) for electrophysiological recording or plated onto glass coverslips (Fisher Scientific, Nepean, ON) for immunocytochemistry.

2. Electrophysiological recordings

2.1 Solutions

Plastic dishes with isolated retinal cells were positioned on the stage of an inverted microscope (Nikon). Müller cells were identified by their distinctive

morphology (Figure 2.1). The recording chamber was perfused with external solution via a gravity inflow system at a rate of 1 – 2 ml/min. The pH of external solutions was 7.6 and that of internal solutions was 7.2, adjusted with HCl, NaOH, or CsOH. The compositions of the various solutions are listed in Table 2.1 and described in more detail in Chapters 3-5. Briefly, Ca channel currents were recorded with 10 mM Ba^{2+} as the charge carrier (solution E, Table 2.1) and a 100 mM CsCl pipette solution (solution K, Table 2.1). K channel currents were recorded in a 100 mM NaCl and 2.5 mM KCl bath solution (solution D, Table 2.1) with 90 mM KCl in the pipette solution (solution J, Table 2.1) or in nearly symmetrical K^+ (~100 mM) external and internal solutions (solutions C and J, Table 2.1). Cl channel currents were recorded in an 88 mM NaCl bath solution (solution H, Table 2.1) with a pipette solution containing 100 mM CsCl (solution K, Table 2.1); Cl^- concentration both externally and internally was ~103 mM.

2.2 Patch clamp techniques

Currents were recorded using the tight-seal, patch-clamp technique (Hamill et al., 1981) in the whole-cell or cell attached patch configuration. A gigaohm resistance seal was formed between the pipette and a small patch of cellular membrane by lowering the pipette to the membrane surface and applying negative pressure. Additional negative pressure was applied to rupture the patch of membrane, while leaving the high resistance seal intact. In whole-cell mode, the contents of the pipette solution dialyze the interior of the cell. In the whole-cell voltage clamp configuration, the voltage at the pipette was controlled by the command potential (V_C) and is equal to the membrane potential (V_m) such that:

Table 2.1. Composition of extracellular and intracellular solutions

Composition of extracellular solutions (mM)

	A	B	C	D	E	F	G	H
NaCl	90	90	-	100	70	70	70	88
KCl	2.5	2.5	102	2.5	2.5	2.5	2.5	0.5
CsCl	-	-	-	-	5.0	5.0	5.0	5.0
$BaCl_2$	-	-	-	-	10	-	-	-
$CaCl_2$	3.0	-	3.0	3.0	-	3.0	10	3.0
TEA Cl	-	-	-	-	15	15	15	-
HEPES	10	10	10	10	15	15	15	10
Glucose	8.0	8.0	8.0	8.0	8.0	8.0	8.0	8.0

Composition of intracellular solutions (mM)

	J	K	L
KCl	90	-	-
CsCl	-	100	8.0
Csglucuronate	-	-	92
$CaCl_2$	0.4	0.4	0.4
$MgCl_2$	1.0	0.8	0.8
EGTA	1.0	1.0	1.0
KOH	4.0	-	-
CsOH	-	4.0	4.0
HEPES	5.0	5.0	5.0
ATP Mg^{2+}	2.0	2.0	2.0
GTP Na^{+}	0.1	0.1	0.1

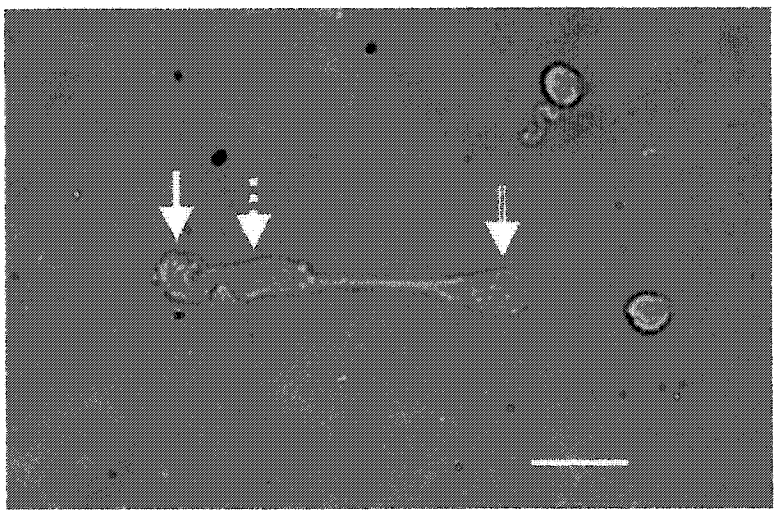

Figure 2.1. Enzymatically isolated salamander Müller cell.
A phase contrast micrograph showing the three distinct regions of the cell: the apical processes, which ensheathes the photoreceptor inner segments (solid arrow), the somatic region (dotted arrow), and the endfoot region, which terminates in the ganglion cell layer adjacent to the vitreous humour (double line arrow). Scale bar, 10 μm.

$$V_m = V_C \quad (2.1)$$

For cell-attached patch continuous recordings of single channel currents, the membrane under the pipette was left intact, and the contents of the pipette solution were only in contact with the extracellular side of the patch of membrane. In the cell-attached patch configuration, V_m was inversely proportional to V_C and shifted by the resting membrane potential (V_{rm}) such that:

$$V_m = V_{rm} - V_C \quad (2.2)$$

Currents were measured using patch pipette electrodes having a resistance of 3 - 10 MΩ. The pipettes were pulled from borosilicate glass with an external diameter of 1.5 mm and an internal diameter of 1.1 mm (Sutter Instrument Co., Novato, CA or Drummond Scientific Co., Bromall, PA) using a two-stage vertical microelectrode puller (Narishige model PP83, Tokyo or Kopf Instruments model 730, Tujunga, CA). Currents were recorded using an Axopatch-1D or -200 patch clamp amplifier (Axon Instruments, Union City, CA), filtered with a 4-pole low pass Bessel filter and digitized at a sampling frequency of 5 - 10 kHz using pCLAMP software (Axon Instruments, Union City, CA), or digitized with an interface (Indec Systems, Sunnyvale, CA) running BASIC-FASTLAB acquisition software. Currents and voltages were also displayed on a Kikuzui 5040 oscilloscope and stored in a computer.

In all experiments, a sealed electrode/salt bridge combination was used as a reference electrode (World Precision Instruments, Inc., Sarasota, FL). The amplifier circuitry was used to zero any offset potentials before the pipette electrode was lowered to the cell membrane to make a seal. The apparent seal

resistances obtained on cells ranged from 500 MΩ to 10 GΩ and series resistance was typically less than 15 MΩ and was uncompensated. All experiments were performed at room temperature (21 – 24 °C).

2.3 Liquid junction potentials

At the interface of the two solutions, a potential difference exists as a result of the tendency of ions with higher mobility to move across the concentration gradient at the junction more quickly than those of lower mobility. Liquid junction potentials (LJP) of appreciable magnitude can arise between the pipette and bath solutions in the whole-cell, patch-clamp configuration (Neher, 1992).

Liquid junction potentials between the pipette and bath solutions were calculated with a software program (JPCalc; P.H. Barry, Sydney, Australia) using a generalized form of the Henderson equation for N polyvalent ions:

$$LJP = V^B - V^P = (RT/F) \sum_{i=1}^{N} S_f \ln \{\sum_{i=1}^{N} z_i^2 u_i a_i^B / \sum z_i^2 u_i a_i^S\} \quad (2.3)$$

where

$$S_f = \sum_{i=1}^{N} [(z_i u_i)(a_i^B - a_i^P)] / \sum_{i=1}^{N} [z_i^2 u_i (a_i^B - a_i^P)]$$

where V^B refers to the potential of the bath solution (B) and V^P refers to the potential of the pipette solution (P); mobility, activity and valency (including sign) of each ion species (i) are represented by u, a, and z; R is the universal gas

constant; T is the temperature in Kelvins; F is Faraday's constant. All data shown in the results that have been corrected for LJPs are indicated as such in the text.

2.4 Pharmacological treatments

All water soluble drugs were dissolved in deionized water to make a concentrated stock solution, aliquoted and stored at -30 °C. On the experiment day, an aliquot of stock solution was thawed and diluted to the desired concentration in either the bath or pipette solution. Stock solutions of lipophilic drugs were made by dissolving the drug in dimethylsulfoxide (DMSO). DMSO drug stocks were aliquoted and kept frozen until needed. When a DMSO-dissolved agent was used, an equal concentration of DMSO alone was first added to the external bath solution as a control. Final DMSO concentrations were always $\leq 0.1\%$. Most drugs were applied extracellularly via perfusion in the external bath solution, but a small number of drugs were dialyzed directly into the cell by the patch pipette. Agents diluted in the intracellular patch pipette solution were allowed ~10 minutes after whole-cell rupture to dialyze into the cell interior before any electrophysiological recordings were made.

Efforts to minimize current rundown were regularly performed. Prior to the application of any pharmacological agents, electrophysiological recordings were made in control solutions until ~5 minutes of stable current recordings were obtained. Once a stable, baseline current was achieved, the pharmacological treatment was begun and continued until ~3 minutes of consecutively steady currents were recorded at which time the drug was washed out via superfusion with the control solution. Furthermore, currents that did not recover or currents

that continued to substantially decrease beyond 10 pA during the wash, i.e., in the absence of drug, were not included in analyses.

2.5 Quantitative and statistical analyses

Current-voltage (I-V) relations were measured during the last 20 milliseconds (ms) of each depolarizing pulse, or tail currents were sampled 30 ms after the end of the voltage step. I-V relations were leak subtracted as indicated in the text. The leak-current is a linear and time-independent current which was calculated by fitting the current present at hyperpolarized potentials, when the contribution of any voltage-dependent currents is minimal, with a linear equation. This estimation of the leak current was then subtracted from the raw current data. Amplitude histograms were constructed from the peak current values with control currents normalized to 100%. The average current remaining after application of the drug is expressed as mean percentage ± standard error (s.e.m.). The n of an experiment is defined as the number of individual isolated Müller cells in a given experiment. All comparisons were carried out using either Student's t test or non-parametric analysis of variance (ANOVA) with Tukey-Kramer multiple comparison post-test, as indicated in the text, with significance defined as $P<0.05$. Activation curves were derived either from leak subtracted currents divided by driving force (or electromotive force) or from isochronal tail current analysis (as indicated in the text). Both activation and inactivation curves were fit with the Boltzmann function:

$$I = \frac{1}{1+\exp((V-V_{½})/m)} \qquad (2.4)$$

where $V_{½}$ is activation midpoint and m is the slope factor.

The equilibrium potential of individual ions in particular solutions was estimated by the Nernst equation:

$$E_X = \frac{RT}{zF} \ln \frac{[X]_o}{[X]_i} \qquad (2.5)$$

where E_X is the equilibrium potential of ion "X", R is the universal gas constant, T is temperature in Kelvin units, z is the charge of ion "X", F is Faraday's constant, $[X]_o$ is the extracellular concentration of ion "X", and $[X]_i$ is the intracellular concentration of ion "X".

3. Immunohistochemistry and immunocytochemistry

Fresh salamander eyes were fixed in 4% paraformaldehyde for ~12 hours at 4 °C and then placed in a 30% sucrose solution for 1-2 days at 4 °C. Following fixation, individual eyes were embedded in Tissue-Tek O.C.T. compound (Sakura Finetek U.S.A., Inc., Torrance, CA), frozen, and sectioned at 14 – 16 μm thickness with a Leica Cryocut 3000 (Nussloch, Germany). Retinal sections were arranged onto silane-treated glass microscope slides. Sections were subjected to three 5 minute washes with phosphate-buffered solution (PBS) and followed by 20 minute incubation with 0.3% Triton X-100. Following three additional 5 minute washes with PBS, a solution of PBS containing 10% goat serum was applied to the retinal sections for 1.5 hours (at room temperature). The PBS/goat serum was removed, and the sections were incubated overnight at 4 °C with a

fresh solution of PBS containing the primary antibody. The next day, the retinal sections were rinsed five times with fresh PBS for 5 minutes per wash and then incubated with the secondary antibodies, Alexafluor goat anti-rabbit IgG or Alexafluor goat anti-mouse IgG, for 1 hr at room temperature. The retinal sections were washed quickly with distilled water once, followed by three washes in PBS at 5 minutes per wash, and finally coverslipped. Control experiments were performed by repeating the protocol but with the primary antibody preadsorbed with its respective control peptides prior to exposure to the tissue. Other control sections were processed with the primary antibody omitted completely to test for any non-specific fluorescence. All other steps and visualization procedures remained the same. Antibody dilutions are described throughout the text (Chapters 3-5).

Müller cells were isolated in the manner described above and fixed in 100% methanol at –30 °C for 5 minutes and then washed three times for 5 minutes in PBS at room temperature. The fixed cells were subjected to an identical protocol of 0.3% Triton-X, washes and blocking as the retinal sections. After removal of the primary antibody solution, the fixed cells were washed five times with PBS and with one or both of the secondary antibodies, Alexafluor goat anti-rabbit and -mouse IgG, was applied for 1 hour, removed, and then washed once with distilled water and once with PBS (all at room temperature). Coverslips containing the antibody-treated fixed cells were aqueously mounted on glass. As a negative control, fixed cells were processed in a manner identical to the above protocol; however, the primary antibody was preadsorbed with its respective

control peptides according to the dilutions recommended by the antibody manufacturer. As an additional control, the above protocol was repeated on fixed cells with complete omission of the primary antibodies by PBS substitution to test for any non-specific staining from the secondary antibody. All other steps and visualization procedures remained the same. Antibody dilutions are described throughout the text (Chapters 3-5).

4. Laser scanning confocal microscopy

4.1 Visualization of antibody-treated retinal sections and isolated cells

Excitation of the Alexafluor goat anti-rabbit IgG and -mouse IgG secondary antibodies was achieved with wavelengths of 488 nm and 543 nm, respectively, via an argon and a helium-neon laser equipped Nikon Eclipse microscope with a C1 laser scanning confocal attachment. Fluorescence emission of Alexafluor goat anti-rabbit IgG was detected with bandpass filter at 515 ± 30 nm by a photomultiplier tube (see Chapter 3 -5). Detection of Alexafluor goat anti-mouse IgG fluorescence emission was with bandpass filter at 586 ± 40 nm (see Chapter 3-5). Antibody-treated retinal sections and isolated cells were visualized with 60X and 40X oil immersion lenses, respectively.

4.2 Visualization of fluorescent-tagged dihydropyridine distribution on isolated cells

Freshly isolated Müller cells (described above) were incubated with both DM-BODIPY (10 nM) and FM1-43 (2.5 μM) for 30 minutes at 4 °C, washed with a NaCl based Ringer, and visualized with a 40X water immersion lens on a laser-

scanning confocal microscope (C-1, Nikon) in 1 μm sections. DM-BODIPY and FM1-43 fluorescence emission was recorded with bandpass filters at 515 ± 30 nm and 586 ± 40 nm, respectively, with a 40X water immersion lens. A neutral density filter (ND8, Nikon) was used for visualizing DM-BODIPY fluorescence. Müller cells used for control experiments were first pre-incubated with 100 μM nifedipine, an L-type Ca channel antagonist, for 30 minutes at 4 °C before application of the fluorescent probes and compared to Müller cells incubated in DM-BODIPY only. Fluorescent labeling of DM-BODIPY was normalized for membrane area by dividing by the FM1-43 fluorescence (Scion Image, NIH software). Pixel intensity was analyzed by subtracting the DM-BODIPY/FM1-43 ratio from the arbitrarily set maximum value of 255 (as defined by the Scion Image program) and dividing by this maximum value of 255 yielding a new ratio between 0 and 1. Regional distribution of DM-BODIPY was analyzed by one-way ANOVA (significance defined as $P<0.05$).

Chapter 3

High-voltage-activated calcium channels in Müller cells acutely isolated from tiger salamander retina

This work has previously been published by Welch NC, Wood S, Jollimore C, Stevens K, Kelly MEM, and Barnes S (2005) High-voltage-activated calcium channels in Müller cells acutely isolated from tiger salamander retina. Glia 49:259-274; Welch NC, Wood S, Jollimore C, Stevens K, Kelly MEM, and Barnes S (2004) Characterization of HVA calcium channels in Müller cells isolated from tiger salamander retina. FASEB J S11525-0056; Welch NC, Barnes S, and Kelly MEM (2003) Uniformly Distributed Calcium Channels in Retinal Müller Cells Exhibit Currents With a Distinctive Pharmacology. Invest. Ophthalmol. Vis. Sci. 44: E-Abstract 4138; Welch NC, Barnes S, and MEM Kelly (2002) Calcium and Calcium-Activated Potassium Currents in Müller Cells Isolated From Tiger Salamander Retina.Invest. Ophthalmol. Vis. Sci. 43: E-Abstract 4757.

ABSTRACT

Müller cells mediate retinal function by stabilizing the ionic environment and signal glial network activity via calcium waves. Using whole-cell patch clamp recording, this thesis describes a high-voltage-activated, slowly inactivating Ca channel current in isolated salamander Müller cells that has unusual pharmacological properties. The Ca channel current has an activation midpoint of ~ –8 mV and an inactivation midpoint near -26 mV in 10 mM Ba^{2+}. The time constant for inactivation is ~380 ms at potentials positive to zero. The current is blocked by Cd^{2+} with an EC_{50} below 100 nM. Nisoldipine (10 μM) blocks ~50%, while nifedipine (1 μM), diltiazem (20 μM) and verapamil (50 μM) each block one third of the current. In contrast to its typical actions, BayK 8644 *blocks* the current by ~ 25%. Blockers of other Ca channel subtypes were also tested: ω-agatoxin IVA (200 nM) blocked only 13% of the Ca channel current, while ω-conotoxin GVIA (1 μM) blocked 84% of the current. Immnohistochemistry and immunocytochemistry supported the presence of α1A, α1B, α1C, and α1D Ca channel subunits. Mapping of dihydropyridine-binding sites with DM-BODIPY revealed a distribution of channels over the entire membrane of the Müller cell with a higher density at the apical region. Overall, these observations suggest either the presence of a mix of L- and N-type Ca channels, or a single, unconventional HVA Ca channel subtype sharing L- and N-type Ca channel characteristics.

1. Introduction

Ca^{2+} influx through voltage-gated Ca channels can influence a wide variety of biological cell processes, depending on the cell type. HVA Ca channels in excitable cells shape the regenerative phase of the action potential. In both excitable and non-excitable cells, $[Ca^{2+}]_i$ is an important second messenger and activates many cellular functions. The $[Ca^{2+}]_i$ is kept low (30 to 200 nM) in living cells, by the combined actions of ATP-dependent Ca^{2+} pumps, a Na^{+}-Ca^{2+} exchange system on the plasma membrane and by ATP-dependent Ca^{2+} pumps on the endoplasmic reticulum. Opening of Ca channels causes an influx of Ca^{2+} into the cytoplasm and transiently raises $[Ca^{2+}]_i$ until Ca^{2+} levels return to normal by diffusion, buffering, and pumping mechanisms. The release of neurotransmitters at nerve terminals is a Ca^{2+}-dependent process requiring an elevation of $[Ca^{2+}]_i$ on the order of 50 – 100 μM. Ca^{2+} regulates the mobilization of neurotransmitter-containing vesicles to the plasma membrane. Furthermore, Ca^{2+} is believed to trigger vesicle fusion with the plasma membrane allowing the vesicle contents, i.e. neurotransmitters, to be released into the synapse. The actions of Ca^{2+} also include direct effects on proteins such as enzymes and ion channels.

Several subtypes of Ca channels have been described and a variety of classification systems have been devised. Initially, Ca channels were categorized according to electrophysiological descriptions, such as LVA or T-type (transient) and HVA or L-type (long-lasting). Pharmacology further distinguished the HVA Ca channels into dihydropyridine-sensitive (L-type), ω-conotoxin GVIA-sensitive (N-type), ω-agatoxin IVA-sensitive (P/Q-type), and toxin-resistant (R-type) Ca

channels. With the advent of molecular techniques, it was determined that Ca channels were comprised of a pore-containing α_1 subunit and three auxiliary subunits, $\alpha 2 - \delta$, β, and γ (Figure 3.1). Drug binding sites are contained within the α_1 subunit which has four homologous domains (I-IV) that are each composed of six transmembrane helices. The fourth transmembrane helix of each domain contains the voltage-sensing function. There are ten α_1 subunits identified which, in turn, are associated with the five classes of Ca channels: L-type have α1C, α1D, α1F, α1S subunits, N-type have α1B subunit, P/Q-type have α1A subunit, and T-type have α1G, α1H, α1I subunits. The nomenclature of Ca channels is further complicated by the addition of a structural name basis which recognizes three broad gene subfamilies: Ca_V1, Ca_V2, and Ca_V3. The types of Ca channels and their respective nomenclature are found in Table 3.1.

Retinal Müller cells signal intercellularly via Ca^{2+}-waves (Newman, 2001), a portion of these signals may be mediated by voltage-gated Ca channels. Both low-voltage-activated (LVA) and high-voltage-activated (HVA) Ca channel currents were found in freshly isolated Müller cells from postnatal rabbits (Bringmann et al., 2000a). The physiological significance of the presence of voltage-gated Ca channels in Müller cells of the mature retina has yet to be fully established, although high voltage-activated (HVA) Ca channels in cultured human Müller cells were shown to be involved in the regulation of cell proliferation (Puro and Mano, 1991). In cultured human Müller cells, an HVA Ca channel has been identified as an α1D, L-type Ca channel ($Ca_v1.3$). The HVA Ca channel was

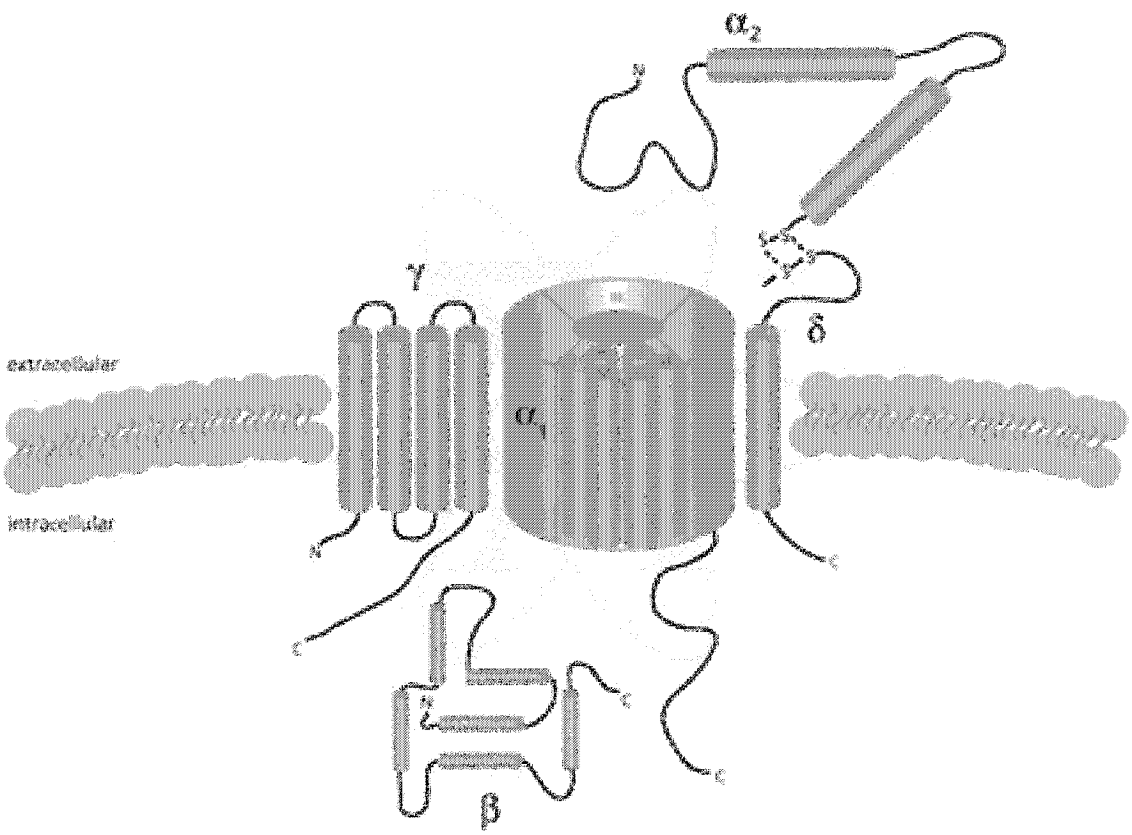

Figure 3.1. Ca channel structure
The heteromultimeric structure of a voltage-gated Ca channel includes the pore-containing α_1 subunit and three auxiliary subunits, α_2-δ, γ, and β. The α_2-δ subunit complex is attached via disulfide bonds with structural support required for Ca channel stimulation provided by α_2 domain while the δ domain modulated activation and inactivation kinetics. The γ subunit is a glycoprotein and the intracellular β subunit is involved in membrane trafficking of α_1 subunits.

Table 3.1. Summary of Ca channel classification

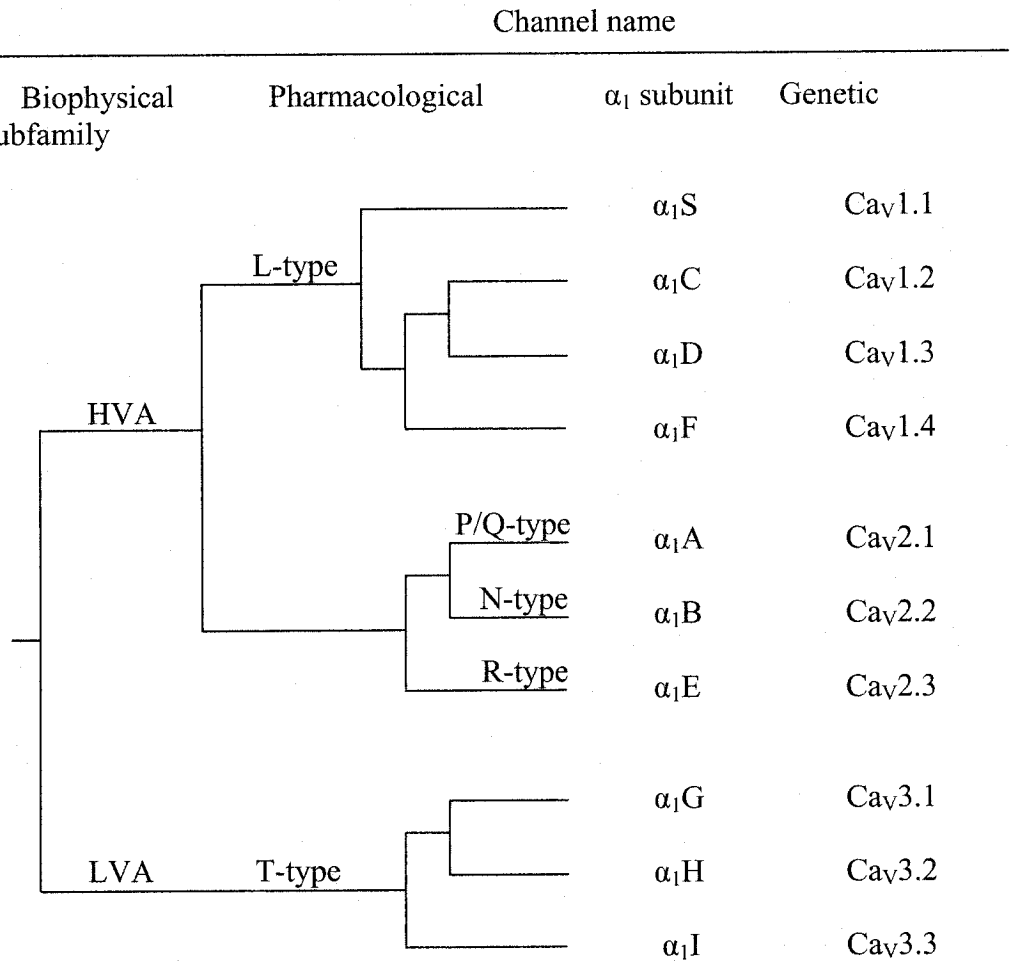

A dendogram linking the different schemes of Ca channel nomenclature. Phenomenological nomenclature recognizes electrophysiological and pharmacological descriptions (HVA vs. LVA, and L, T, N, P/Q, R). The Snutch gene class distinguishes Ca channels according to α_1 subunit variation. Sequence similarities and gene subfamilies are the most recent classification system differentiating Ca channels according to structure.

blocked by dihydropyridines (DHP), indicating the presence of L-type Ca channels and was insensitive to the N-channel blocker ω-conotoxin GVIA and P/Q- channel blocker ω-conotoxin MVIIC (Puro et al., 1996a). Freshly isolated Müller cells from the salamander were found to have a verapamil-sensitive HVA current (Newman, 1985a) suggesting an L-type Ca channel while both HVA and LVA currents were detected in freshly isolated Müller cells from the toad (Bringmann et al., 2000c) indicating the presence of an L-type as well as a T-type Ca channel. The L-type Ca channel subtypes α1C and α1D have been immunohistochemically localized to Müller cells of the salamander (Nachman-Clewner et al., 1999; Henderson et al., 2001). While Ca channel immunoreactivity in the rat retina has identified two L-type Ca channel subtypes, α1D and α1C, in Müller cells, but staining for the N-type (α1B) and P/Q-type (α1A) Ca channels was not found (Xu et al., 2002).

The objectives of this study were to examine the biophysical, pharmacological, and molecular properties of the Ca channel subtype(s) in freshly isolated salamander Müller cells and to define their spatial distribution. It is still unknown whether Müller cell Ca channels are localized to a particular region of the cell, as is the case with the K_{IR} channel (Newman, 1985a). A detailed knowledge of Müller cell Ca channel pharmacology is essential so that the participation of Müller cells in mediating the effects of modulators, drugs, and other agents applied to the retina can be predicted and understood.

2. Materials and Methods

2.1 Cell isolation

Larval tiger salamanders (*Ambystoma tigrinum*) were killed by decapitation, the eyes were enucleated and dissected to remove the retina. Retinas were enzymatically treated to dissociate cells as previously described (see Chapter 2, General Methods; section 1). Retinal cells were aliquoted onto plastic dishes for patch-clamp recording or glass coverslips for immunocytochemistry and visualized in a Nikon Diaphot microscope. Müller cells were identifiable by their distinct morphology.

2.2 Patch clamp recording

Müller cell Ca channel currents were recorded with the whole-cell, patch-clamp recording technique, using recording techniques previously described (see Chapter 2, General Methods; section 2.2). Briefly, isolated Müller cells were held at –60 mV and stepped in 10 mV increments from –60 to +40 mV. The duration of the depolarizing steps was 100 ms. Electrodes were filled with a solution designed to isolate Ca^{2+} channel currents, containing (in mM): 100 CsCl, 0.8 $MgCl_2$, 0.4 $CaCl_2$, 1 EGTA, 5 HEPES, 1 ATP, 0.1 GTP at pH 7.2 (solution K, Table 2.1 in Chapter 2, General Methods). The extracellular bathing solution was composed of (in mM): 70 NaCl, 2.5 KCl, 5 CsCl, 10 $BaCl_2$, 15 TEA, 15 HEPES, 8 glucose at pH 7.6 (solution E, Table 2.1 in Chapter 2, General Methods). Drugs were added to the extracellular solution and superfused during electrophysiological recording. Nisoldipine and (±)BayK 8644 were each prepared as 10 mM stock solutions in DMSO and diluted in the bathing solution.

In each case, control electrophysiological recordings were made in the presence of an equal concentration of DMSO in the external bathing solution. In some experiments, extracelluar Ba^{2+} was replaced by either 3 mM $CaCl_2$ or 10 mM $CaCl_2$ (solutions F and G, Table 2.1 in Chapter 2, General Methods). All recordings were performed at room temperature (21 – 25 °C).

2.3 Immunohistochemistry and immunocytochemistry

Salamander retinal sections were stained for four different Ca channel proteins using the generalized protocols described in Chapter 2, General Methods (section 3). The primary antibodies used on retinal sections were: monoclonal mouse anti-glial fibriallary acidic protein (GFAP, 1:200), polyclonal rabbit anti-α1A, -α1B, -α1C, or -α1D (each at 1:200 dilution). The secondary antibodies used were Alexafluor goat anti-rabbit IgG (1:500) and Alexafluor goat anti-mouse IgG (1:500). Control experiments were performed by repeating the protocol but with the primary antibodies preadsorbed with their respective control peptides, according to the dilutions recommended by the antibody manufacturer (1:1 ratio of control peptide to antibody for anti-α1A and -α1D and 1:10 ratio for anti-α1B and -α1C). Additional control experiments were carried out by omitting the Ca channel primary antibodies completely. Antibody-fluorescence was detected using laser-scanning confocal microscopy (described in Chapter 2, General Methods; section 4.1).

Fixed isolated Müller cells were stained for each of the rabbit Ca channel anti-α1A, -α1B, -α1C, or -α1D subunit polyclonal antibodies (each at 1:1500 dilution). The immunocytochemical protocol is detailed in Chapter 2, General

Methods (section 3). The secondary antibody used was Alexafluor goat anti-rabbit IgG (1:500 dilution). As a negative control, fixed cells were processed in a manner identical to the immunocytochemical protocol; however, the primary antibodies were preadsorbed with their respective control peptides according to the dilutions recommended by the antibody manufacturer (1:1 ratio of control peptide to antibody for anti-α1A and -α1D and 1:10 ratio for anti-α1B and -α1C). As an additional control, the above protocol was repeated on fixed cells with complete omission of the primary antibodies to account for any non-specific staining from the secondary antibody. Antibody-treated cells were visualized with laser-scanning confocal microscopy (described in Chapter 2, General Methods; section 4.1).

2.4 Distribution of fluorescent-tagged dihydropyridines

Freshly isolated Müller cells were incubated with both DM-BODIPY (10 nM) and FM1-43 (2.5 μM) and visualized with a laser-scanning confocal microscope as described in Chapter 2, General Methods (section 4.2). Müller cells used for control experiments were first pre-incubated with 100 μM nifedipine for 30 minutes at 4 °C before application of the fluorescent probes.

2.5 Drugs and chemicals

Most chemicals used in electrophysiological recordings were obtained from Sigma Chemical Co. (St. Louis, MO) including: ω-agatoxin IVA (AgTX), (±)BayK 8644 (BayK), cadmium chloride (Cd^{2+}), ω-conotoxin GVIA (CTX), nifedipine (Nif), diltiazem, and verapamil. Nisoldipine (Nis) was a gift of Bayer Inc (Toronto, ON). The fluorescent-tagged dihydropyridine, DM-BODIPY, the

styryl dye, FM1-43, and the Alexafluor secondary antibodies, goat anti-rabbit and goat anti-mouse, were purchased from Molecular Probes, Inc (Eugene, OR). The Ca channel subunit antibodies used in immunohistochemistry and immunocytochemistry, rabbit anti-α1A and -α1D, were purchased from Alomone laboratories (Jerusalem, Israel); rabbit anti-α1B and -α1C was purchased from Chemicon (Temecula, CA). GFAP was purchased from Novocastra Laboratories Inc. (Newcastle upon Tyne, UK). The peroxidase-labelled anti-rabbit IgG used in the Western blotting was obtained from Vector Laboratories (Burlington, ON).

2.6 Quantitative and statistical analyses

Current-voltage (I-V) relations were measured near the end of each depolarizing pulse, 80 ms after the beginning of the voltage step, and leak subtracted. Amplitude histograms were constructed from the peak current values with control currents normalized to 100%. Average current remaining after application of drug is expressed as mean ± standard error (s.e.m.). All comparisons were carried out using either Student's t test or non-parametric analysis of variance (ANOVA), as indicated in the text, with significance defined as $P<0.05$. Statistical analyses of drug block were performed on raw currents as paired t test. Activation curves were derived either from leak subtracted currents divided by driving force (or electromotive force) or from isochronal tail current analysis (as indicated in the text). Both activation and inactivation curves were fit with the Boltzmann function (2.4).

3. Results

3.1 Properties of Ca channels in isolated Müller cells

LVA and HVA Ca channels can be distinguished by the voltage dependence of their activation and their sensitivity to divalent cation block. Measured in 10 mM Ba^{2+} bath solution with the CsCl pipette solution, Ca channels activated at membrane potentials positive to –20 mV as shown in Figures 3.2*A* and *C*. Peak inward current was seen at 0 mV in the cell illustrated, but the peak's value was often seen between –10 and +20 mV in other cells. An estimate of the activation parameters was obtained from the I-V relation by dividing by the driving force and fitting with the Boltzmann function. This revealed an activation midpoint of –6.9 ± 1.7 mV and a slope factor of 3.4 ± 0.3 in a sample of six cells.

The current traces in figure 3.2*A* suggest that a slow inactivation process occurs. Steady-state inactivation of the Ca channel currents was measured in the presence of 10 mM Ba^{2+} by applying depolarizing prepulses to potential between –90 and +20 mV for 500 ms and then testing the current at +10 mV (Fig. 3.3*A*). Fit with the Boltzmann function (Fig. 3.3*B*), the steady-state inactivation properties obtained from this protocol included an inactivation midpoint of -26 ± 2 mV and a slope factor of -7 ± 1 mV (n=4). Upon replacement of Ba^{2+} with Ca^{2+} as the charge carrier, the same inactivation protocol did not elicit a significant difference in the steady-state inactivation midpoint (ANOVA, $P<0.05$) between 10 mM Ba^{2+}, 10 mM Ca^{2+}, or 3 mM Ca^{2+}.

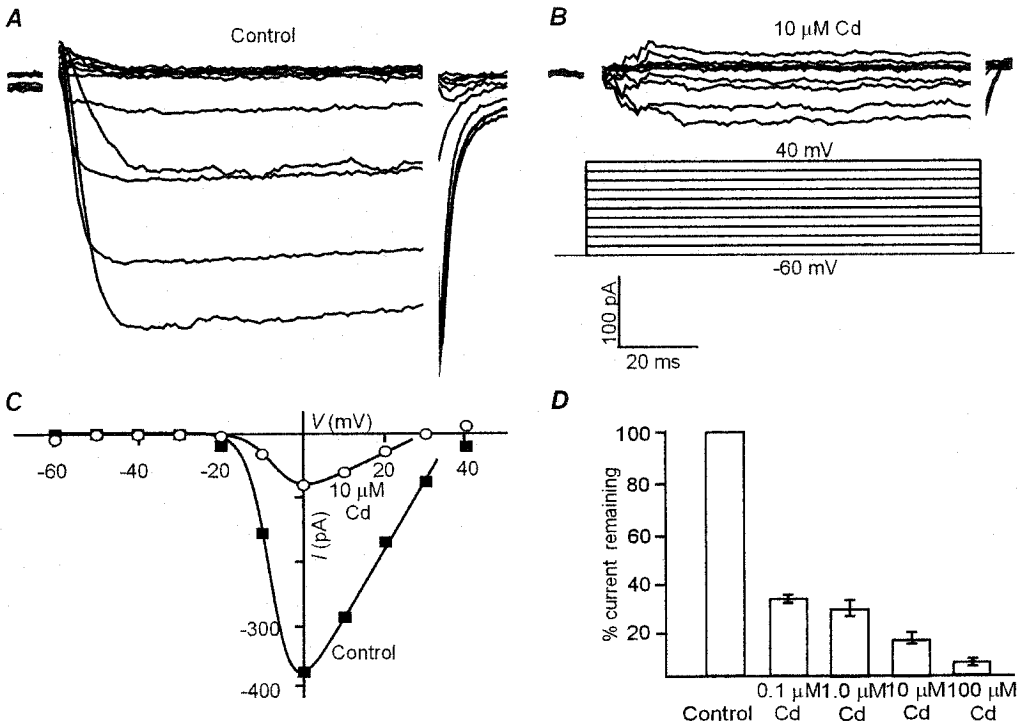

Figure 3.2. Ca channel currents in isolated Müller cells and their sensitivity to Cd^{2+}.

A, Whole-cell, capacitance-subtracted Ca channel currents in a Müller cell elicited during steps to voltages between –60 and +40 mV, in 10 mV increments, from a holding potential of –60 mV, recorded in 10 mM Ba^{2+}. *B*, The current was reduced significantly in the presence of 10 μM Cd^{2+}. *C,* I-V relation for currents shown in *A&B* in the absence (closed squares) and the presence (open circles) of 10 μM Cd^{2+}. *D,* Concentration response data was compiled with control currents normalized to 100% and the current after administration of Cd^{2+} (0.1 μM Cd^{2+}; n=3, 1.0 μM Cd^{2+}; n=3, 10 μM Cd^{2+}; n=5, 100 μM Cd^{2+}; n=6) expressed as percent of current remaining. Values were averaged from currents evoked at the peak of the I-V relation for each cell.

When the cell was depolarized for 2 s (Fig. 3.3*C*), the resulting Ba^{2+}-conducting Ca channel current decayed exponentially with a time constant of ~170 ms at –10 mV and ~380 ms at potentials positive to -10 mV (Fig 3.3*D*). The Ca^{2+}-dependent portion of inactivation of the Müller cell Ca channel was revealed by superimposing currents recorded in Ba^{2+} (solid line) and Ca^{2+} (dotted line; Fig 3.3*E*). The difference in current remaining after a 100 ms depolarization to 0 mV in 10 mM Ba^{2+} (83 ± 4%, n=6) compared to that in 10 mM Ca^{2+} (66 ± 5%, n=7) was significant (Fig 3.3*F*, unpaired t test, $P<0.05$). Lowering the concentration of Ca^{2+} from 10 mM to 3 mM reduced the Ca^{2+}-dependent portion of inactivation (72 ± 4%, n=4).

The Ca channel currents recorded with Ba^{2+} as the charge carrier were only slightly smaller when recorded in the presence of 3 mM and 10 mM Ca^{2+} (data not shown). This preference for conducting Ba^{2+} over Ca^{2+} is shared by all HVA Ca channels (Hille, 2001).

3.2 Block of Müller cell Ca channels by Cd^{2+}

Cadmium is a potent blocker of some HVA and LVA channels. Figures 3.2*B* and *C* show that Müller cell Ca channel currents were blocked by Cd^{2+}, and that the reduction occurred in a dose-dependent manner (Fig. 3.2*D*). The average Ca channel current remaining in the presence of Cd^{2+} (measured at the peak of the I-V relation) was 31 ± 1% (n=3), 27 ± 3% (n=3), 15 ± 2% (n=5), and 5 ± 1% (n=6) for 0.1, 1.0, 10, and 100 μM Cd^{2+}, respectively, indicating that the EC_{50} lies at concentrations below 100 nM. Statistical analyses of the currents confirmed

Figure 3.3. Inactivation of Ca channel currents in retinal Müller cells. *A,* Ca channel currents tested at –10 mV preceded by depolarizing conditioning steps made to voltages between –90 mV and +20 mV in 10 mV increments. *B,* The steady-state inactivation curve (closed squares, n = 6) was constructed from data like those derived in Figure 3.2*A*, measured at the peak of the current during the test step, and fit with a Boltzmann function. The closed circles show the activation curve constructed from 6 leak-subtracted I-V relations which were divided by the driving force and fit with a Boltzmann function. *C,* Ca channel currents in response to 2000 ms steps to –10 mV and +10 mV. *D,* Slow inactivation time constants measured during 2000 ms depolarizing steps to –10, 0, +10 and +20 mV. Current records such as those shown in *C* were fit with a single exponential (n = 6). *E,* The response of Ca channel currents to a 100 ms depolarization to 0 mV in the presence of 10 mM Ba^{2+} (solid line) and 10 mM Ca^{2+} (dotted line). *F,* Ratio of peak to sustained currents (such as those in *E* measured at the peak and at the end of the 100 ms depolarization) measured in 10 mM Ba^{2+} and in 10 mM and 3 mM Ca^{2+}. A significant difference was observed between 10 mM Ba^{2+} and 10 mM Ca^{2+}.

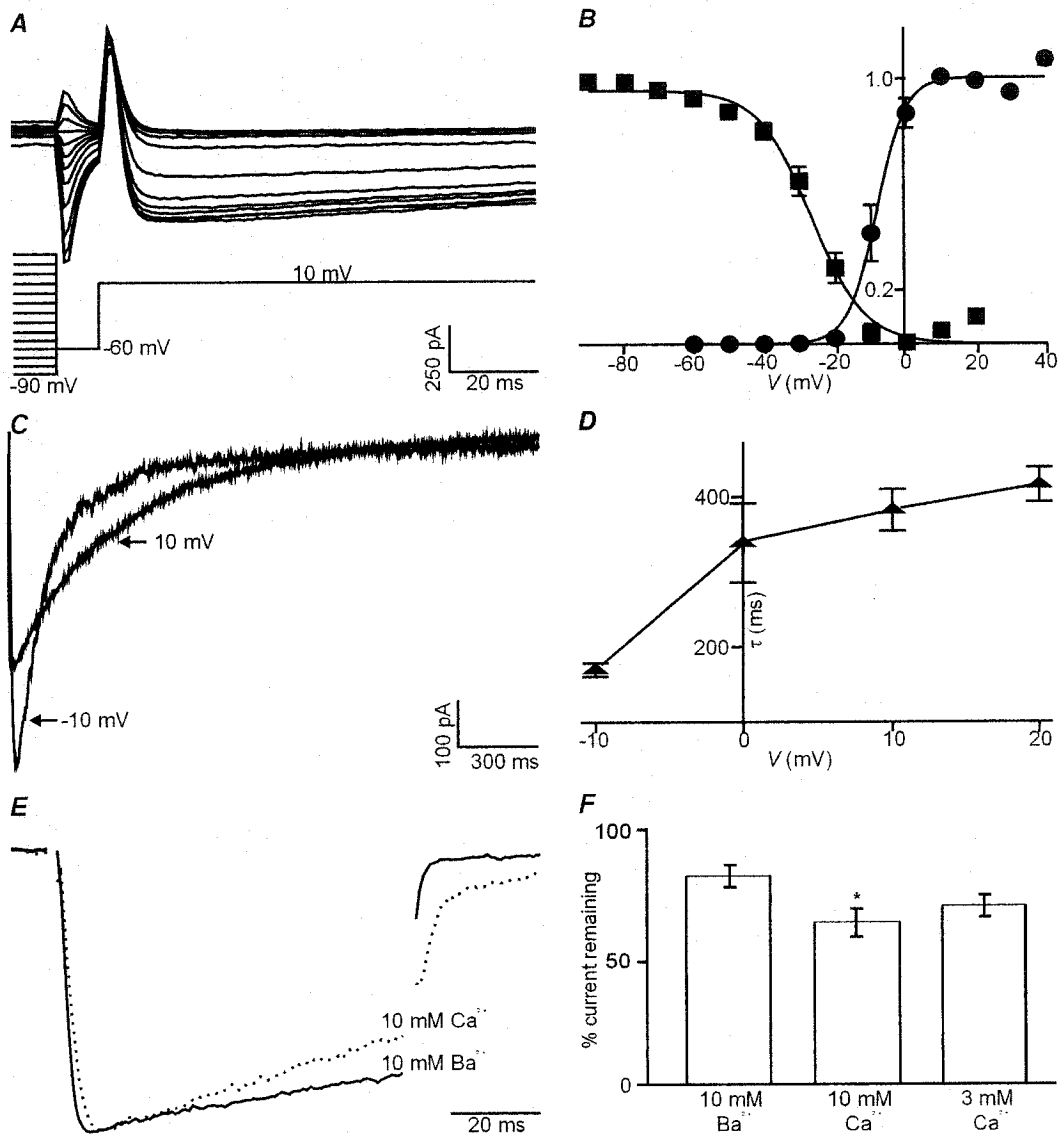
A
10 mV
-60 mV
-90 mV
250 pA
20 ms
B
1.0
0.2
-80
-60
-40
-20
0
20
40
V (mV)
C
10 mV
-10 mV
100 pA
300 ms
D
400
200
τ (ms)
-10
0
10
20
V (mV)
E
10 mM Ca2+
10 mM Ba2+
20 ms
F
100
50
0
% current remaining
*
10 mM Ba2+
10 mM Ca2+
3 mM Ca2+

Figure 3.3.

that a significant decrease was observed in the presence of each concentration of Cd^{2+} (paired t test, $P<0.05$).

3.3 Modulation of Ca channels by L-type Ca channel blockers

L-type Ca channel subtypes (α1C, α1D, and α1F) are preferentially blocked by lipid-soluble drugs such as the benzothiazepines, the phenylalkylamines, and the 1,4-dihydropyridines (DHPs). These three classes of drugs are thought to bind to three separate, allosterically linked, receptor sites (Hockerman et al., 1997). Figure 3.4*A* shows currents from a cell evoked by a test depolarization to 0 mV in control and in the presence of 20 μM diltiazem, a benzothiazepine. The I-V relation for this cell is shown in Figure 3.4*B*. In the sample of cells tested (n=9), diltiazem blocked 37 ± 5% of the Ca channel current, a significant effect (paired t test, $P<0.05$), which was partially reversible once the drug was removed from the bath. Verapamil, a phenylalkylamine Ca channel blocker, was also tested (Fig. 3.4*C* & *D*). In the presence of 50 μM verapamil, 38 ± 8% of the Ca channel current was blocked (n=8), and the current could not be recovered upon removal of the drug from the perfusate. Statistical analysis of the currents revealed that the decreased current in the presence of verapamil was significant compared to control currents (paired t test, $P<0.05$)

A defining criterion for L-type Ca channels is sensitivity to DHPs. Nisoldipine is a DHP which binds to the L-type Ca channel favoring a closed state and suppressing Ca channel current. Figure 3.5*A* illustrates Ca channel currents evoked by successive depolarizations from a holding potential of –60 mV which,

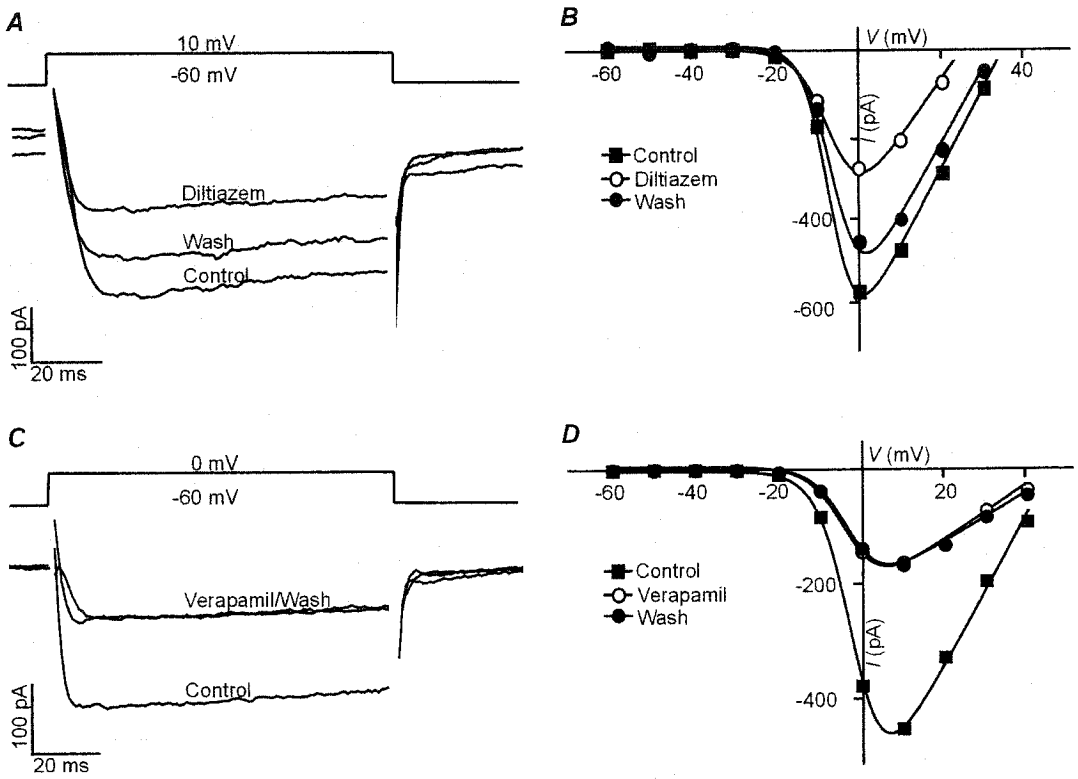

Figure 3.4. Partial block of Ca channel currents by diltiazem and verapamil in Müller cells.

A, Capacitance-subtracted Ca channel currents from a cell stepped to 0 mV from a holding potential of –60 mV, before (control), in 20 μM diltiazem, and upon removal (wash) of diltiazem. *B,* I-V relations for the currents in *A* in control (closed squares), 20 μM diltiazem (open circles), and wash (closed circles). C, Capacitance-subtracted Ca channel currents recorded from a cell before (control), in verapamil (50 μM), and after removal (wash) of verapamil. The Ca channel currents were elicited during steps to -10 mV from a holding potential of –60 mV. *D,* I-V relations from the isolated Müller cell in *A* in control (closed squares), 50μM verapamil (open circles), and wash (closed circles).

when repeated in the presence of 10 μM nisoldipine, produced a reduced current (Fig. 3.5*B*). The corresponding I-V relations are shown in Figure 3.5*C*. The actions of nisoldipine were dose-dependent as shown in Fig. 3.5*D*, which illustrates the effects of decreasing concentrations of DHP with 48 ± 7% (n=5), 44 ± 3% (n=4), and 72 ± 6% (n=3) of Ca channel current remaining upon the administration of 10 μM, 1 μM, and 0.1 μM nisoldipine, respectively. Statistical analyses of the control currents compared to the nisoldipine-treated currents revealed a significant block by 10 μM nisoldipine, while the block by lower concentrations of nisoldipine was not significant (paired t test, $P<0.05$). Another DHP antagonist, 1 μM nifedipine had a significant effect on Ca channel currents (paired t test, $P<0.05$) leaving 71 ± 4% of the Ca channel current (n=7). For each of the four Ca channel blockers (diltiazem, verapamil, nisoldipine, and nifedipine), there was no significant difference between the activation midpoints of the Ca channel current (Table 3.2; ANOVA, $P<0.05$). In the presence of each of the four L-type Ca channel blockers a considerable portion of the current remained suggesting that if the Ca channel subtype contributing to the current in Müller cells is attributable principally to an L-type Ca channel, then the efficacy of the L-type Ca channel blockers is relatively low in this cell type.

3.4 Suppression of Ca channel currents by BayK 8644

DHPs can both decrease and increase activation of L-type Ca channels depending on the structure of the drug and its interaction with the DHP binding sites on the channel. The agonist BayK 8644 appears to increase Ca channel current by favoring the channel's open state (Hille, 2001). A BayK 8644-induced

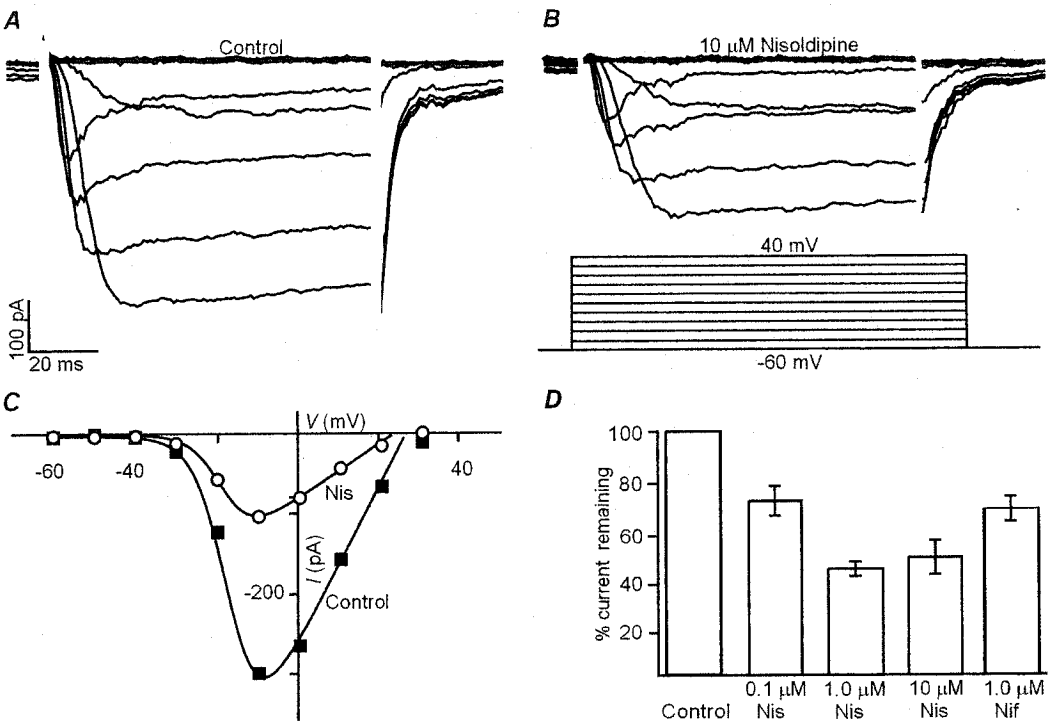

Figure 3.5. Dose-dependence of weak nisoldipine block.
A, Capacitance-subtracted whole-cell Ca channel currents from an isolated Müller cell elicited during steps to voltages between –60 and +40 mV in 10 mV increments from a holding potential of –60 mV in the absence (control) and *B,* presence of 10 μM nisoldipine (Nis). *C,* Leak subtracted I-V relations from the same cell in *A&B* in control (closed squares) and nisoldipine (open circles) *D,* Histogram displays the concentration response data of all cells tested with control currents normalized to 100% of the Ca channel current after administration of nisoldipine (0.1 μM; n=3, 1.0 μM; n=4, 10 μM; n=5) and nifedipine (1.0 μM; n=5) expressed as percent current remaining. Values were averaged from currents evoked at the peak of the I-V relation for each cell.

Table 3.2. Summary of Ca channel activation kinetics in isolated Müller cells

Drug	$V_{½}$ (mV)		m (mV)	
	Unblocked	Blocked	Unblocked	Blocked
Diltiazem (20 μM; n=9)	1 ± 1	-4 ± 2	-4 ± 1	-3 ± 1
Verapamil (50 μM; n=6)	1 ± 1	-4 ± 2	-5 ± 1	-3 ± 1
Nisoldipine (10 μM; n=5)	7 ± 5	2 ± 5	-3 ± 1	-3 ± 1
Nifedipine (1 μM; n=5)	-1 ± 1	1 ± 3	-4 ± 1	-5 ± 1
BayK (1 μM; n=7)	-3 ± 2	-1 ± 4	-4 ± 1	-2 ± 1
CTX (1 μM; n=6)	2 ± 3	4 ± 1	-6 ± 1	-4 ± 1
AgTX (200 nM; n=7)	-2 ± 2	-1 ± 1	-4 ± 1	-3 ± 1

Activation curves were derived from leak-subtracted I-V relations and fitted with the Boltzmann function: $1/(1+\exp((V-V_{½})/m))$. Values are expressed as means ± s.e.m.

net current increase is also diagnostic, taken together with block by the other DHPs, for the L-type Ca channel's presence. To verify the presence of an L-type Ca channel current in salamander Müller cells, (±)BayK 8644 (BayK) was tested on isolated Müller cells. In seven cells tested, BayK was found to modestly suppress the peak Ca channel current with 75 ± 5% of the current remaining upon application of the drug. Statistical analysis of the currents revealed that this block was significant (paired t test, $P<0.05$). Successive depolarizing steps from a holding potential of –60 mV generated the currents in Figure 3.6 in the presence of 10 mM Ba^{2+} before and after the application of 1 μM BayK. Some slowing of the tail current relaxation is evident in the presence of BayK. The I-V relation (Fig. 3.6*C*) for the same cell reveals the reduction in peak Ca channel current but also an apparent negative shift in channel activation at potentials below –10 mV, reminiscent of the agonist actions of BayK. Similar results were also observed upon application of the pure enantiomer (-)BayK 8644 with 83% of the Ca channel current remaining after administration of (-)BayK (data not shown). Isochronal tail current analysis provided activation curves for this cell with and without BayK as shown in Figure 3.6*D*. Enhanced channel activation at the foot of the activation curve is typical of the actions of BayK. However, the activation midpoint in BayK did not differ significantly from the other L-type Ca channel blockers (Table 3.2; ANOVA, $P<0.05$). In a parallel series of experiments, the normative actions of the racemic mixture of BayK (1 μM) were confirmed in cone photoreceptors (Wilkinson and Barnes, 1996), shown in Figure 3.6*E*, with (±) BayK producing substantial increases in Ca channel current (n=3).

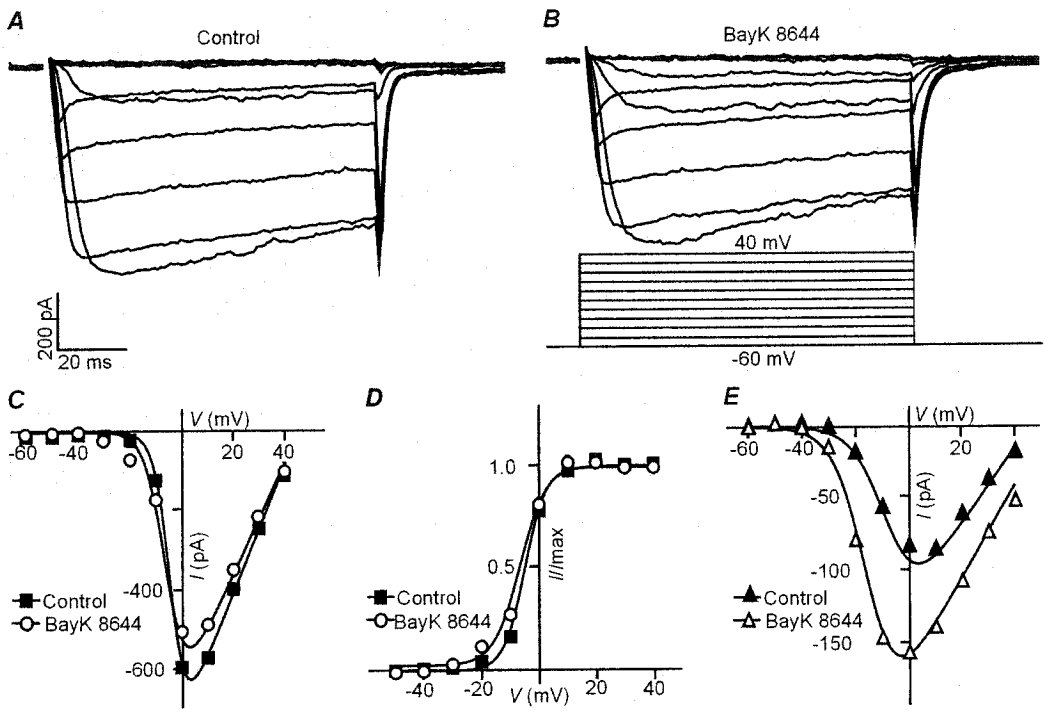

Figure 3.6. BayK 8644 reduces the Müller cell Ca channel current.
A, Capacitance-subtracted Ca channel currents recorded from an isolated cell generated during steps to voltages from –60 mV to +40 mV in 10 mV increments from a holding potential of –60 mV before (control) and *B,* after the application of 1 μM (±) BayK 8644 (BayK). *C,* I-V relations from the cell in *A & B* before (control, closed squares) and after BayK (open circles). *D,* Normalized activation curves derived from the tail current records in *A & B* before (closed squares) and after (open circles) the application of BayK. *E,* (±) BayK enhances Ca channel currents in cone photoreceptors at the same concentration and under the same conditions for which reduction was seen in Müller cells.

3.5 Toxin-sensitivity of Ca channels

While nearly all of the Ca channel current could be blocked by Cd^{2+}, but not by nisoldipine, the possibility that other Ca channel subtypes are present needed to be tested. Ca channel subtypes have been classified according to their pharmacology and, in particular, to their sensitivity to toxins such as CTX and AgTX, blockers selective for N (α1B)- and P/Q (α1A)-type Ca channel subtypes, respectively, in mammalian neurons. Application of 1 μM CTX, shown in Figure 3.7 (*A* & *B*), significantly inhibited Ca channel current (paired t test, $P<0.05$) with only 16 ± 4% (n=10) of the current remaining even upon removal of CTX from the bath, suggesting that CTX binds irreversibly to the Ca channel. Simultaneous application of nifedipine (1 μM) and CTX (1 μM) completely abolished the Ca channel current (Fig. 3.7*C*). This additive inhibition of the Ca channel current was observed in each of the five cells tested (Fig. 3.7*D*) with 66 ± 5% of the current remaining after the administration of 1 μM nifedipine and 3 ± 2% of the Ca channel current remaining after co-application of 1 μM nidedipine and 1 μM CTX. Application of 200 nM AgTX (AgTX) (Fig. 3.8*A*) slightly, but significantly (paired Student's t test, $P<0.05$) reduced Ca channel current by 13 ± 6% (n=4). A higher concentration of AgTX, 500 nM, produced greater block (Fig. 3.8*B*) (50 ± 7%; n=7), but this concentration is far beyond that at which AgTX blocks P/Q currents in other neurons (e.g. 92% block at 200 nM in Purkinje cells; Mintz et al., 1992).

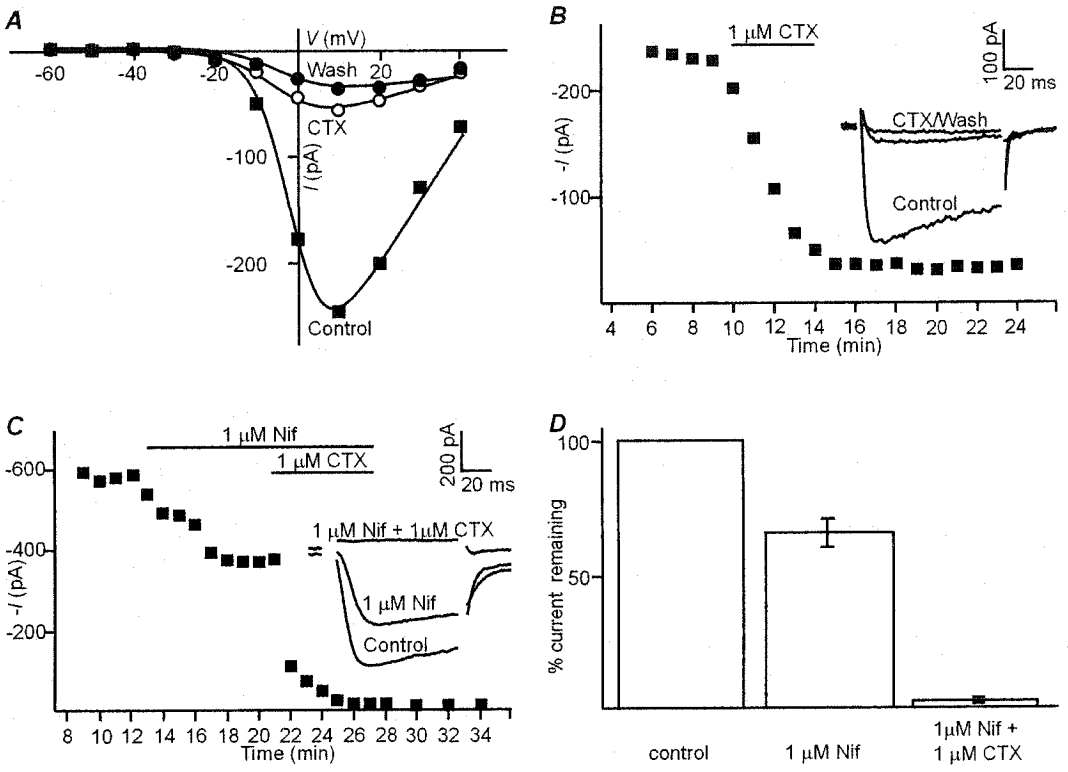

Figure 3.7. ω-Conotoxin GVIA suppresses the Müller cell Ca channel current.

A, Leak-subtracted I-V relation from an isolated Müller cell in control (closed squares), 1 μM CTX (open circles) and wash (closed circles). *B,* Time course of CTX block of the cell shown in *A*. Peak current amplitudes were evoked every 60 s with voltage steps from –60 to +10 mV and plotted against time. CTX inhibition could not be reversed. Capacitance-subtracted current records are shown in the inset and were taken before (control), at peak CTX block, and after 10 min wash. *C,* Time course of currents, elicited at 0 mV, from a different isolated Müller cell exposed first to 1 μM nifedipine and then to co-application of 1 μM Nif and 1 μM CTX. Inset shows capacitance-subtracted current records sampled before drug application (control), 8 minutes after the administration of 1 μM Nif, and after 10 minutes of exposure to both 1 μM Nif and 1 μM CTX. *D,* Ca channel currents after administration of 1 μM Nif and 1 μM Nif + 1 μM CTX expressed as percent of current remaining.

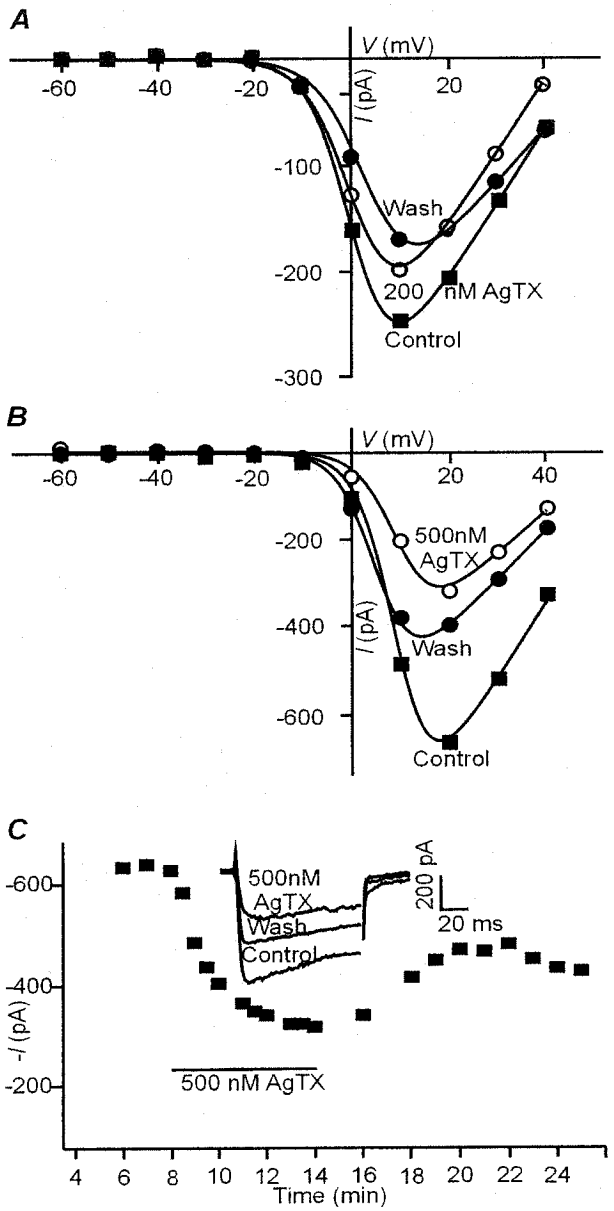

Figure 3.8. ω-Agatoxin IVA blocks Ca channel currents in Müller cells. A, Leak-subtraced I-V relations from an isolated Müller cell in 10 mM Ba^{2+} in control (closed squares), in the presence of 200 nM AgTX (open circles) and after removal of AgTX (wash, closed circles). *B*, Leak-subtracted I-V relations from an isolated Müller cell in the presence of 10 mM Ba^{2+} before (control, closed squares), during (AgTX, open circles) the application of 500 nM AgTX, and after removal of AgTX from the bath (wash, closed circles). *C*, Time course of current block from the cell in *A* in the presence of AgTX. Voltage steps from –60 to +20 mV every 60 s elicited a peak current and was plotted against time. Capacitance-subtracted barium current records taken before (control), at peak AgTX block and after 10 min wash for the cell in *A&B* are shown in the inset.

3.7 Immunoreactivity of α_1B, α_1C, and α_1D Ca channel subunits

Immunohistochemistry was also performed on salamander retinal sections by employing a double-labeling technique using a glial specific marker, anti-GFAP, in combination with each of the Ca channel subunit antibodies. Antibody specificity had been previously confirmed in salamander retina (Welch et al., 2005). Figure 3.9 shows fluorescent images of retinal slices stained with the Ca channel antibodies anti-α1A (Fig. 3.9*A*), -α1B (Fig. 3.9*D*), -α1C (Fig. 3.9*G*), and -α1D (Fig. 3.9*J*) in green and the corresponding anti-GFAP-positive images in red (Fig. 3.9*B*, *E*, *H*, &*K*). The GFAP-positive cells are identified as the Müller cells from the distinctive long stretches of GFAP staining extending from the outer nuclear layer (*onl*) through the outer plexiform layer (*opl*), inner nuclear layer (*inl*) and inner plexiform layer (*ipl*). Colocalization of GFAP-positive cells and Ca channel subunit-positive immunoreactivity is distinguished as orange. Retinal slices treated with the Ca channel anti-α1A antibody did not exhibit significant staining of Müller cells (Fig. 3.9*A*). However, a small degree of colocalization (Fig. 3.9C) can be observed in the outer retina surrounding the photoreceptor inner segments which the Müller cell apical processes are known to ensheath (Sarantis & Mobbs, 1992) suggesting that the α1A, P/Q-type, Ca channel may be expressed in this region of the glial cell. The overlapping staining patterns of anti-GFAP and anti-α1B antibodies indicate that Müller cells do express N-type Ca channel epitopes (Fig. 3.9*D*, *E*, *F*). Similarly, two types of L-type Ca channel epitopes were found to be expressed on salamander Müller cells as the antibodies for both α1C and α1D were found to exhibit the

Figure 3.9. Immunohistochemical analysis of Ca channel subunits reveals that α1A, α1B, α1C, and α1D are expressed in GFAP-positive Müller cells. *A*, Laser scanning confocal microscopy (LSCM) image of a 14 – 16 μm retinal cross-section stained with an α1A-specific Ca channel antibody (green). *B*, The same retinal section in *A* stained with the glial-specific marker GFAP (red). *C*, The same retinal section in *A* and *B* is dual labeled with anit-α1A and anti-GFAP with some colocalization of the two antibodies apparent only in the outer plexiform layer when both green and red fluorescence was visualized together. *D*, A 14 – 16 μm cross-section of a salamander retina viewed with LSCM showing the distribution of α1B Ca channel subunit expression (green). *E*, GFAP-positive cells from the same retinal section in *D* viewed in red. *F*, Colocalization of anti-α1B and -GFAP are displayed in orange for the retinal section in *D* and *E*. The green staining in the *opl* and *ipl* represents non-glial cells expressing α1B. *G*, LSCM image of a salamander retinal section, 14 – 16 μm thickness, typifies the expression of α1C (green). *H*, The same cross-section in *G* stained with anti-GFAP (red). *I*, Double-labeling of the retinal section in *G* and *H* reveal areas of overlap of α1C and GFAP immunoreactivity (orange). *J*, The retinal distribution of α1D Ca channel subunit expression (green) is exemplified in this cross-section viewed with LSCM. *K*, The retinal section in *J* is stained for the glial-specific marker, GFAP (red). *L*, Colocalization of α1D and GFAP immunoreactivity appears as orange in the retinal section in *J* and *K*. The green staining of α1D indicates that this Ca channel subunit is also expressed on non-glial cells in both of the plexiform layers. *M*, Anti-rabbit secondary antibody (2°) only negative control retinal sections processed without any primary antibodies viewed with LSCM. Only the photoreceptors exhibit any fluorescence, and this is likely due to autofluroescence. *N*, Negative controls for the anti-mouse 2° only of the same retinal cross-section shown in *M*. Fluorescence is noted only in the photoreceptors and is attributed to autofluorescence. *N*, Merging of the 2° only negative controls reveals non-specific fluorescence is limited to the photoreceptors. Scale bar, 10 μm.

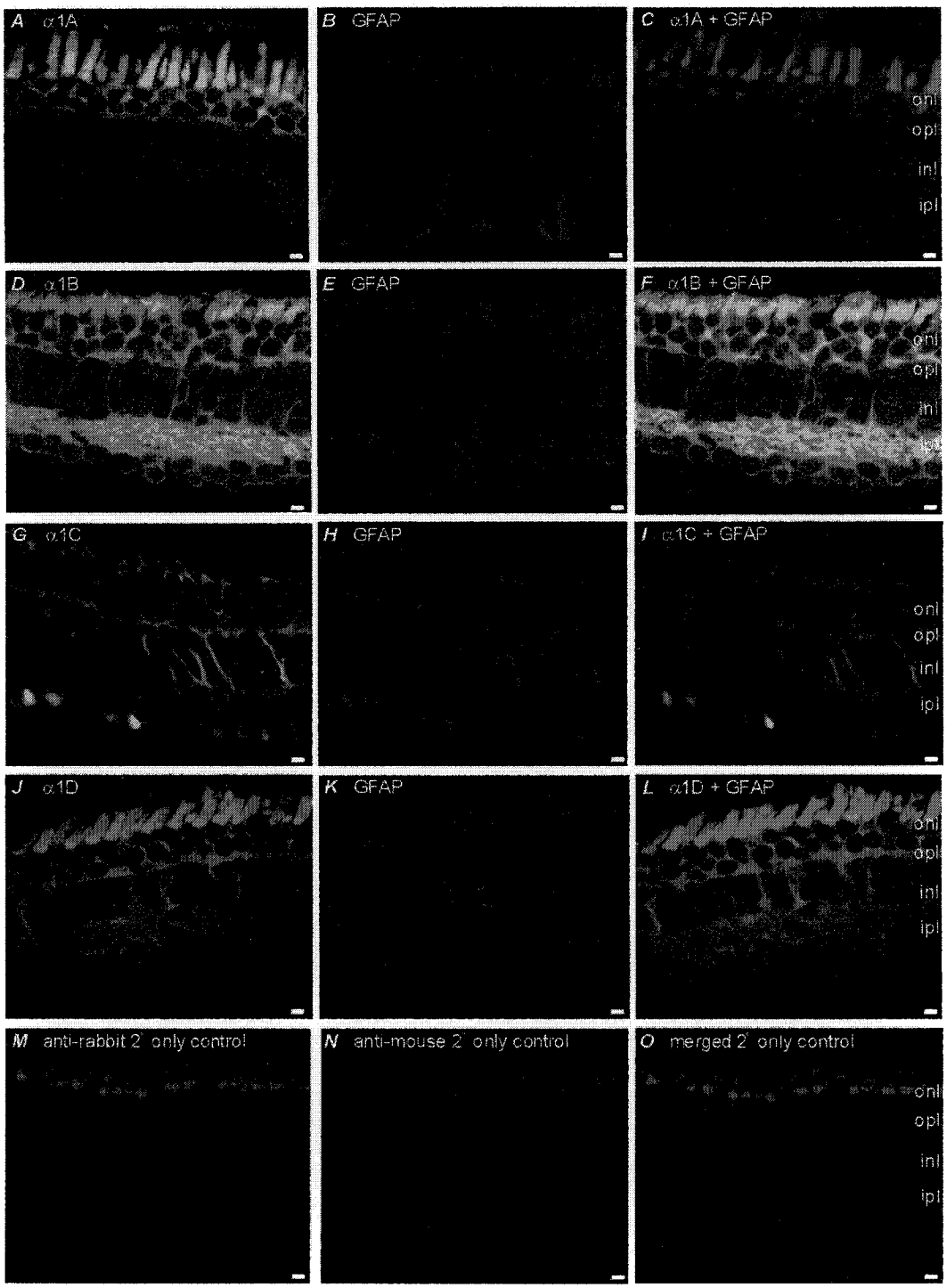
A α1A
B GFAP
C α1A + GFAP
onl
opl
inl
ipl
D α1B
E GFAP
F α1B + GFAP
onl
opl
inl
G α1C
H GFAP
I α1C + GFAP
onl
opl
inl
ipl
J α1D
K GFAP
L α1D + GFAP
onl
opl
inl
ipl
M anti-rabbit 2° only control
N anti-mouse 2° only control
O merged 2° only control
onl
opl
inl
ipl

Figure 3.9

characteristic Müller cell staining pattern (Fig. 3.9*G* & *J*) and colocalize with GFAP (Fig. 3.9*I* & *L*). The salamander photoreceptors are autofluorescent but retinal sections did not exhibit any non-specific staining when only the secondary antibodies were applied (Fig. 3.9*M, N &O*). Controls were also performed by preadsorbing each of the four Ca channel antibodies (anti-α1A, -α1B, -α1C, and -α1D) with its respective control peptide and then testing these in retinal sections. No distinct fluorescence labeling was detected (data not shown).

The immunoreactivity of acutely isolated Müller cells was also investigated and showed the same patterns of staining (Fig. 3.10). The Ca channel anti-α1A antibody only faintly stained the apical processes and somatic region of Müller cells (Fig. 3.10). In contrast, staining for each remaining Ca channel antibody (anti-α1B, -α1C, and -α1D) was found over the entire Müller cell (Fig. 3.10*C, E*, &G). There was no apparent immunoreactivity evident when each of the four primary antibodies was preadsorbed with its respective control peptide (CP) (Fig. 3.10*B, D, F, &H*). As well, when the primary antibodies were omitted from the protocol, there was an absence of any non-specific fluorescence which may have been due to the secondary antibody (Fig. 3.10*I*). Fig. 3.10*J* is a phase contrast photograph of the Müller cell from the secondary only control (Fig. 3.10*I*) and is representative of the size and shape of the other Müller cells used in the primary antibody + CP negative controls (Fig. 3.10*B, D, F*, &H).

3.8 Distribution of L-type Ca channels

L-type Ca channels were visualized in the membranes of isolated Müller

Figure 3.10. Immunoreactivity of isolated Müller cells detects regional expression of α1A Ca channel subunit and expression of α1B, α1C, and α1D Ca channel subunits over the entire cellular membrane.
A, An isolated Müller cells stained with anti-α1A Ca channel subunit antibody reveals immunopositive fluorescence (green) in the apical processes and somatic region of the Müller cell. *B*, LSCM image of a Müller cell treated with preadsorbed anti-α1A antibody + control peptide (CP). The lack of fluorescence in this negative control experiment confirms specificity of the anti-α1A Ca channel subunit antibody. *C*, Enzymatically isolated Müller cells were incubated with anti-α1B Ca channel antibody and expression of N-type Ca channels are displayed in green on the LSCM image. Fluorescence is noted in all areas of the Müller cell. *D*, There is an absence of fluorescence in this LSCM image of a Müller cell incubated with anti-α1B antibody preadsorbed with CP affirming the specificity of this antibody. *E*, LSCM image of a typical Müller cell stained with anti-α1C Ca channel antibody (green) over all regions of the cell. *F*, A Müller cell incubated with anti-α1C Ca channel antibody + CP typically displays a lack of fluorescence as evidenced in this LSCM image. *G*, LSCM image of an isolated Müller cell incubated with anti-α1D Ca channel antibody (green) indicates expression of this Ca channel subtype over all areas of the cell. *H*, LSCM image of an isolated Müller cell incubated with preadsorbed anti-α1D + CP exhibits a lack of fluorescence. *I*, A Müller cell processed without the addition of any primary antibodies is viewed with LSCM and exhibits no fluorescence confirming the specificity of the secondary anti-rabbit antibody (2°). *J*, A phase contrast photograph of the cell from *I* which is of a typical size and shape of the cells representing all of the negative controls, including 2° only and + CP.

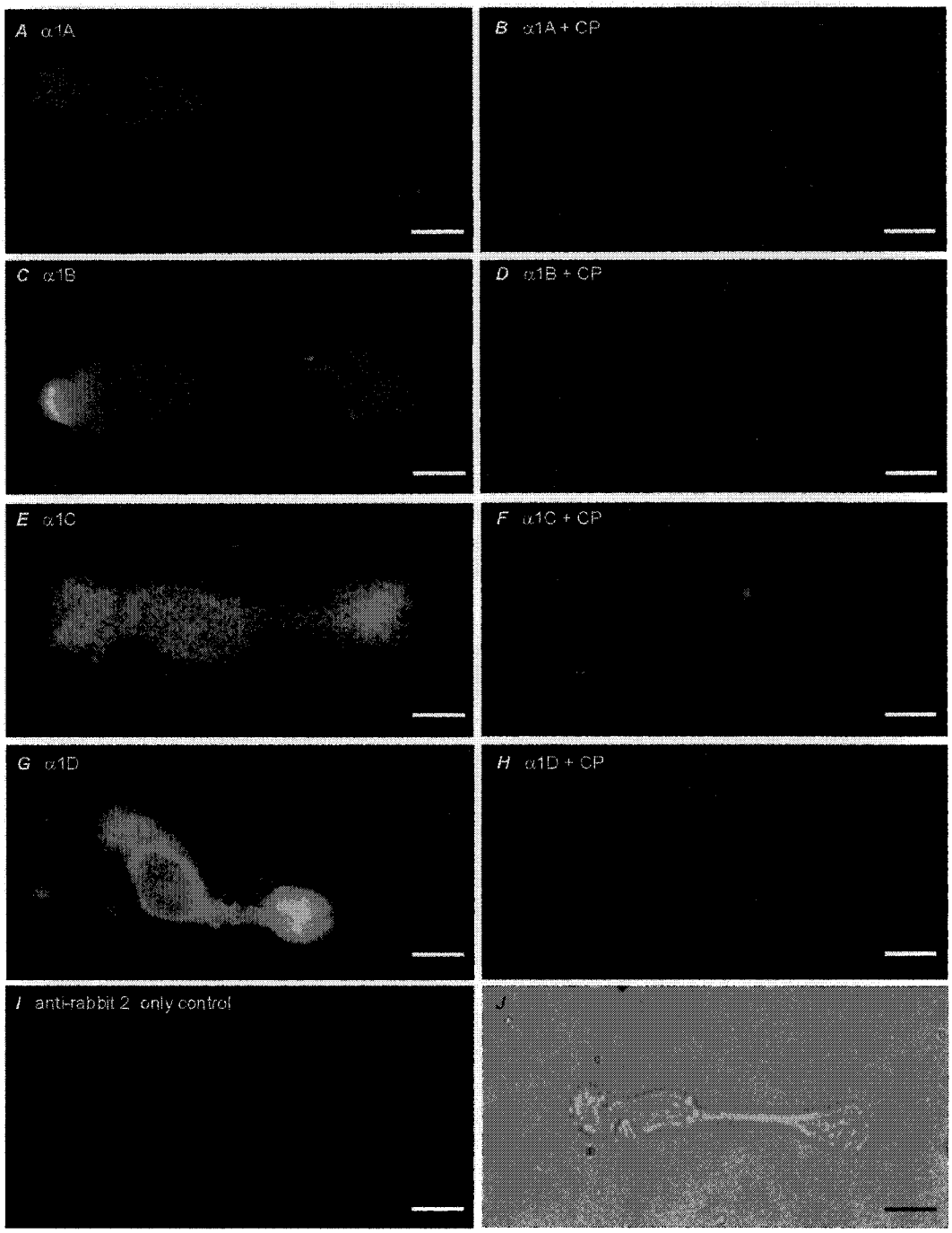
A α1A
B α1A + CP
C α1B
D α1B + CP
E α1C
F α1C + CP
G α1D
H α1D + CP
I anti-rabbit 2° only control
J

Figure 3.10

cells after incubation with a fluorescent-tagged DHP, DM-BODIPY. The styryl membrane dye, FM1-43 was used to normalize membrane density. Figure 3.11*A* shows a laser scanning confocal micrograph of a Müller cell labeled with DM-BODIPY (top), FM1-43 (middle) and a merged image of DM-BODIPY and FM1-43 (bottom). DM-BODIPY labeling was found over the entire surface of the Müller cell, although it was not uniform. To normalize areas of exceptional membrane density, the labeling intensity of DM-BODIPY was divided by that of FM1-43. The resulting ratio (Fig. 3.11*B*) represents the density of L-type Ca channels. To confirm that DM-BODIPY is indeed labeling a DHP-sensitive channel, control experiments were performed by pre-incubating Müller cells with 100 μM of nifedipine before application of DM-BODIPY and FM1-43 (Nachman-Clewner et al., 1999). DM-BODIPY fluorescence was strongly reduced in the cells pre-incubated with nifedipine indicating that the fluorescent-tagged DHP had been blocked from binding to the Ca channel by the DHP antagonist (Fig. 3.11*C*; student's t-test, $P<0.05$; n=5). Figure 3.11*C* also shows that a significant difference in the density of L-type Ca channels between the endfoot, somatic, and apical processes regions was found 0.11 ± 0.02 (0.002 ± 0.001; 100 μM nifedipine pre-incubation), 0.10 ± 0.02 (0.004 ± 0.006; 100 μM nifedipine pre-incubation), and 0.15 ± 0.03 (0.02 ± 0.02; 100 μM nifedipine pre-incubation), respectively (one-way ANOVA, $P<0.05$; n=8). The apical processes region of the Müller cell appeared to display a stronger labeling of DHP-sensitive Ca channels.

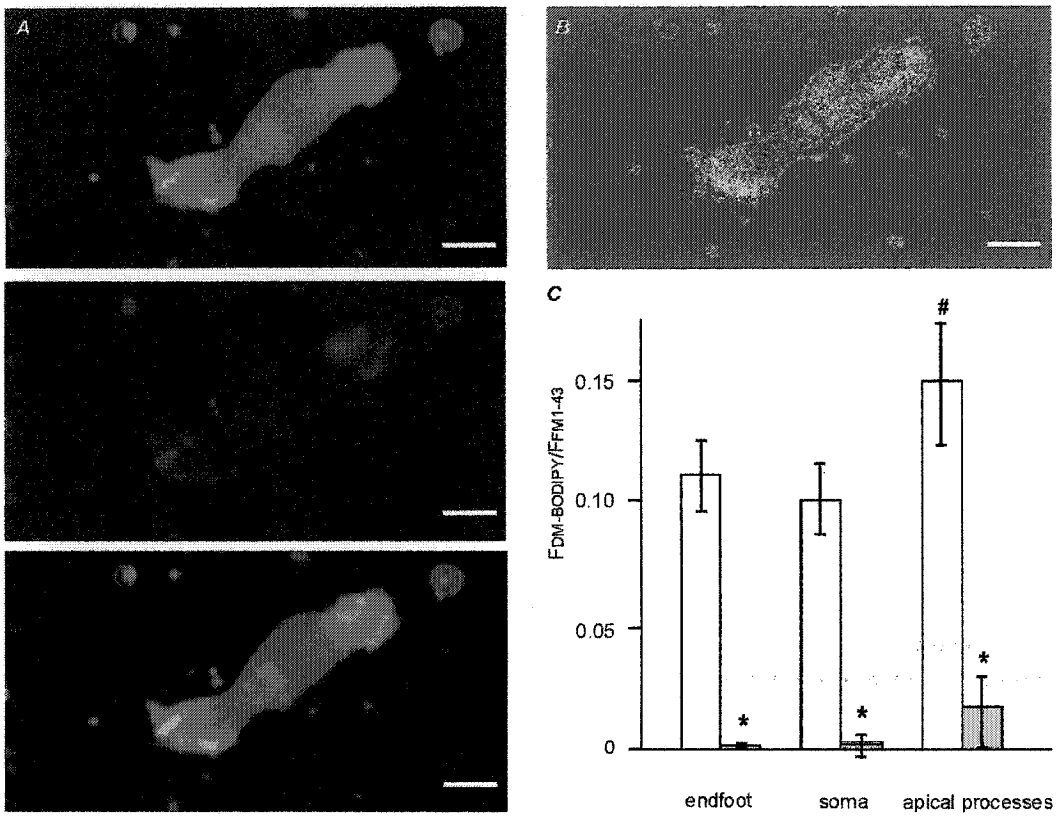

Figure 3.11. Normalized distribution of L-type Ca channels on the Müller cell membrane.

A, LSCM image of an isolated Müller cell incubated with DM-BODIPY (10 nM) (top), FM1-43 (2.5 μM) (middle), and both DM-BODIPY and FM1-43 (bottom) at room temperature. DM-BODIPY fluorescence is displayed in green and that for FM1-43 is shown with red so that colocalization of fluorescence shows as orange. *B,* Ratio of labeling intensity of DM-BODIPY/FM1-43 fluorescence for the cell shown in *A*. Areas with no difference ($F_{DM\text{-}BODIPY}/F_{FM1\text{-}43}$ value of 0) in fluorescence are displayed as dark blue while yellow and red indicate $F_{DM\text{-}BODIPY}/F_{FM1\text{-}43}$ values of approximately 0.26 and 0.05 (the higher $F_{DM\text{-}BODIPY}/F_{FM1\text{-}43}$ value, the stronger labeling for DM-BODIPY), respectively. Scale bars, 10 μm. *C,* Histogram of labeling intensity ratios ($F_{DM\text{-}BODIPY}/F_{FM1\text{-}43}$) sampled from distinct regions of several Müller cells including those cells pre-exposed to 100 μM nifedipine (shaded boxes) and those incubated only with the fluorescent probes (open boxes). Data were collected from the endfoot, soma and apical processes of the Müller cells.

4. Discussion

4.1 Ca channel properties

These results suggest that HVA Ca channels account for the Ca channel current in salamander Müller cells. LVA Ca channels in neurons activate at more negative potentials, exhibit faster inactivation and are distinguishable from typical HVA Ca channels which lack rapid inactivation. HVA Ca channel recordings can be isolated from LVA Ca channel currents by holding potential. However, in salamander Müller cells, even when holding at a potential of –90 mV, an LVA Ca channel current was not detected. This finding is in contrast to studies done on rabbit, human, and toad retinal glial cells reporting the presence of an LVA Ca channel current (Bringmann et al., 2000a,b,c). The density of LVA Ca channels in rabbit Müller cells was found to be highest at early postnatal days and decreased within the first three postnatal weeks (Bringmann et al., 2000a). In human Müller cells, the ratio between peak HVA and LVA Ca currents increased with the age of the donors (Bringmann et al., 2000b). While the study of Ca channel-mediated Na^+ currents in the toad did find a current attributable to an LVA Ca channel, these currents were not demonstrable under normal conditions with physiological concentrations of Ca^{2+} and Mg^{2+} present (Bringmann et al., 2000c). Since the Bringmann study (2000c) using toad Müller cells used Na^+ as a charge carrier by omitting divalent cations from the bath solution, a direct comparison with my Ba^{2+}-conducting Ca channel current kinetics is limited.

In our study with 10 mM Ba^{2+}, the voltage at which half maximum activation occurred was –6.9 ± 1.7 mV, similar to another report of an L-type Ca

channel ($Ca_V1.3$; α1D) current recorded in 15 mM Ba^{2+} with a $V_{½}$ of –4 ± 1 mV (Koschak et al., 2001) and a $Ca_V1.4$ α1F-type channel expressed with β2a subunits which has a $V_{½}$ of –10.7 ± 1.4 mV (Koschak et al., 2003). However, the slope factor was –3.4 ± 0.3 mV in salamander Müller cells and about –8 mV for the α1D and α1F channels. The kinetics of inactivation was also similar with inactivation midpoints of Ca channel currents of –26 ± 2 mV in salamander Müller cells vs. –28 ± 3 mV in rabbit cells (Bringmann et al., 2000a). However, in the case of inactivation, our estimation of the slope factor in salamander Müller cells was much smaller at about 7 mV compared to +14 ± 2 mV for the α1D (Koschak et al., 2001). Ca^{2+}-dependent inactivation was observed when Ca^{2+} was used as the charge carrier, typical of all HVA except for α1F, L-type Ca channel ($Ca_V1.4$; McRory et al., 2004). In the present study, the overlap of the activation and inactivation curves made possible a window current between –30 and +10 mV. The activation midpoints in the presence of the various blockers tested were compared, and statistical analysis showed no significant changes in the activation midpoint of the Ca channel current in any of the drugs tested (Table 3.2), suggesting that the channels involved have near identical kinetics. In other descriptions of N-type Ca channel biophysics, these Ca channels activate with midpoints of -13.8 ± 0.9 mV (n=13) or -9.1 ± 0.7 mV (n=10), depending on the isoform of the N-type Ca channel expressed (Lin et al., 1997) or -13.2 mV, in frog sympathetic neurons (Delcour et al., 1993); a trend towards more negative activation than what is observed from our results for Müller cell Ca channel currents.

The time constant of inactivation, τ, in salamander Müller cells was more rapid at negative voltages, τ = 170 ms (Ba^{2+}) and τ = 195 ms (Ca^{2+}), compared to a slower inactivation at voltages above 0 mV where τ = ~ 380 ms (in Ba^{2+} only). However, none of the time constants are consistent with accepted values for any of the HVA channel subtypes where L-type Ca channels inactivate very slowly with τ > 500 ms and other HVA channels (P/Q-, N-, and R-type) partially inactivate with τ = 50 – 80 ms (for review see Hille, 2001). Many T-type Ca channels inactivate at rates in a 20 – 50 ms time range.

4.2 Ca channel pharmacology

In this study, this thesis attempted to pharmacologically classify the HVA Ca channel subtype in salamander Müller cells. Although the currents responded with high sensitivity to the nonselective blocker, cadmium, the pharmacological profile of the salamander Müller cell Ca channel is not characteristic of any one of the traditionally classified HVA Ca channel subtypes. Ca channel current in salamander Müller cell was sensitive to both L-type Ca channel blockers (~50%) and CTX (~84%), and a combination of nifedipine and CTX blocked the current completely. The overlap of blockade indicates either both L- and N-subtypes co-exist or that one subtype is present and is sensitive to both drugs. The notion of an atypical Ca channel subtype in a lower vertebrate species such as the salamander is not unprecedented: Incomplete block by DHP antagonists and a CTX-sensitive component of the current characterize an L-type Ca channel in salamander cone photoreceptors (Wilkinson and Barnes, 1996). Furthermore, partial block of Ca channel current by CTX is a distinguishing feature of the

human L-type $Ca_v1.3$ (α1D; Williams et al., 1992, Koschak et al., 2001, Xu and Lipscombe, 2001, Bell et al., 2001). Williams et al. (1992) also reported a CTX-sensitive fraction of the current which, in contrast with our results, was reversible.

Notably distinct in the salamander Müller cell Ca channel pharmacology is the current's suppression by BayK. The studies on the $Ca_v1.3$ (α1D) Ca channel mentioned above all reported the typical L-type Ca channel current enhancement upon application of the DHP agonist BayK. Each of the other subclasses of L-type Ca channels including $Ca_v1.1$ (α1S) (Cognard et al., 1986), $Ca_v1.2$ (α1C) (Wilkens et al., 2001), and $Ca_v1.4$ (α1F) (Koschak et al., 2003) conduct currents that can be enhanced by BayK. Suppression of Ca channel currents in cardiac tissue have been reported with higher concentrations of BayK (1-5 μM) and with stimulation paradigms that either hold the cells at more positive membrane potentials (e.g. > -50 mV) or pulse to positive potentials more frequently (0.1 Hz) than the paradigms employed in this work. Inhibition of L-type Ca channel current by BayK in the presence of the diphenylalkalamine, fendiline, has also been described in guinea-pig cardiac myocytes and was attributed to changes in affinity of the DHP-receptor site for BayK (Schreibmayer et al., 1992). This effect of BayK could not be repeated in the presence of verapamil, diltiazem, or nifedipine nor was it observed when BayK alone was added.

BayK binding and its agonist actions were abolished in a mutant $Ca_v1.2$ (α1C) Ca channel indicating that Ser^{1115} from the pore-forming region between IIIS5 and IIIS6 was a vital DHP binding site (Yamaguchi et al., 2000). This thesis postulates that the Ca channel in salamander Müller cells is an atypical L-

type Ca channel with altered DHP-binding sites accounting for the unusual effect of BayK. Analysis of the molecular structure of the salamander Müller cell Ca channel subunits should aid in the pursuit of defining DHP binding constraints, revealing critical deviations in amino acid sequences. However, the data presented in this thesis do not preclude the possibility that a traditional N-type Ca channel subtype is present and exhibiting unusually high affinity for DHPs, as has been previously described (Mansvelder et al., 1996).

4.3 Ca channel distribution

Evidence for the possible expression of four types of HVA Ca channel subtypes in salamander Müller cells was found in this investigation, these being the CTX-sensitive, α1B, N-type Ca channel, two types of DHP-sensitive L-type Ca channels, α1C and α1D, and to a much lesser degree, the AgTX-sensitive, α1A, P/Q-type Ca channel. Although antibody staining suggested that both N- and L-type Ca channels are expressed over the entire salamander Müller cell, biophysical or pharmacological approaches were not able to clearly distinguish whether one or both these Ca channel subtypes are responsible for the unusual pharmacology of the Müller cell Ca channel current. Dense labeling of Müller cells with anti-α1C Ca channel antibody has also been observed in salamander retinal sections (Nachman-Clewner, et al., 1999). I found that DHP-sensitive Ca channels, including both α1C and α1D subtypes, are localized over the membrane of the salamander Müller cell, with a higher density at the apical processes region of the cell. While the role of Müller cell Ca channels is not yet clear, these channels could serve a number of Ca-dependent processes in the cell such as

propagation of Ca^{2+} waves and the activation of Ca^{2+}-dependent K^+ currents (Newman, 2001; Newman, 1985b). For example, in hippocampal neurons, Ca^{2+}-dependent K channels are selectively activated by co-localized Ca channels (Marrion and Tavalin, 1998). Salamander Müller cells express a large conductance Ca^{2+} -dependent K channel (Newman, 1985b) which has been implicated in regulation of DNA synthesis in (Kodal et al., 2000) and proliferation of Müller cells (Puro and Mano, 1991). Our observation that Ca channels are found over the entire cell membrane is consistent with widespread roles for Ca channels in Müller cells.

However, the role of Ca channels in Müller cells remains enigmatic as most consider that the membrane potential of Müller cells is strongly hyperpolarized under normal conditions due to the high membrane K^+ conductance. It remains possible that fine, electrically isolated processes of the Müller cell, especially those in the outer retina, may become depolarized to membrane potentials at which Ca channels could activate, and it may be in these cell compartments that signaling via changes in $[Ca^{2+}]_i$, brought about by Ca channel activity, may be important.

Chapter 4

Large conductance calcium-activated potassium channels in freshly isolated tiger salamander Müller cells

This work has been previously published by Welch NC, Barnes S, and MEM Kelly (2002) Calcium and Calcium-Activated Potassium Currents in Müller Cells Isolated From Tiger Salamander Retina. Invest. Ophthalmol. Vis. Sci. 43: E-Abstract 4757.

ABSTRACT

The resting membrane potential of Müller cells is set by K^+ conductance through K channels. While K_{IR} channels dominate the Müller cell K^+ conductance other K channels are also expressed, such as large conductance Ca^{2+}-activated K channels. Whole-cell patch-clamp recordings have been used to characterize K_{Ca} channels in salamander Müller cells. A23187, a Ca^{2+} ionophore, enhanced the outward current at +60 mV by 130%, which was blocked by the application of the large conductance K_{Ca} channel blocker, iberiotoxin (ibTX). The K_{Ca} channel current was isolated by substituting Na^+ in the external Ringers with choline, along with the addition of 100 μM Ba^{2+}. Isolated K_{Ca} channel current was partially sensitive to TEA. A23187 enhanced the isolated K_{Ca} channel current by 138%, and the A23187-enhanced current was blocked by TEA. Cd^{2+} had a small effect on both inward and outward currents blocking ~ 25 – 30 % of the current, respectively. Dialysis of IP_3 into the Müller cell interior enhanced the outward current by 228%, and the IP_3-enhanced current was subsequently blocked by the application of ibTX. These observations suggest that a large conductance K_{Ca} channel is present in salamander Müller cells, and that the activation of this K channel is not solely dependent on Ca^{2+} influx through voltage-gated Ca channels, but may require release of Ca^{2+} from intracellular stores.

1. Introduction

The broad diversity of K channel subtypes underscores the many cellular functions in which these ion channels participate. In excitable cells, activation of K channels generally lowers the effectiveness of excitatory inputs, since these channels tend to push the membrane potential closer to E_K and away from the firing threshold. In all cell types, K channels help set the resting potential, repolarize the cell after a depolarization event, and hyperpolarize the cell. The range and proportions of K channels expressed in an individual cell depends upon cellular function. The super-family of K channels, including K_V, K_{IR}, and K_{Ca} subgroups, is molecularly diverse. However, all K channels are tetrameric structures with four α subunits arranged symmetrically around a central pore (Doyle et al., 1998). Each of the α subunits of K_V and K_{Ca} channel subgroups contain six transmembrane segments (Figure 4.1*A*). This is structurally different from the K_{IR} channel subgroup, which has two transmembrane regions in each α subunit (Figure 4.1*B*). Auxiliary subunits may also be associated with K channels and seem to be involved in regulation of expression levels and functional properties but do not contribute to ion selectivity (reviewed by Coetzee et al., 1999). A schematic representation of K channel classification is presented in Table 4.1.

K_V channels can be described as slow or fast delayed rectifier K channels. Slow K_{DR} channels (or simply K_{DR} channels), the subfamily KCNQ, are tonically open but may be closed indirectly by neurotransmitters such as acetylcholine. Fast K_{DR} channels are transient, rapidly activating and inactivating, and

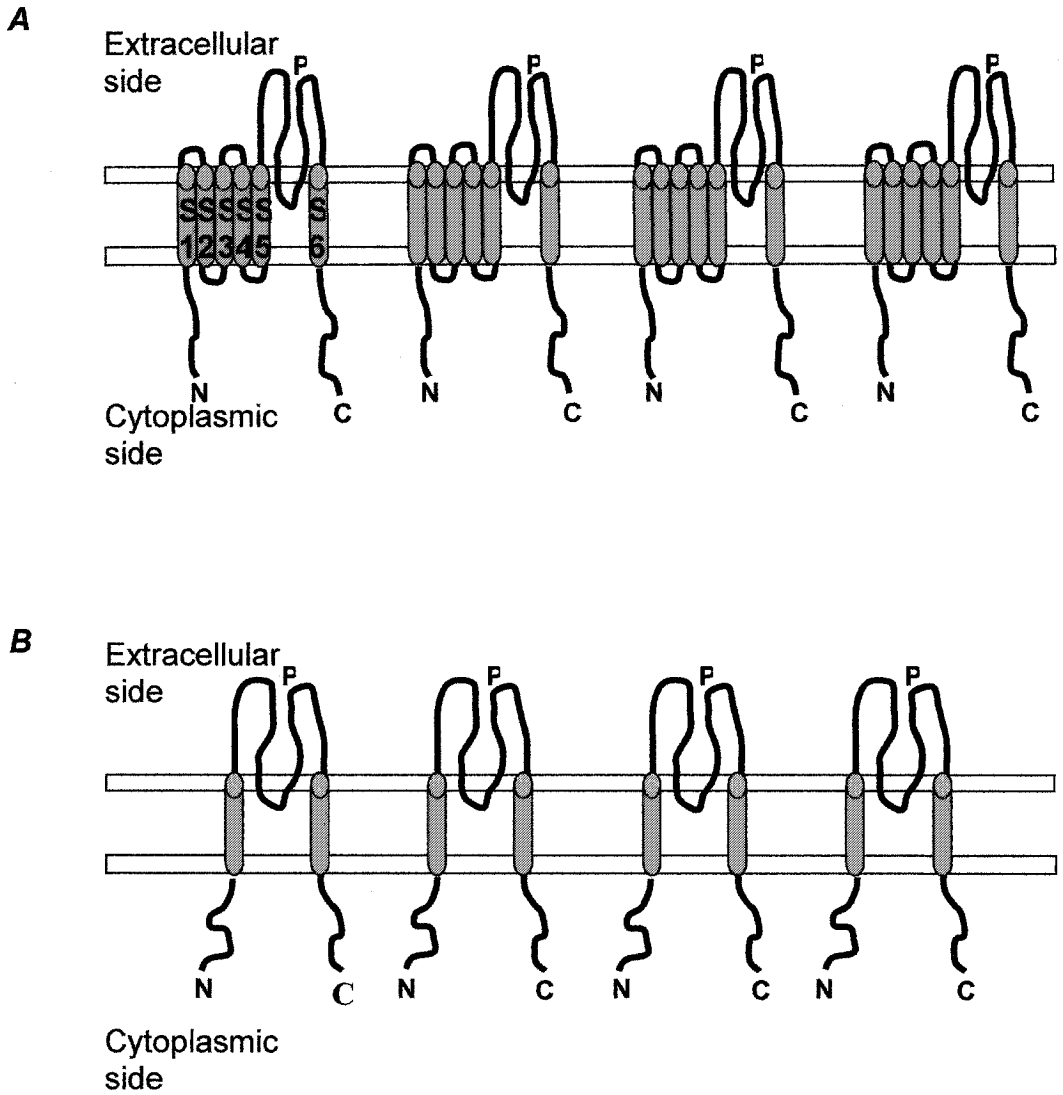

Figure 4.1. Structure of the pore-forming region of K channels
A, The pore-forming region of vertebrate K channel structures is comprised of 4 α subunits. The composition of the individual α subunit varies depending on the subtype of K channel. Each of the α subunits of voltage-gated K_V channels (including K_{DR} and K_A channels) and K_{Ca} channels consist of 6 transmembrane domains or segments (S1-S6). *B*, The pore-forming region of the inward rectifier K channels is composed of 2 transmembrane domain α subunits. The extracellular loop (P) forms the selectivity filter of the K channel (Doyle et al., 1998). The N-terminal (N) and C-terminal (C) regions of K channels are located on the cytoplasmic side.

contribute to repetitive firing. Traditional classification of fast K_{DR} channels uses the terms A-type or K_A channels, but recent nomenclature describes $K_{Vm.n}$, where *m* and *n* are integers denoting subfamilies and order of discovery. K channels with characteristics of both K_{DR} and K_A channels are expressed by Müller cells (Newman, 1985b; Chao et al., 1994) however, the functional relevance of these channel types on glial membranes is unknown.

K_{IR} channels in Müller cells are involved in the regulation of retinal K^+ homeostasis. Inward rectification describes the tendency of K_{IR} channels to act as a valve with K^+ influx favored at membrane potentials negative to E_K (Hille, 2001). K_{IR} channel gating is dependent upon membrane potential and extracellular $[K^+]$. Rapid local elevations in extracellular $[K^+]$, such as those occurring in the synaptic layers of the retina, shifts E_K to more depolarized potentials. The membrane potential of the entire Müller cell is unchanged since most regions of the membrane are not exposed to high $[K^+]_o$. Therefore, in local regions, E_K is positive to the resting membrane potential of the Müller cell, and K_{IR} channels open. Extracellular K^+ ions flow through open K_{IR} channels, located in the membrane of the Müller cell near the plexiform layers, into the glial cell interior. In other regions of the Müller cell, where $[K^+]_o$ is not elevated by neuronal activity, the resting membrane potential is positive to E_K. K^+ efflux through K_{IR} channels can then result. There is a large transmembrane K^+ concentration gradient across the Müller cell endfoot region and the vitreous humour which drives the efflux of K^+ through K_{IR} channels as part of the proposed role of K_{IR} channels in retinal K^+ siphoning (Newman, 1993).

Table 4.1. Summary of K channels classification

# TMS	Subfamily	Phenotype	
6 Nonselective	NCN1	Hyperpolarization-activated	cation
6 channels	CNG1	Cyclic nucleotide-gated	
6	mslo	Large conductance Ca^{2+}-activated	K_{Ca} channels
6	SK1	Small and intermediate Ca^{2+}-activated	
6	$K_V1.1$	Voltage-gated Shakers	Fast K_{DR} (aka K_A) channels
6	$K_V3.1$	Voltage-gated Shaws	
6	$K_V4.1$	Voltage-gated Shals	
6	$K_V2.1$	Voltage-gated Shabs	
6	$K_V5.1$	Voltage-gated outlier	
6	$K_V6.1$		
6	$K_V8.1$	Modifiers/silencers	
6	$K_V9.1$		
6	KCNQ1	Voltage-gated KCNQs	Slow K_{DR} channels
2	$K_{IR}4.1$	Inward rectifiers	Classical K_{IR} channels
2	$K_{IR}7.1$		
2	$K_{IR}1.1$		
2	$K_{IR}2.1$		
2	$K_{IR}5.1$		ATP-sensitive
2	$K_{IR}6.1$		
2	$K_{IR}8.1$		G- protein -coupled K_{IR} channels

K channel subfamilies are grouped together according to the number of transmembrane segments (TMS) and biophysical similarities. Only one representative member of each subfamily is presented for simplicity.

Another class of K channels has been described in Müller cells which are activated by $Ca^{2+}$and are not transient in nature (Newman, 1985b). The K_{Ca} channels have been divided into three subfamilies, which can be distinguished biophysically and pharmacologically. Small conductance K_{Ca} channels are voltage-insensitive with a single channel conductance of 2-20 pS while intermediate conductance K_{Ca} channels have slightly larger single channel conductances, 20-100 pS, and are also voltage-insensitive (reviewed by Stocker, 2004). Large conductance K_{Ca} channels, 200-400 pS single channel conductance, require both Ca^{2+} and membrane depolarization for activation (reviewed by Faber and Sah, 2003) and are selectively blocked by iberiotoxin (ibTX) (Candia et al., 1992). The primary structure of the voltage-insensitive K_{Ca} channels does not contain any Ca^{2+}-binding domains, but rather a Ca^{2+}-dependent calmodulin (CaM) domain (Shumacher et al., 2001). The crystal structure of the voltage-sensitive, large-conductance K_{Ca} channels is not yet known, however, these channels are believed to contain a linker-gating ring complex (Niu et al., 2004). The channel's gating mechanism is connected to a ring of intracellular regulator domains via a spring-like linker. The ring of intracellular regulator domains contains both a voltage-sensor and Ca^{2+}-binding site(s), each of which might compress the linker and apply a force to the gating mechanism, thus, opening the channel.

In excitable cells, all K_{Ca} channels play a role in after-hyperpolarization, but, in glia, the function of these channels remains unclear. There are few reports of any K_{Ca} channels expressed in glial cells, although large-conductance K_{Ca} channels have been reported in Schwann cells of rat sciatic nerve (Mi et al.,

1999), cultured mouse astrocytes (Nowak et al., 1987), and in retinal Müller cells (Newman, 1985b). While the function of large conductance K_{Ca} channels in glial cells is still unknown, K_{Ca} channels have been implicated in the regulation of Müller cell proliferative activity (Puro at al., 1989). Large conductance K_{Ca} channels in Müller cells are highly regulated by a wide variety of cellular mechanisms. Large conductance K_{Ca} channel activation is enhanced by PKA and down-regulated by PKC in rabbit Müller cells (Schopf et al., 1999). Glutamate, the major neurotransmitter in the retina, was found to increase the amplitude of large conductance K_{Ca} channels in mammalian Müller cells (Bringmann and Reichenbach, 1997). For example, Müller cells express metabotropic glutamate receptors that are linked to a G-protein cascade which stimulates the release of Ca^{2+} from intracellular stores (Schwartz, 1993; Keirstead and Miller, 1997). Increases in intracellular Ca^{2+} may contribute to activation of K_{Ca} channels. Other sources of elevated $[Ca^{2+}]_i$ might include Ca^{2+} influx through voltage-gated Ca channels. In salamander Müller cells, K_{Ca} channel current was blocked by application of Cd^{2+}, a non-specific blocker of Ca channels (Newman, 1985b). Although it has yet to be demonstrated in glial cells, K_{Ca} in hippocampal neurons were found to be selectively activated by co-localized Ca channels (Marrion and Tavalin, 1998).

The objectives of this study were to confirm the presence of a large conductance K_{Ca} channel in freshly isolated salamander Müller cells and to pharmacologically characterize this ion channel. The K^+ conductance in Müller cells is vital for proper retinal functioning but the significance of K_{Ca} channels

remains unknown. Investigating the properties of K_{Ca} channels in Müller cells may provide functional insight into how these channels contribute to Müller cell and retinal physiology.

2. Materials and methods

2.1 Cell isolation

Müller cells were isolated from the retinas of tiger salamanders (*Ambystoma tigrinum*; larval stage) as previously described (see Chapter 2, General Methods; section 1). Briefly, animals were sacrificed by decapitation, eyes removed and retinas dissected. Retinas were treated with an enzyme solution, and isolated cells were aliquoted onto plastic dishes for patch-clamp recording. Müller cells were visualized using a Nikon Diaphot microscope and were identifiable by their distinct morphology.

2.2 Patch clamp recording

Müller cell K channel currents were recorded with the cell-attached-patch and the whole-cell patch-clamp recording technique, as previously described (see Chapter 2, General Methods; section 2.2). Briefly, cell-attached-patch currents were continuously recorded at a given voltage for 1500 ms. Whole-cell patch-clamp recordings were obtained by holding the isolated Müller cell at –70 mv and stepping for 100 ms in 20 mV increments from –120 to +60 mV. Electrodes were filled with a solution designed to isolate K channel currents, containing (in mM): 90 KCl, 1 $MgCl_2$, 0.4 $CaCl_2$, 1 EGTA, 5 HEPES, 1 ATP, 0.1 GTP at pH 7.2 (solution J, Table 2.1 in Chapter 2, General Methods). For single channel recordings, the extracellular bathing solution was composed of (in mM): 102 KCl, 3 $CaCl_2$, 10 HEPES, 8 glucose at pH 7.6 (solution C, Table 2.1 in Chapter 2, General Methods). Whole-cell recordings were made in an extracellular solution composed of (in mM): 100 NaCl or 100 choline chloride, 2.5 KCl, 3 $CaCl_2$, 10

HEPES, 8 glucose at pH 7.6 (solution D, Table 2.1 in Chapter 2, General Methods). Drugs were added to the extracellular solution and superfused during electrophysiological recording. A23187, a Ca^{2+} ionophore, was prepared as 10 mM stock solutions in DMSO and diluted in the extracellular solution. Control electrophysiological recordings were made in the presence of an equal concentration of DMSO in the external bathing solution. All recordings were performed at room temperature (21 – 25 °C).

2.3 Drugs and chemicals

Chemicals used in electrophysiological recordings were obtained from Sigma Chemical Co. (St. Louis, MO) including: A23187, barium chloride (Ba^{2+}), cadmium chloride (Cd^{2+}), choline chloride (Choline), iberiotoxin (ibTX), inositol triphosphate (IP_3), and tetraethylammonium chloride (TEA).

2.4 Quantitative and statistical analyses

I-V relations were measured during the final 20 ms of the depolarizing pulse. Amplitude histograms were constructed by normalizing the peak current values of control currents to 100%. Current remaining after application of drug is expressed as a percentage of control as mean ± standard error (s.e.m.). All comparisons were carried out using Student's t test with significance defined as $P<0.05$. Statistical analyses of drug block were performed on raw currents with a paired t test while comparison between two drug treatments were analyzed with an unpaired t test, as indicated in the text.

3. Results

3.1 Properties of a large conductance K_{Ca} channels in isolated Müller cells

A large conductance channel was found to be present in cell-attached patch recordings made from a salamander Müller cell. Figure 4.2 shows representative single channel currents. At negative potentials ($-V_p$), there were very few channel openings, and these were of a short duration. With increasing depolarization, the number and duration of channel openings increased (Figure 4.2*A*). The reversal potential of the large conductance K channel was –3.8 mV with 102 mM K^+ in the extracellular bath solution and 90 mM K^+ in the intracellular pipette solution and was close to the predicted equilibrium potential of –3.3 mV, as calculated by the Nernst equation. The channel from this representative experiment had a slope conductance of 185 pS (Figure 4.2*B*), which is consistent with previous descriptions of large conductance K_{Ca} channels recorded in mammalian Müller cells (Bringmann et al., 1997; Schopf et al., 1999).

Whole-cell patch-clamp recordings in isolated Müller cells were carried out to further characterize the salamander Müller cell large conductance K channel. Ca^{2+}-dependence was confirmed by the application of the Ca^{2+} ionophore, A23187. Whole-cell currents were generated from a holding potential of –70 mV with voltage steps from –120 mV to +80 mV in 20 mV increments. Elevation of intracellular Ca^{2+} levels with A23187 increased the amplitude of the outward current by 30 ± 6% at +60 mV (n=6) (Figure 4.3). Extracellular application of 50 nM iberiotoxin (ibTX), a potent blocker of large conductance K_{Ca} channels (Candia et al., 1992), significantly decreased the Ca^{2+}-enhanced

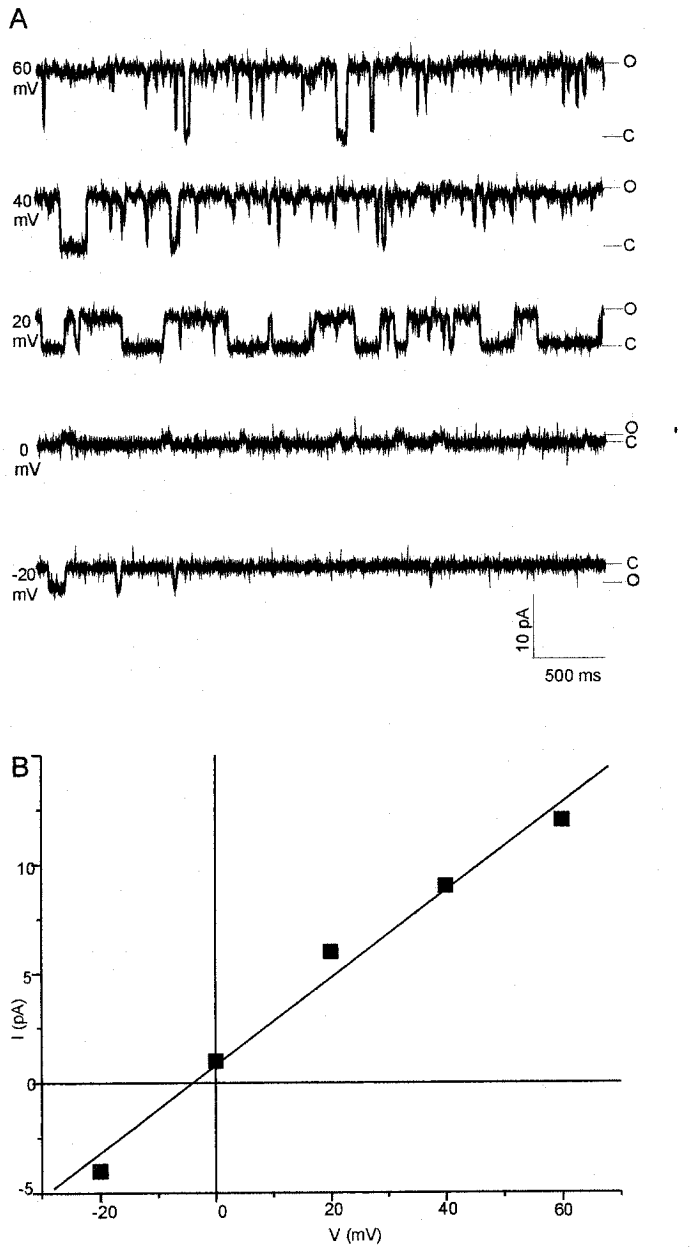

Figure 4.2. Large-conductance K channel in Müller cells
A, Cell-attached patch recording of a single K^+ channel in symmetrical K solutions. Single channel recordings were made at –20, 0, +20, +40, and +60 mV where $V = -V_{pipette}$. Unitary currents reversed at –3.8 mV and were outwardly rectifying. *B*, Current-voltage relation for unitary currents from *A*. Channel slope conductance was 185 pS, consistent with presence of BK channels in Müller cells.

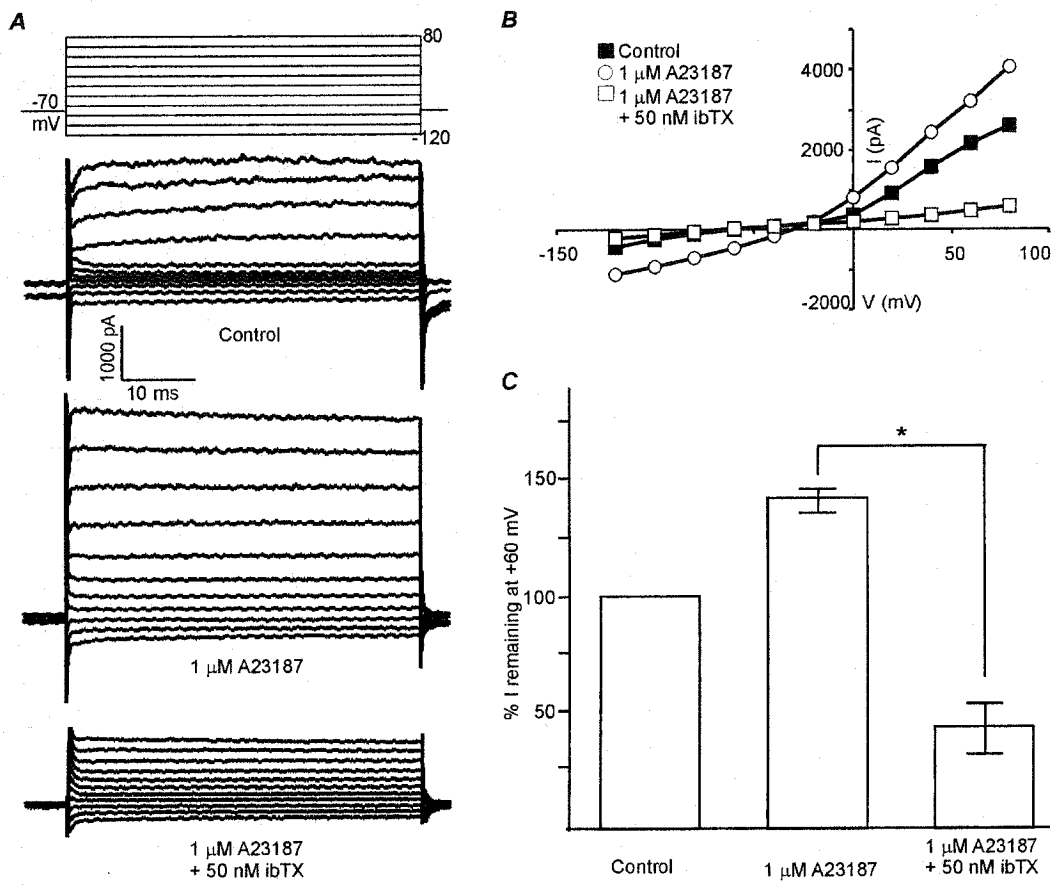

Figure 4.3. Activation of K_{Ca} channel current by the Ca^{2+} ionophore, A23187, in isolated Müller cells

A, Representative whole-cell current traces recorded in a Müller cell in 2.5 mM K^+-containing external Ringers and with 90 mM K^+ in the pipette. Current was elicited by voltage steps from –120 to +80 mV, in 20 mV increments, from a holding potential of –70 mV before (Control) and after application of the Ca^{2+} ionophore 1 μM A23187. *B*, I-V relation for currents shown in *A* in the absence (closed squares) and presence of A23187 (open circles). *C*, Control currents were normalized to 100% and expressed as percent current remaining following the application of A23187 alone or A23187 and iberiotoxin. Values are mean ± sem measured at +60 mV.

current with 41 ± 10% of the A23187-enhanced current remaining at +60 mV (paired Student's t test; $P<0.05$; n=3) (Figure 4.3).

3.2 Isolating the K_{Ca} channel current

The currents presented in Figure 4.3*A* are a compilation of all conductances in the Müller cell including K_{IR}, K_{DR}, and K_A. By taking advantage of the differential K channel sensitivity to particular K channel blockers, such as Ba^{2+}, the contribution of K_{Ca} channels was investigated (Bringmann and Reichenbach, 1997). As well, Müller cells express an electrogenic Na^+-dependent co-transporter that may also be contributing to the whole-cell current. Therefore, choline was substituted for Na^+ in the extracellular solution. Ba^{2+}, 100 μM, was added to the choline-based extracellular solution to inhibit K_{IR} channels (Newman, 1993). Perfusion of choline Ringers with Ba^{2+} blocked the inward K^+ current with 15 ± 4 % (n=10) of the current remaining at –120 mV and a significantly smaller decrease in outward current (47 ± 3% of the current remaining at +60 mV) (paired t test, $P<0.05$; n=13). Figure 4.4*A* shows a representative Müller cell exposed first to the Na^+-based Ringer (Na^+, right panel) and then in the choline + Ba^{2+}-based Ringer (Choline + Ba^{2+}, left panel). Cells were held at –70 mV and stepped in 20 mV increments from –120 mV to +80 mV. The I-V relation of the cell shown in Figure 4.4*A* demonstrates Müller cell whole-cell currents in a Na^+-based solution and has the typical I-V relation of a K_{IR} channel in Müller cells (Figure 4.4*B*; closed squares). In the presence of choline and Ba^{2+} (open circles), the I-V relation indicates a complete block of the

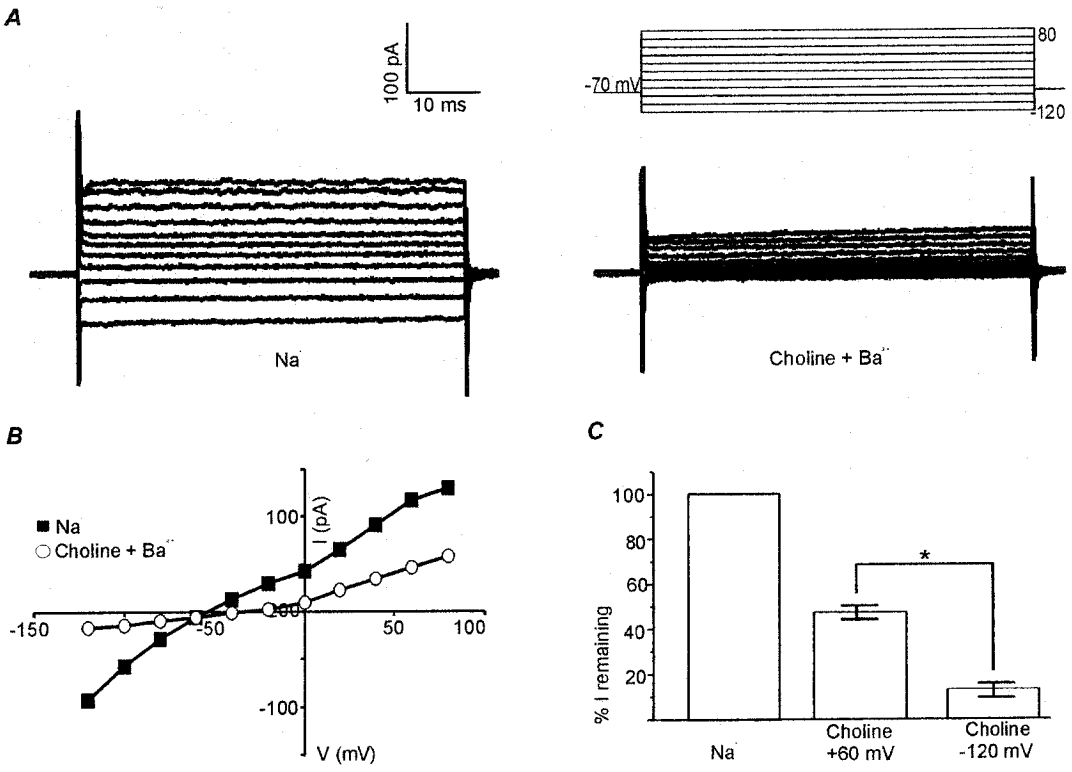

Figure 4.4. Isolation of outward K^+ current in choline + Ba^{2+} Ringers in isolated Müller cells

A, Representative Müller cell currents measured in the same cell under control conditions in Na^+-based Ringers (Na^+) with 2.5 mM K^+ extracellularly and 90 mM K^+ solution in the pipette (upper left), after the substitution of choline for Na^+ and exposure to 100 μM Ba^{2+}(Choline + Ba^{2+}) (upper right). Currents were elicited from a holding potential of –70 mV and stepped from –120 to +80 mV in 20 mV increments. *B*, The I-V relation for the cell shown in *A* is displayed with control conditions (Na^+, closed squares) and choline + Ba^{2+} (open circles). *C*, Data from several cells was compiled in a histogram with control conditions (Na^+) normalized to 100 and choline + Ba^{2+} expressed as the percentage (mean ± sem) of current remaining after treatment at +60 mV and –120 mV.

inward current with only a portion, ~ 47%, of the outward current remaining in the modified Ringers (Figure 4.4*B*).

In the presence of 100 μM external Ba^{2+} in a choline-based Ringer, 1 mM TEA, a non-selective K channel blocker, reduced the outward current with 61 ± 4% of the current at +60 mV remaining (n=6) (Figure 4.5). However, statistical analysis of the currents before and during the application of TEA did not reveal a significant current inhibition (paired t test; $P<0.05$). The current response of a representative Müller cell is shown in Figure 4.5*A* in choline + Ba^{2+} extracellular solution before (Control, left panel), and after the addition of 1 mM TEA (right panel). The I-V relations for the cell shown in Figure 4.5*A* are presented in Figure 4.5*B* before (Control, closed squares), after the application of 1 mM TEA (open circles), together with the difference between control and drug block (TEA-sensitive, gray triangles). The TEA-sensitive I-V relation displays the typical N-shape of a K_{Ca} channel current (Hille, 2001).

The choline + Ba^{2+} extracellular solution inhibited the inward current and ~ 53% of the outward current suggesting that the K_{IR} channels were blocked. To confirm that the large conductance K_{Ca} channel continued to be active under these conditions, the Ca^{2+} ionophore, A23187, which had previously (Figure 4.3) induced an enhancement in the current in Na^{+}-based Ringers, was applied. In the extracellular solution of choline + Ba^{2+} (Figure 4.6*A*; Control, top panel), application of 1 μM A23187 increased the amplitude of the outward current (Figure 4.6*A*, middle panel) by 138 ± 25% (n=3). Treatment of the A23187-enhanced current with 1 mM TEA reduced the outward current back to the

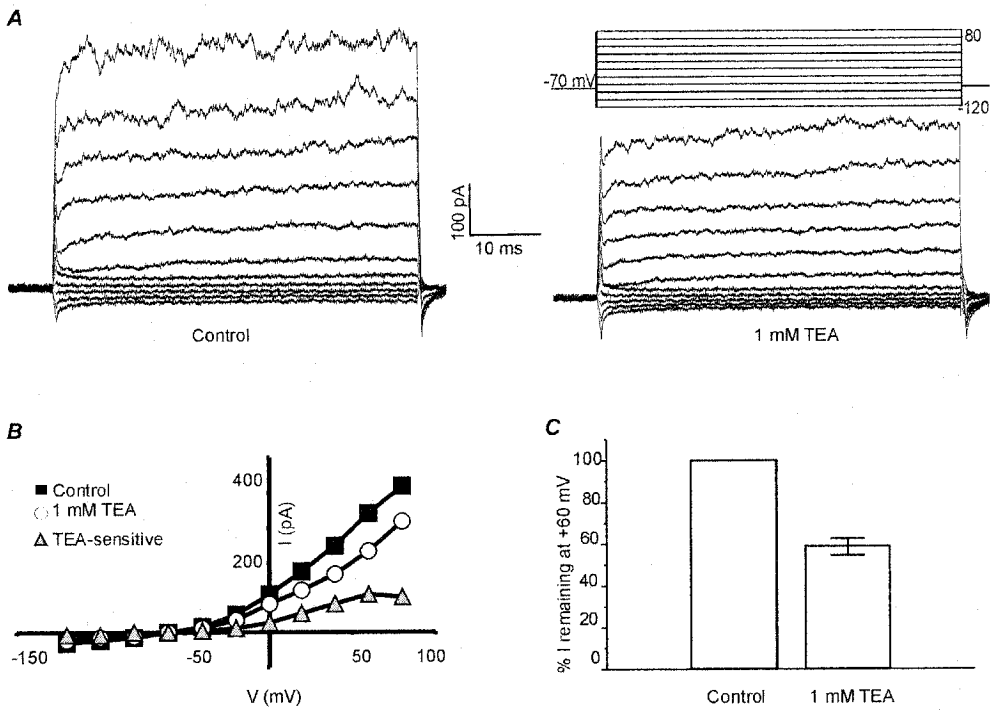

Figure 4.5. Tetraethylammonium-sensitive K^+ current in isolated Müller cells *A*, Whole-cell current traces recorded from a representative salamander Müller cell in 2.5 mM K^+- and 100 μM Ba^{2+}-containing external Ringers and 90 mM K^+-containing internal pipette solution. Current was elicited by voltage steps between –120 and +80 mV, in 20 mV increments, from a holding potential of -70 mV. Outward current was reduced in the presence of 1 mM TEA (upper right). *B*, Current-voltage relations from the cell in *A* in the absence (closed squares) and presence (open circles) of 1 mM TEA. The TEA-sensitive current (gray triangles) was obtained by subtracting current records in the presence of TEA from control currents. *C*, Control current was normalized to 100% and current remaining after application of 1 mM TEA was expressed as mean ± sem remaining current measured at +60 mV.

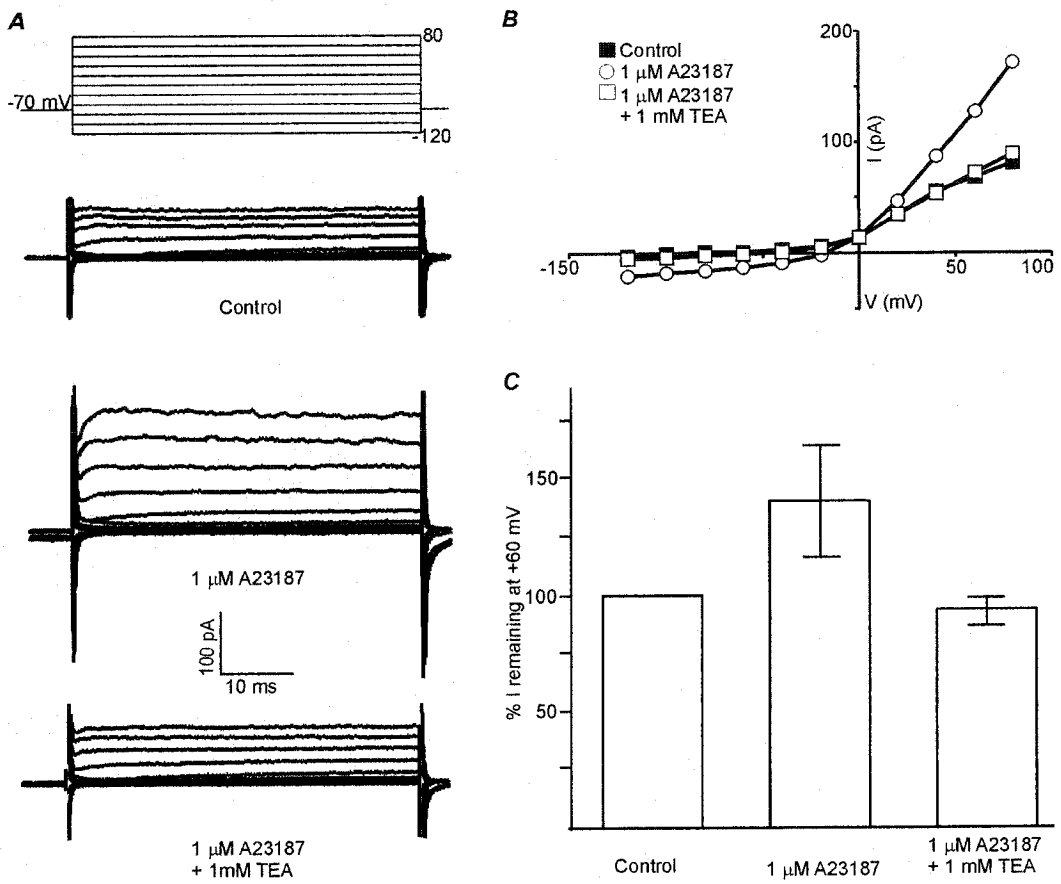

Figure 4.6. Block of the A23187-enhanced K channel current by TEA in isolated Müller cells

A, Whole-cell current traces recorded from a representative salamander Müller cell in 2.5 mM K^+- and 100 μM Ba^{2+}-containing choline-based external Ringers and 90 mM K^+-containing internal pipette solution elicited during steps to voltages between –120 mV and + 80 mV, in 20 mV increments, from a holding potential of –70 mV. Enhancement of the K channel current by the Ca^{2+} ionophore, A23187, (middle left) was blocked by TEA (bottom left). *B*, I-V relation for the currents shown in *A* before (Control, closed squares), during application of A23187 alone (open circles) and during co-application of A23187 and TEA (open squares). *C*, Control currents were normalized to 100% and expressed as percentage of current remaining following the application of A23187 alone or A23187 and TEA. Values are mean ± sem current measured at +60 mV.

baseline level with 102 ± 5% (n=3) of the current remaining at +60 mV compared to the control.

3.3 Ca^{2+} source for K_{Ca} channel activation

Figures 4.3 and 4.6 provided evidence that elevated $[Ca^{2+}]_i$ could enhance K_{Ca} channel current amplitude. Next, the potential source of Ca^{2+} in Müller cells was investigated. Influx of Ca^{2+} through voltage-gated Ca channels can activate K_{Ca} (Marrion and Tavalin, 1998). Cd^{2+} is a non-selective, potent blocker of Müller cell Ca channels (Welch et al., 2005). In 3 of the 4 cells tested, application of 100 μM Cd^{2+} blocked ~ 23% of the outward currents with 77 ± 4% of the current remaining at +60 mV (Figure 4.7). In the same 3 cells, there was also a small reduction in the inward current in the presence of 100 μM Cd^{2+} at – 120 mV with 71 ± 10% of the current remaining. Statistical analyses of the currents revealed that the effect of Cd^{2+} was not significant (paired t test; $P<0.05$). The fourth cell did not respond to the application of Cd^{2+} (data not shown). The current records of a representative Müller cell which responded to application of Cd^{2+} are shown in Figure 4.7*A* (Control, solid line; 100 μM Cd^{2+}, dotted line). The corresponding I-V relations for the cell displayed in Figure 4.7*A* are shown in Figure 4.7*B* before the application of Cd (Control, closed squares) and during the application of Cd (open circles). Also presented in Figure 4.7*B* is the I-V relation of the Cd-sensitive component (gray triangles), which was calculated by subtracting the I-V relation in Cd from the control I-V relation. Compiled data from the 3 cells which responded to 100 μM Cd^{2+} is presented in Figure 4.7*C* with control current normalized to 100%. The current remaining in the presence

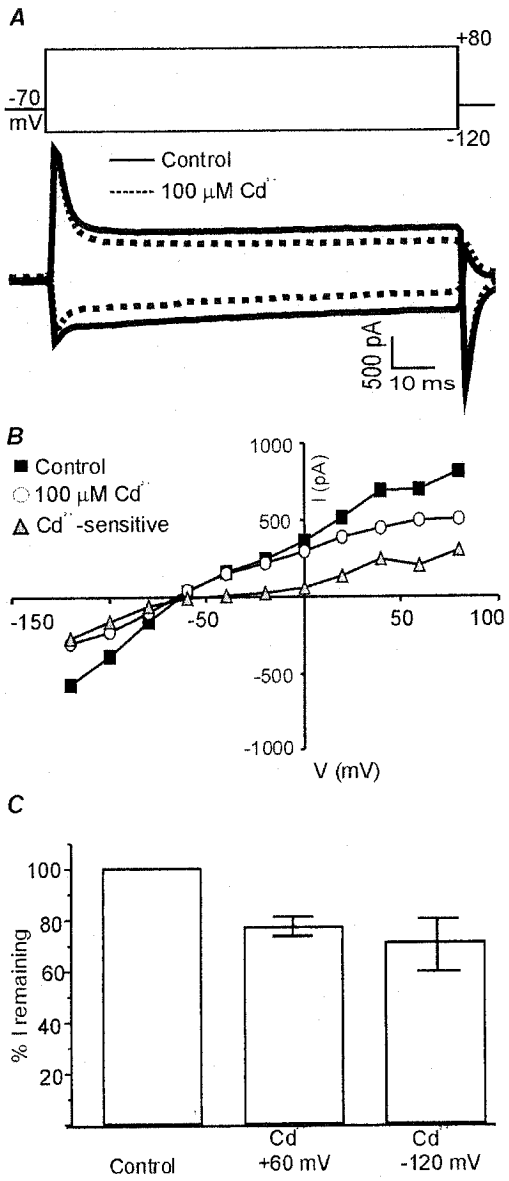

Figure 4.7. Cd^{2+} has a small effect on K_{Ca} channel current in isolated Müller cells

A, Current traces from a representative isolated Müller cell were recorded in 2.5 mM K^+-containing Na^+-based external Ringers and with 90 mM K^+ in the pipette. Currents were elicited from a holding potential of –70 mV with voltage steps from -120 mV to +60 mV before (Control; solid line) and after (100 μM Cd^{2+}; dotted line) the application of Cd^{2+}. *B*, I-V relations for the currents in *A* in control (closed squares), in Cd^{2+} (open circles) and the Cd^{2+}-sensitive difference (gray triangles) *C*, Data from 3 different cells which responded to Cd^{2+}. Control currents are normalized to 100% and the current remaining at +60 mV and at –120 mV in the presence of 100 μM Cd^{2+} is expressed as percentage of control.

of Cd^{2+} at both –120 mV and +60 mV is described as the percentage of control current.

The contribution of Ca^{2+} release from intracellular stores to K_{Ca} channel activation was investigated via dialysis of IP_3 into the interior of the Müller cell. Inclusion of 500 nM IP_3 in the pipette resulted in a significant increase in the mean amplitude of outward current at +60 mV compared to recordings of Müller cells when IP_3 was not present (Figure 4.8). The currents were measured at ~ 10 minutes after rupture in a choline + Ba^{2+} extracellular solution. Cells recorded without IP_3 in the pipette were defined as control, and currents were normalized to 100%. Compared to control, currents measured with IP_3 included in the pipette were significantly enhanced with 100 ± 23% pA (control, n=9) and 228 ± 15 pA (IP_3, n=3) (unpaired t test, *, $P<0.05$). In cells recorded with IP_3 included in the pipette, currents could also be significantly reduced to near control levels (136 ± 20%, n=3) by application of 50 nM ibTX, a large conductance K_{Ca} channel blocker, in the extracellular solution (paired t test, #, $P<0.05$). A representative Müller cell current, with IP_3 included in the pipette, is presented in Figure 4.8*A* before (IP_3) and after the application of iberiotoxin (IP_3 + 50 nM ibTX). The I-V relations for the cell presented in Figure 4.8*A* are shown in Figure 4.8*B*. Current traces acquired before (IP_3, closed squares), during exposure to ibTX (IP_3 + 50 nM ibTX, open circles), and the difference (ibTX-sensitive, gray triangles) are shown. There is a reduction in the outward current in the presence of ibTX, and the ibTX-sensitive I-V relation is characteristic of a K_{Ca} channel (Hille, 2001).

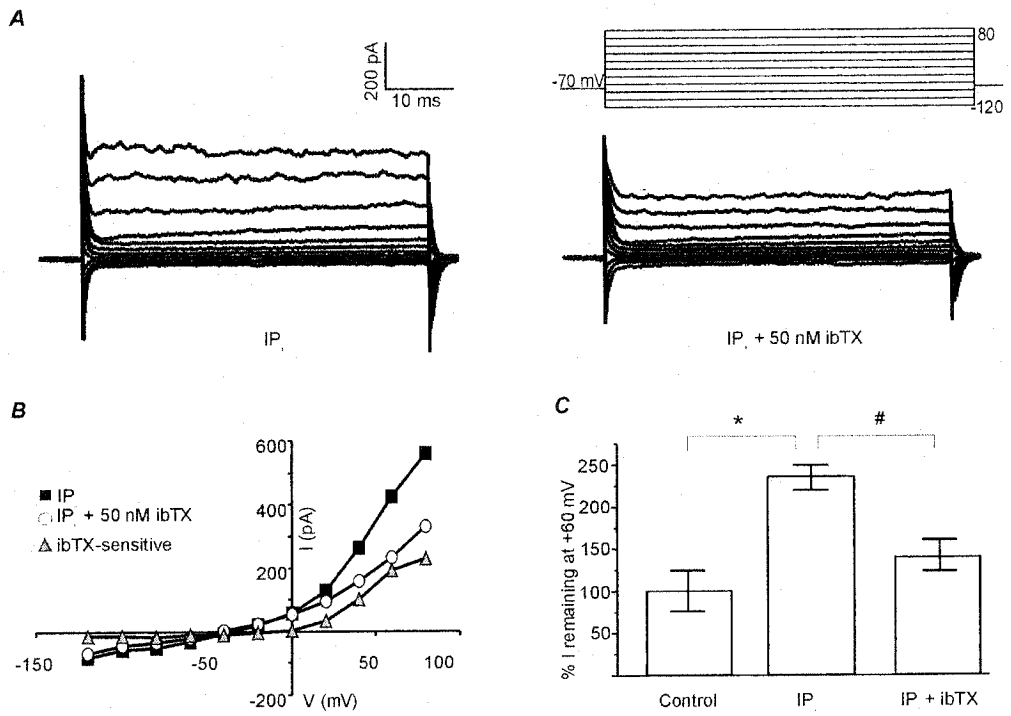

Figure 4.8. IP_3-enhanced K channel current is sensitive to ibTX
A, Whole-cell current traces recorded from a typical salamander Müller cell in 2.5 mM K^+- and 100 μM Ba^{2+}-containing choline-based external Ringers. The internal pipette solution contained 90 mM K^+ and 500 nM IP_3. Current was elicited from a holding potential of –70 mV and from voltage steps between –120 and +80 mV, in 20 mV increments. *B*, I-V relations from the cell in *A* before (IP_3, closed squares) and during (IP_3 + 50 nM ibTX, open circles) application of ibTX. The ibTX-sensitive current (gray triangles) was obtained by subtracting current records in the presence of IP_3 and ibTX from currents recorded in the presence of IP_3 only. *C*, Control currents were recorded from isolated Müller cells in 2.5 mM K^+- and 100 μM Ba^{2+}-containing choline-based external Ringers and 90 mM K^+ -containing pipette solutions. The mean control current was normalized to 100%. The currents recorded before and during the application of ibTX are expressed as a percentage of the control currents. All currents are presented as mean ± sem measured at +60 mV.

4. Discussion

A Ca^{2+}-enhanced component of the whole-cell K channel currents in isolated Müller cells was ibTX-sensitive. These results are consistent with the presence of a large conductance K_{Ca} channel in salamander Müller cells. The single channel conductance of the K_{Ca} channel was 185 pS and similar to those in previous reports of large conductance K_{Ca} channels in Müller cells of the salamander (Newman, 1985b) and mammals (Bringmann and Reichenbach, 1997). Small conductance K_{Ca} channels have not been reported to be present in any glial cell, including Müller cells. In a study examining the developmental expression of small conductance K_{Ca} channels in the rat retina, these channels were found only in neuronal cell types and not in Müller cells or astrocytes (Klöcker et al., 2001).

This study attempted to isolate the contribution of the large conductance K_{Ca} channel currents from the total currents in the salamander Müller cell using whole-cell patch clamp recordings. The current was sampled 80 ms after the beginning of the voltage step to avoid any contribution from K_A channels, which inactivate in rabbit Müller cells within 70 ms (Chao et al., 1994). As well, both K_A and K_{IR} channels are highly sensitive to the application of external Ba^{2+} (Chao et al., 1994). In this study 100 μM Ba^{2+} was included in the extracellular solution to block, or minimize, any contribution from K_A and K_{IR} channels. An electrogenic Na^+/HCO_3^- transporter is expressed on salamander Müller cells (Newman, 1991), which may contribute to the whole-cell outward current. Therefore, choline was substituted for Na^+ to inhibit the Na^+/HCO_3^- transporter.

Under conditions optimized to record K_{Ca} channel contributions to the whole-cell currents, application of 1 mM TEA was found to block a portion of the outward current. The TEA-sensitive current displayed a typical I-V relation of a K_{Ca} current. K_{Ca} channel I-V relations are characteristically N-shaped which reflects their Ca^{2+} dependence. K_{Ca} channel conductance tends to increase with depolarization peaking at ~ +40 mV, and falls again for large depolarizations which permits little Ca^{2+} into the cell due to a reduction in the electrochemical driving force for Ca^{2+} (Hille, 2001). If K_{Ca} channel currents alone were contributing to the total whole-cell K^+ current, then a complete block in the presence of TEA would have been expected. Furthermore, application of TEA to the Ca^{2+}-enhanced current only returned the current back to baseline, pre-Ca^{2+}-enhanced levels. In the presence of ibTX, a selective blocker of large conductance K_{Ca} channels, a larger percentage of the Ca^{2+}-enhanced current was blocked compared to the current inhibited with TEA. Neither blocker could completely inhibit the whole-cell current. This may be due to the presence of TEA-insensitive K channels, such as K_{DR}, or a Ca^{2+}-dependent non-selective cation channel (Puro, 1991). Application of the Ca^{2+} ionophore, A23187, caused an enhancement in outward current, typical of K_{Ca} channel activation. However, a small increase in the inward current was also observed after application of A23187, which was blocked by both ibTX and TEA. A Ca^{2+}-dependent nonselective cation channel has been reported in human Müller cells (Puro, 1991), which may be contributing to the Ca^{2+}-activated whole-cell currents observed in salamander Müller cells.

Elevations in $[Ca^{2+}]_i$ activate K_{Ca} channels, as was observed by the application of A23187. The potential sources of elevated intracellular Ca^{2+}, which could lead to activation of K_{Ca} channels, were investigated. Influx of Ca^{2+} through voltage-gated Ca channels was examined by monitoring the effects of 100 μM Cd^{2+} on Müller cell currents. This experiment was conducted in the Na^+-based Ringer, including 3 mM Ca^{2+}, and not in the choline + Ba^{2+} extracellular solution due to the higher permeability of Ca channels for Ba^{2+} over Ca^{2+} (Hille, 2001). Influx of Ba^{2+} through Ca channels would not activate a K_{Ca} channel current even if K_{Ca} and Ca channels were colocalized in the membrane. Furthermore, voltage-gated Ca channel conductance has been shown to be further decreased in external solutions containing a mixture of Ca^{2+} and Ba^{2+} than with external solutions containing Ca^{2+} only or Ba^{2+} only (Wakamori et al., 1998); a phenomenon known as the anomalous mole-fraction effect (Hille, 2001). Application of 100 μM Cd, a concentration previously shown to block Ca channels (Welch et al., 2005), had only a small effect on the K channel currents. This suggests that activation of large conductance K_{Ca} channels does not depend solely on Ca^{2+} influx through Ca channels. If Ca^{2+}-influx through Ca channels were the primary source of elevated $[Ca^{2+}]_i$, then a larger effect should have been observed. Furthermore, the small Cd^{2+}-induced inhibition that was observed affected both inward and outward currents. This argues towards a non-specific action of Cd^{2+} since the Ca channels in salamander Müller cells are inactive at membrane potentials below –20 mV. Cd^{2+} may be blocking the K_{IR} channel directly or blocking Ca^{2+}-activated nonselective cation channels. Ca^{2+}-activated

nonselective cation channels expressed in human Müller cells are voltage-independent, and inward currents were recorded at negative membrane potentials in the presence of Ca^{2+} (Puro, 1991). The pharmacology characterizing this Ca^{2+}-activated nonselective cation channels is lacking, and a direct interaction of Cd^{2+} and this channel must also be considered.

The small effect of Cd^{2+} on large conductance K_{Ca} channels observed in this study is in contrast to the Newman study (1985b) where 2 mM Cd^{2+} was found to block K_{Ca} currents in the presence of 10 mM external Ca^{2+}. However, this thesis has shown that 100 μM Cd^{2+} is sufficient to block Müller cell Ca channels (Welch et al., 2005) and that increasing the concentration of Cd^{2+} to 2 mM results in a higher probability of non-specific interactions of Cd and the K_{Ca} channel itself (or the Ca^{2+}-activated nonselective cation channel). Alternatively, my study used 3 mM $[Ca^{2+}]_e$ compared to Newman's 10 mM $[Ca^{2+}]_e$. Perhaps, the elevated extracellular Ca^{2+} concentration exerts a stronger driving force on the Ca channel making Ca channel activation more probable under Newman's recording conditions.

The other obvious source of elevated intracellular Ca^{2+} levels is release from Ca^{2+} stores. Dialysis of IP_3 into the interior of the cell resulted in a significant increase in K_{Ca} channel activity, which could be blocked by ibTX. Metabotropic glutamate receptors have been found on Müller cell membranes (Schwartz, 1993), and metabotropic glutamate receptor agonists can evoke Ca^{2+} waves in isolated Müller cells via the release of Ca^{2+} from intracellular stores (Keirstead and Miller, 1997). In fact, glutamate has been shown to increase the

activity of K_{Ca} channels in Müller cells (Bringmann and Reichenbach, 1997). High affinity glutamate transporters on Müller cells remove excess glutamate from the extracellular space, but metabotropic glutamate receptors might also respond to the neurotransmitter via an increase in $[Ca^{2+}]_i$, and, consequently, activate a large conductance K_{Ca} channel.

The functional significance of large conductance K_{Ca} channels on mature Müller cells continues to be speculative. There remains the possibility that electrically isolated regions of the Müller cell membrane, such as the apical processes, might shift to more positive potentials to allow for activation of voltage-dependent ion channels. Considering the large conductance a single K_{Ca} channel, only a small number of K_{Ca} channels need to open to have a significant effect on membrane potential. K_{Ca} channels may function to maintain or restore Müller cell resting potential or participate in the K^+ siphoning mechanism. Large conductance K_{Ca} channels in Müller cells are modulated by an array of mediators including glutamate, PKA, PKC, and pH (Bringmann and Reichenbach, 1997; Schopf et al., 1999; Bringmann et al., 1997). The finely controlled regulation of the channel activity suggests that large conductance K_{Ca} channels are important and warrants further investigation into the role of K_{Ca} channels in retinal physiology.

Chapter 5

Calcium-activated chloride channels in acutely isolated Müller cells from tiger salamander retina

ABSTRACT

This study used whole-cell patch-clamp recordings to demonstrate the presence of Cl_{Ca} channels in salamander Müller cells. Cl_{Ca} channels were fully activated by the application of the Ca^{2+} ionophore, ionomycin. The Ca channel blocker, Cd^{2+}, abolished the Cl_{Ca} tail currents. Increasing or decreasing the duration of the depolarizing pulse immediately preceding the tail currents resulted in either an enhancement or reduction of of the Cl_{Ca} channel tail current, respectively. Repetitive depolarizations with rapid pulses to +20 mV produced a "build-up" of Cl_{Ca} tail currents, which reversed at 0 mV in symmetrical [Cl^-] and at –40 mV in asymmetrical [Cl^-] when intracellular [Cl^-] was reduced to 10%. Cl_{Ca} channel currents were blocked by the Cl channel blocker niflumic acid, while niflumic acid had no effect on voltage-gated Ca channels. The Cl_{Ca} channel tail currents were not sensitive to dialysis of antibodies directed towards ClC-3 Cl channels and immunohistochemical analysis of ClC-3 staining confirmed that, in Müller cells under isotonic conditions, ClC-3 is found primarily at intracellular sites and is distinct from the plama membrane channels giving rise to Cl_{Ca}.

1. Introduction

The most abundant physiological anion is Cl^-, with Cl channels participating in many cellular processes including volume regulation, intracellular pH regulation, transepithelial transport and control of water flow. When E_{Cl} is negative to the resting membrane potential, the opening of anion selective ion channels would permit an influx of Cl^- which is defined as an outward current. Current is defined as the movement of positive charge and, therefore, the influx of negatively charged ions, such as Cl^-, is described as an efflux of positive charge, and thus, an outward current. Therefore, when E_{Cl} is negative to the resting membrane potential, opening of Cl channels produces an outward current, to facilitate cellular repolarization. Conversely, when E_{Cl} is positive to the resting membrane potential, an inward current, i.e. Cl^- efflux, produces a depolarizing response.

Several families of voltage-dependent Cl channels are present in the vertebrate retina, including calcium-activated chloride (Cl_{Ca}) channels and members of the ClC family of anion channels. In photoreceptors, Cl_{Ca} channels mediate a Cl^- current that is outwardly rectifying and is functionally coupled to Ca^{2+} influx through voltage-gated Ca channels (Barnes and Bui, 1991; Barnes and Hille, 1989). As with K_{Ca} channels, the depolarization required to open photoreceptor Cl_{Ca} channels is lowered with increasing $[Ca^{2+}]_i$. Although the mode of Ca^{2+} activation in Cl_{Ca} channels remains unknown, the steep dependence on $[Ca^{2+}]_i$ suggests that several Ca^{2+} ions bind to activate the channel.

The molecular structure of Cl_{Ca} channels has not been resolved, and to-date there is only limited sequence data available on this family. A region of the Cl_{Ca} channel has been cloned from bovine tracheal epithelium and expressed in *Xenopus* oocytes (Cunningham et al., 1995). The resulting current was outwardly rectifying and enhanced by the application of ionomycin, a Ca^{2+} ionophore, however channel activation required very high, non-physiological $[Ca^{2+}]i$ and the biophysical properties of this channel are signficantly different from the Cl_{Ca} channel described in photoreceptors (Barnes and Hille, 1989; Barnes and Bui, 1991). The bovine tracheal epithelial Cl_{Ca} channel could be inhibited by the nonspecific Cl channel blockers 4,4`-diisothiocyanostilbene-2,2`-disulfonic acid (DIDS) and dithiothreitol (DTT), but was insensitive to niflumic acid (Cunningham et al., 1995). A second epithelial Cl_{Ca} channel has now been cloned from human lung, trachea and mammary gland. This channel when expressed in HEK293 cells also required high $[Ca^{2+}]_i$ to be activated, was slightly outwardly rectifying, enhanced by ionomycin, and inhibited by DIDS, DTT, and niflumic acid (Gruber et al., 1999). A five transmembrane topology for the epithelial Cl_{Ca} channel has now been proposed. Whether these epithelial channels are part of the same Cl channel family as Cl_{Ca} channels described in other cell types is not yet resolved, as is the functional requirement for additional accessory subunits for Ca^{2+} sensitivity (Nilius and Droogmans, 2003).

While there is little evidence of Cl_{Ca} channels in astrocytes, ClC channels have been well characterized in glia and have been described in a number of different cell types in the retina, including bipolar cells and retinal pigment

epithelial cells (Enz et al., 1999; Wills et al., 2000). Currently, there are nine members of the ClC family of Cl channels. The proposed structure of ClC channels is double-barreled dimers with 10-13 transmembrane domains in each subunit (Jentsch et al., 1999). Members of the ClC family of Cl channels are characterized by their voltage-dependence. Some ClC channels are expressed on intracellular membranes, such as ClC-3, ClC-5, ClC-6, and ClC-7. ClC-3, highly expressed in brain and ClC-5, expressed predominantly in kidneys, are involved in acidification of intracellular vesicles by providing the parallel anion conductance required for efficient pumping of the H^+-ATPase (Duan et al., 1997; Günther et al., 1998). Both ClC-3 and ClC-5 are outwardly rectifying Cl^- currents (Duan et al., 1997; Günther et al., 1998). ClC-6 and ClC-7 are ubiquitously expressed Cl channels, and their function is unclear (Jentsch et al., 1999). ClC-1, ClC-2, ClC-K1/2 are expressed at the plasma membranes in a wide variety of tissues. ClC-1 is activated by depolarization and stabilizes the plasma membrane potential in skeletal muscle (Steinmeyer et al., 1991). The broadly expressed ClC-2 is activated by hyperpolarization and cell swelling, and has been implicated in regulating cell volume and $[Cl^-]_i$ (Gründer et al., 1992). ClC-K channels are found nearly exclusively in the kidney and maintain epithelial secretory function (Jentsch et al., 1999). The physiological functions of ClC-4 are unclear, although it is expressed in several tissues (Jentsch et al., 1999). ClC-3 has been found in many cell types and has been shown to alter intracellular vesicle acidification (Stobrawa et al., 2001). However, a role for ClC-3 as a plasma membrane channel is controversial with some studies favouring ClC-3 as the volume-

sensitive anion channel (Duan et al., 1997) and other studies disputing this claim (Stobrawa et al., 2001). Studies in ClC-3 knock-out mice demonstrated a normal volume-regulated Cl^- conductance which argues against a function for ClC-3 as the membrane cell-swelling activated Cl channel (Stobrawa at al., 2001).

In Müller cells, expression of a voltage-dependent anion conductance has not been reported. However, GABA-evoked currents, via ionotropic $GABA_A$ receptors, in human Müller cells were found to be mediated by Cl^- (Biedermann et al., 2004) and the uptake of glutamate in salamander Müller cells was coupled to an anionic conductance (Eliasof and Jahr, 1996). Immunohistochemical evidence suggested that salamander Müller cells express ClC-3 Cl channels as GFAP-positive cells were found to co-localize with anti-ClC-3 staining (Wood, 2004). The presence of ClC-3 was shown to be necessary for normal retinal development when ClC-3 knockout mice were demonstrated to suffer from retinal degeneration and vision loss (Stobrawa et al., 2001).

The overall objective of this study was to identify voltage-dependent Cl channels in Muller cells. Specifically, to determine if a Ca^{2+}-activated Cl channel was present in isolated Müller cells and, if so, whether the biophysical and pharmacological properties of this channel resembled the previously described photoreceptor Cl_{Ca}. Furthermore, this study sought to determine whether ClC-3 channels contribute to the Muller whole-cell Cl_{Ca} channel.

2. Materials and methods

2.1 Cell isolation

Tiger salamanders (*Ambystoma tigrinum*), in the larval stage, were sacrificed by decapitation, the eyes were enucleated and dissected to remove the retina. Retinas were treated with the enzyme papain to dissociate cells as previously described (see Chapter 2, General Methods; section 1). Retinal cells were aliquoted onto plastic dishes for patch-clamp recording or onto glass coverslips for immunocytochemistry and visualized using a Nikon Diaphot microscope. Müller cells were identifiable by their distinct morphology.

2.2 Patch clamp recording

Müller cell Ca^{2+}-activated Cl currents were recorded with the whole-cell, patch-clamp recording technique, using recording techniques previously described (see Chapter 2, General Methods; section 2.2). Electrodes were filled with a solution designed to isolate Cl_{Ca} channel currents, containing (in mM): 100 CsCl, 0.8 $MgCl_2$, 0.4 $CaCl_2$, 1 EGTA, 5 HEPES, 1 ATP, 0.1 GTP at pH 7.2 (solution K, Table 2.1 in Chapter 2, General Methods). The extracellular bathing solution was composed of (in mM): 88 NaCl, 2.5 KCl, 5 CsCl, 3 $CaCl_2$, 10 HEPES, 8 glucose at pH 7.6 (solution H, Table 2.1 in Chapter 2, General Methods). During experiments in which the intracellular [Cl^-] was reduced, the pipette solution contained (in mM): 8 CsCl, 92 Csglucuronate, 3 $CaCl_2$, 10 HEPES, 8 glucose at pH 7.6 (solution L, Table 2.1 in Chapter 2, General Methods). Ca channel currents were recorded in an extracellular bath solution containing (in mM): 70 NaCl, 2.5 KCl, 5 CsCl, 10 $BaCl_2$, 15 TEA, 15 HEPES, 8 glucose at pH 7.6

(solution E, Table 2.1 in Chapter 2, General Methods). Drugs were added to the extracellular solution and superfused during electrophysiological recording. Niflumic acid and ionomycin were each prepared as 10 mM stock solutions in DMSO and diluted in the bathing solution. In each case, control electrophysiological recordings were made in the presence of an equal concentration of DMSO in the external bathing solution. A polyclonal antibody directed towards ClC-3, anti-ClC-3, was added to the pipette solution and dialyzed into the cell's interior. Controls for anti-ClC-3 dialysis were performed by preincubating anti-ClC-3 with its control peptide (CP) (1:3 ratio) prior to electrophysiological recordings. All recordings were performed at room temperature (21 – 25 °C).

2.3 Immunocytochemistry

Fixed isolated Müller cells were stained using a rabbit Cl channel anti-ClC-3 polyclonal antibody (1:500 dilution) and the mouse lysosome-associated membrane protein marker anti-LAMP-1 monoclonal antibody (1:100). The immunocytochemical protocol is detailed in Chapter 2, General Methods (section 3). The secondary antibodies used were Alexafluor goat anti-rabbit IgG (1:500 dilution) and goat anti-mouse IgG (1:500 dilution). As a negative control, the above protocol was repeated on fixed cells with complete omission of the primary antibodies to account for any non-specific staining from the secondary antibody. Antibody-treated cells were visualized using laser-scanning confocal microscopy (described in Chapter 2, General Methods; section 4.1).

2.4 Drugs and chemicals

Most chemicals used in electrophysiological recordings were obtained from Sigma Chemical Co. (St. Louis, MO) including: cadmium chloride (Cd^{2+}), ionomycin, and niflumic acid. The Alexafluor secondary antibodies, goat anti-rabbit and goat anti-mouse, were purchased from Molecular Probes, Inc (Eugene, OR). The rabbit anti-ClC-3 antibody was purchased from Alomone laboratories (Jerusalem, Israel). The mouse anti-LAMP-1 antibody was purchased from Stressgen Biotechnologies (Victoria, BC).

2.5 Quantitative and statistical analyses

I-V relations for the tail currents were sampled 30 ms after the end of the voltage step. I-V relations have been corrected for liquid junction potentials (equation 2.3; Chapter 2, General Methods; section 3). During the successive voltage depolarization, the individual tail current with largest amplitude was defined as the peak tail current. Control currents were identified as the peak tail current and defined as 100%, and tail current remaining after application of drug is expressed as a percentage of control normalized currents. Data are expressed as mean percentage ± standard error (s.e.m.). All comparisons were carried out using Student's t test with significance defined as $P<0.05$. Statistical analyses of drug block were performed on raw currents with a paired t test while comparison between two drug treatments were analyzed with an unpaired t test, as indicated in text.

3. Results

3.1 Cl channels in isolated Müller cells are dependent on $[Ca^{2+}]_i$

Cl_{Ca} channels exhibit a strong dependence on intracellular Ca^{2+}. A Cl_{Ca} channel current was observed in whole-cell patch clamp recordings from freshly isolated Müller cells. The intracellular pipette solution was Cs-based to block contributions from K channels. Recording solutions were made in symmetrical $[Cl^-]$ and contained 3 mM Ca^{2+} in the extracellular bath solution. Under these conditions, stepping the Müller cell from –70 mV to +60 mV in 10 mV increments from a holding potential of –60 mV, elicited a small inward current between –10 mV and +20 mV, and an outward current positive to +20 mV (Figure 5.1; closed circles). During the voltage protocol, step depolarizations positive to –30 mV elicited an inward tail current, measured at –60 mV, which continued to increase as the voltage was stepped positive in 10 mV increments. Tail currents reached maximum amplitude with depolarations to ~ +20 mV and decreased as the step potential exceeded +20 mV (Figure 5.1*A*, *B*; closed squares). The tail currents, measured 30 ms after the end of the voltage step, were plotted against the potential of the preceding pulse and shown in Figure 5.1*B*.

Superfusion with 5 μM ionomycin, a Ca^{2+} ionophore, in the extracellular Ringers activated an outwardly rectifying current which reversed at 0 mV (Figure 5.2*C*,*D*; open circles). Analysis of the corresponding tail currents in the presence of ionomycin revealed the I-V relation of a Ca^{2+}-activated channel with a current amplitude of ~ 400 pA (Figure 5.2*D*; open squares) in the representative cell

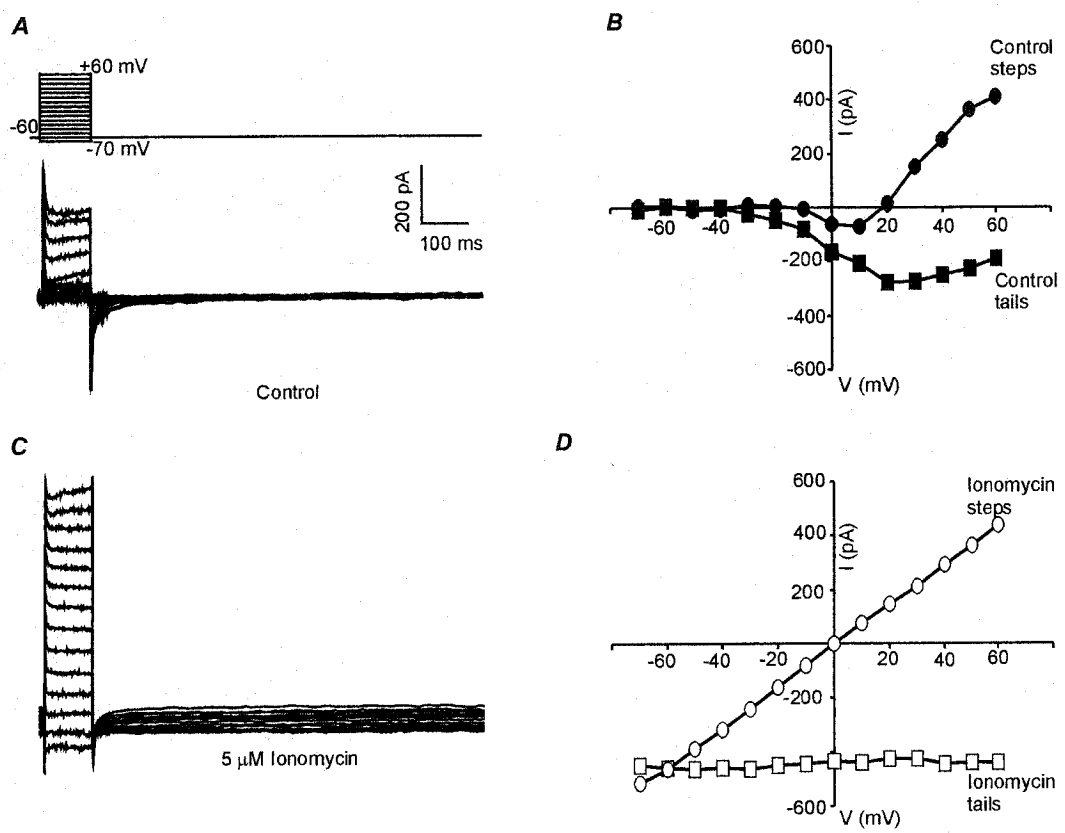

Figure 5.1. Ionomycin enhances a Ca^{2+}-activated chloride channel current in isolated Müller cells

A, Cl_{Ca} channel currents elicited from a holding potential of –60 mV during steps to voltages between –70 and +40 mV, in 10 mV increments, and recorded in 3 mM Ca^{2+}. *B*, I-V relations for the currents shown in *A* measured from the voltage steps (closed circles) and the tail currents plotted against the potential of the preceding depolarization (closed squares). *C,* The current in *A* was activated by application of 5 μM ionomycin. *D*, I-V relation for ionomycin-enhanced currents shown in *C* sampled from the currents during voltage step (open circles) and from the tails (open squares).

shown in Figure 5.2. Ionomycin elevates intracellular Ca^{2+} independent of voltage-gated Ca channels and thus, the activated tail current no longer exhibits any voltage-dependence. The average tail current amplitude observed in 3 cells exposed to ionomycin was 320 ± 79 pA. To isolate Cl_{Ca} channel currents, the contributions from Ca^{2+}-activated K channels were minimized by including Cs^+ in the extracellular and intracellular solutions. Under these conditions, and in symmetrical $[Cl^-]$, Ca^{2+}-activated Cl^- currents reversed at 0 mV.

The currents measured during the depolarizing steps are a compilation of whole-cell currents that included all Cl channel currents as well as Ca channel currents. However, tail currents provide a more direct measurement of Cl_{Ca} channels, which do not inactivate in the presence of available Ca^{2+} (Currie et al., 1995). Since tail current recordings, measured at –60 mV after steps to depolarized potentials, provide a more isolated measure of Cl_{Ca} channel currents, the analyses of all subsequent experiments have focused on the tail currents. In salamander cone photoreceptors, the steep dependence of Cl_{Ca} channels on $[Ca^{2+}]_i$ has been linked to Ca^{2+} influx through voltage-gated Ca channels (Barnes and Hille, 1989).

Therefore, the next experiment investigated whether the tail currents at -60 mV required influx of Ca^{2+} through Ca channels during the preceding depolarization step. Tail currents were maximal between the voltage range of 0 to +20 mV (Figure 5.2*B*), similar to voltage-gated Ca channel currents in salamander Müller cells (Welch et al., 2005). Tail currents were smaller at larger depolarization steps to +50 or +60 mV (Figure 5.2*B*; closed squares) since at

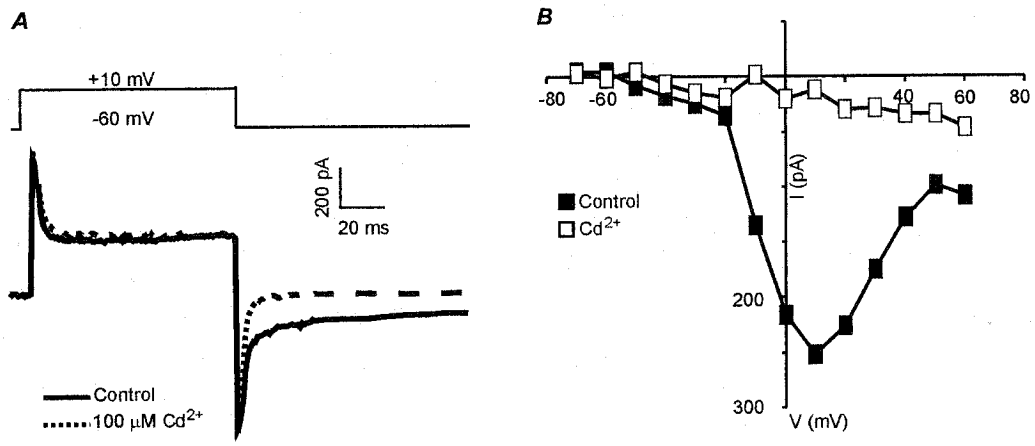

Figure 5.2. Cl_{Ca} channel currents in retinal Müller cells are sensitive to Cd^{2+}
A, Cl_{Ca} channel tail currents at -60 mV preceded by depolarizing conditioning steps to +10 mV before (Control; solid line) and during the application of 100 μM Cd^{2+} (dotted line). *B*, I-V relations for the currents in *A* in control (closed squares), and 100 μM Cd^{2+} (open squares).

potentials near the equilibrium potential of Ca^{2+}, the driving force for Ca^{2+} influx via voltage-gated Ca channels is minimal. Application of 100 μM Cd^{2+} blocks voltage-gated Ca channels in Müller cells (Welch et al., 2005) and also significantly blocked the tails currents through Cl_{Ca} channels (paired Student's t test; $P<0.05$; n=5) (Figure 5.2*A*; dotted line) with 0 ± 1% of the peak tail current remaining in the presence of Cd^{2+}.

If activation of Cl_{Ca} channel tail currents is dependent upon activation of Ca channels, then an increase in the duration of the voltage step should enhance the tail currents; Ca channels open with depolarization and increasing the duration of depolarization allows for increased influx of Ca^{2+}. A time-dependent depolarization effect was observed in Müller cells (Figure 5.3). The response of a representative Müller cell depolarized to +20 mV for 50, 100, 200, 400 ms is displayed in Figure 5.3*A*. The I-V relations for the cell shown in Figure 5.3*A* reveals that a 50 ms depolarization step elicits a small tail current (Figure 5.3*B*; closed diamonds) which is ~ half the peak current (54 ± 12%; n=4) of a tail current preceded by a 100 ms test pulse (Figure 5.3*B*; closed squares). Tail currents measured after a 200 ms (Figure 5.3*B*; closed circles) and 400 ms (Figure 5.3*B*; closed triangles) voltage step to +20 mV were 122 ± 9% and 184 ± 40% larger than those recorded after a 100 ms test pulse (n=4).

Figure 5.4 shows that a similar enhancement of tail currents was observed when brief test pulses of 400 ms were applied several times in rapid succession. Steps to +20 mV, followed by tail currents measured at –80 mV, were applied

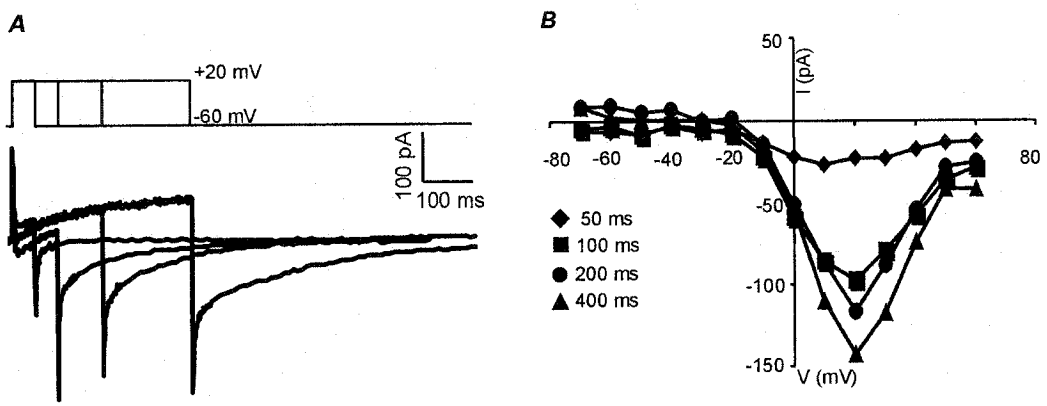

Figure 5.3. Increasing the length of time of the depolarizing pulse enhances Cl_{Ca} channel tail currents

A, Enhancement of the tail current with longer depolarizing pulses in an isolated Müller cell. The cell was stepped to +20 mV for durations of 50 ms, 100 ms, 200 ms, and 400 ms from a holding potential of –60 mV, and tail currents were recorded at –60 mV. *B,* I-V relations for the tail currents in *A* with a voltage step to +20 mV for 50 ms (closed diamonds), 100 ms (closed squares), 200 ms (closed circles), and 400 ms (closed triangles).

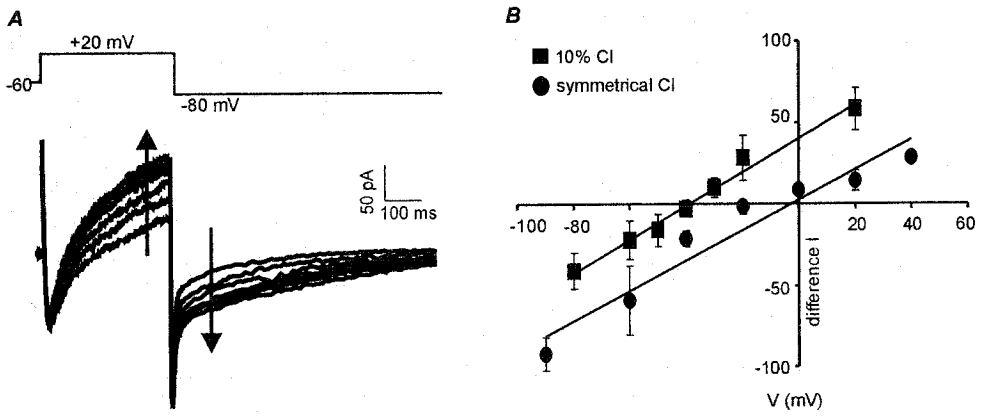

Figure 5.4. Cumulative effect of rapid depolarizations estimated E_{Cl}
A, Cl_{Ca} channel currents from an isolated Müller cell elicited during steps to +20 mV and tail currents at –60 mV from a holding potential of –80 mV recorded in asymmetrical $[Cl^-]$. Growth of outward step and inward tail currents was observed during successive 400 ms depolarizations every 3 seconds. *B*, The difference current of the cumulative current increases plotted vs. the step voltage. The I-V relations for Cl_{Ca} channel currents recorded in symmetrical $[Cl^-]$ (closed circles) and asymmetrical $[Cl^-]$ with intracellular $[Cl^-]$ reduced to 10% (closed squares).

every 3 seconds and caused tail currents to increase cumulatively or "build up" (Figure 5.4*A*). The "build up" is thought to be a reflection of a localized increase in $[Ca^{2+}]_i$ which is caused by reduced Ca^{2+}-buffering and/or diffusion. The available mechanisms for rapidly removing Ca^{2+} from the area near the membrane become saturated by the repeated depolarizations, which continually allow Ca^{2+} to enter the cell (Barnes and Bui, 1991).

3.2 Properties of Cl_{Ca} channels in isolated Müller cells

The reversal potential of the Cl_{Ca} channel current can be estimated by examining the "build up" of current observed at different tail potentials. As predicted for a Cl channel, an inward current would be expected at potentials below E_{Cl} and an outward current observed at potentials above E_{Cl}. Since several currents may be activated by the voltage protocol used to elicit Cl_{Ca} channel currents, an estimate of the current flux through only Cl_{Ca} channels was obtained by subtracting the first pulse from subsequent pulses to reduce contaminating currents. This assumes that Cl_{Ca} channels mediate the tail current sensitive to rapid depolarizations that cause Ca^{2+} build-up. Therefore, if the current trace associated with the first depolarization is subtracted from the last in a rapidly applied series of pulses, then the difference current should reflect an isolated Ca^{2+}-enhanced Cl^- current. In symmetrical $[Cl^-]$, E_{Cl} is estimated to be 0 mV by the Nernst equation (equation 2.5; Chapter 2, General Methods; section 5). Under recording conditions of symmetrical $[Cl^-]$ together with rapid depolarizations to +20 mV, the difference tail currents measured between –90 mV and +40 mV reversed at ~ 0 mV (Figure 5.4*B*; closed circles) and had a linear relationship with

a slope of 1 (n=4; mean ± sem). Figure 5.4*B* (closed squares) shows that when the $[Cl^-]_i$ was reduced to 10%, 10.3 mM Cl^-, by the substitution of Cl^- with glucuronate in the pipette solution, the reversal potential shifted to ~ -40 mV (n=4; mean ± sem). The linear relationship had a slope of 0.9.

The analogous relationship between E_{Cl} and the reversal potential of the tail currents suggests that these Ca^{2+}-sensitive currents are mediated through Cl channels. To further confirm this, the nonselective Cl channel blocker niflumic acid was applied to freshly isolated Müller cells via superfusion. Figure 5.5*A* shows examples of currents from a representative Müller cell before (Control; solid line) and after the application of 100 μM niflumic acid (dotted line). For the cell shown in *A*, the tail currents, sampled at –60 mV, are plotted against the voltage step immediately preceding the tail current before (Control; closed squares) and after exposure to niflumic acid (open squares). The average Cl_{Ca} channel current remaining in the presence of 100 μM niflumic acid was 4 ± 2% of control at +20 mV (n=3). Statistical analysis of the currents revealed that reduction in current observed in the presence of niflumic acid was significant (paired Student's t test; $P<0.05$).

The blocking effects of niflumic acid were selective for Cl channels since 100 μM niflumic acid did not affect voltage-gated Ca channels in salamander Müller cells. The Ca channel currents and corresponding I-V relations for a representative Müller cell before (Control; solid line; closed diamonds) and during the application of 100 μM niflumic acid (dotted line; open diamonds) are shown in Figure 5.5*C&D*. The percentage of the Ca channel current remaining at

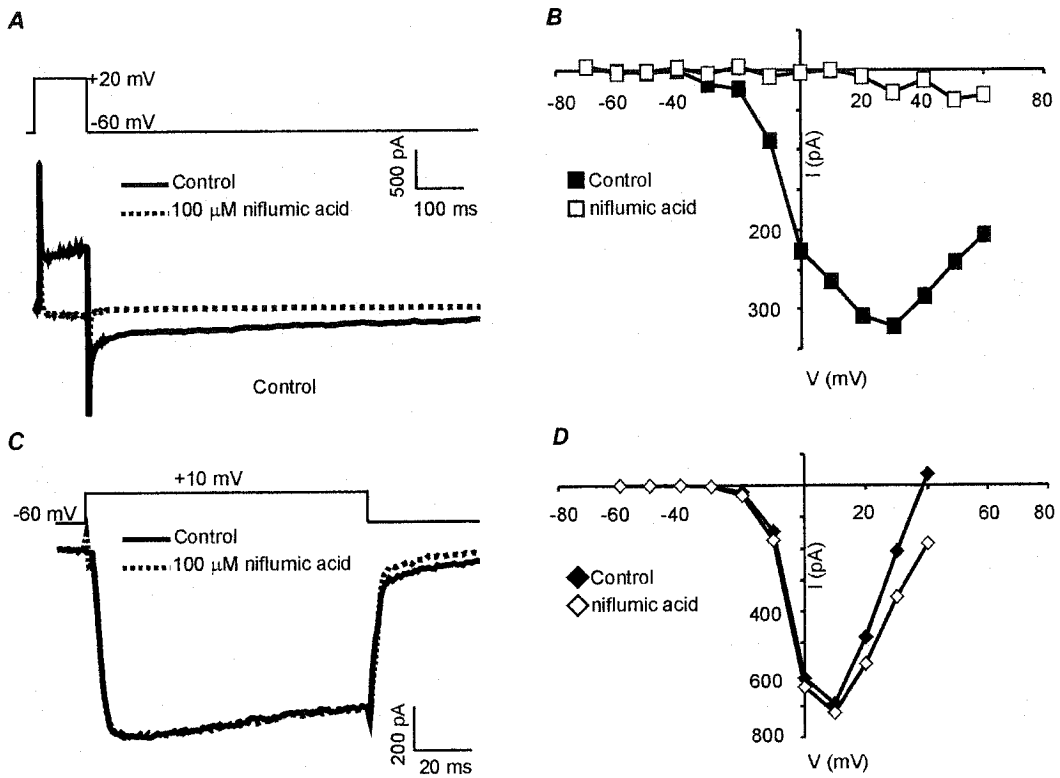

Figure 5.5. Niflumic acid reduces the Müller cell Cl_{Ca} channel current. *A,* Cl_{Ca} channel tail currents recorded at –60 mV from an isolated Müller cell generated during voltage steps to +20 mV from a holding potential of –60 mV before (Control; solid line) and after the application of 100 μM niflumic acid (dotted line). *B,* I-V relations of the tail currents plotted against the preceding depolarization voltages from the cell in *A* before (control, closed squares) and after niflumic acid (open squares). *C,* Ca channel currents recorded in 10 mM Ba^{2+}, generated from a holding potential of –60 mV, and stepped to +10 mV, before (Control; solid line), and during application of 100 μM niflumic acid (dotted line). *D,* The I-V relations for the cell shown in *C* before (Control, closed diamonds) and during exposure of niflumic acid (open diamonds).

+10 mV in the presence of niflumic acid was 103 ± 5% (n=3) compared to control .

3.3 ClC-3 does not contribute to the Cl_{Ca} channel current

The molecular nature of Cl_{Ca} channel is not yet resolved. However, it has been reported that ClC-3, a member of the ClC family of Cl channels, is Ca^{2+} and calmodulin sensitive (Huang et al., 2001). The biophysical properties of cloned ClC-3 appear different from Cl_{Ca} channel. ClC-3 is constitutively open when present in the plasma membrane. The current is outwardly rectifying but shows slight inactivation at very depolarized potentials (>80 mV) and activates with cell swelling (Duan et al., 1997). This is different from Cl_{Ca} channels recorded in salamander Müller cells, which were not constitutively open and required activation by Ca^{2+} and depolarization. However, it is possible that ClC-3 may contribute to Cl_{Ca} channel currents since ClC-3 has also been localized to retinal Müller cells (Wood, 2004). To assess the putative contribution that ClC-3 makes to the Cl_{Ca} channel currents under isotonic conditions, a polyclonal antibody directed towards a region of the intracellular C-terminus of ClC-3, was dialyzed into the cell via the pipette solution. Time zero was set when the membrane was ruptured to obtain the whole-cell configuration, and the tail currents were compared 2 minutes post rupture to those remaining 15 minutes post rupture. Figure 5.6*A* shows that the response of representative Müller cell currents at 15 minutes post rupture (solid line) was reduced compared to currents at 2 minutes post rupture (dotted line). Currents were elicited from a holding potential of -60 mV, stepped to +10 mV, and tails observed at -60 mV. The tail currents from the

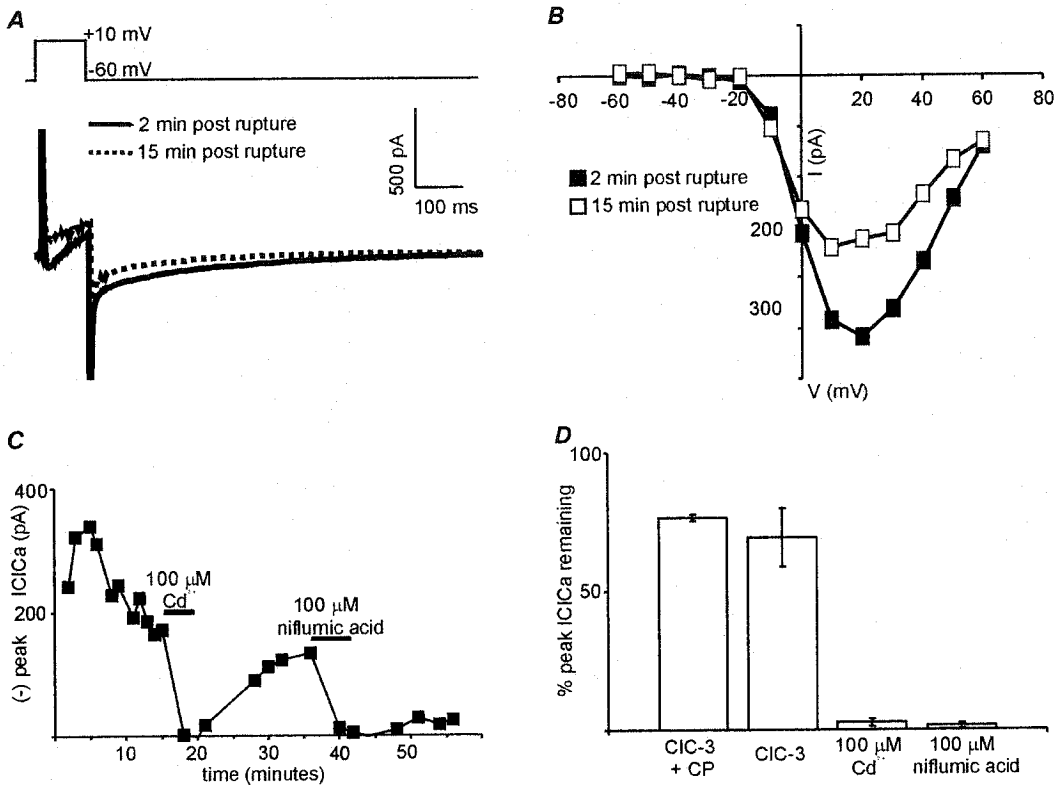

Figure 5.6. Dialysis of anti-ClC-3 did not affect Cl_{Ca} channel currents in isolated Müller cells

A, Isolated Müller cell Cl_{Ca} channel currents presented with tail currents recorded at –60 mV, generated during voltage steps to +10 mV from a holding potential of –60 mV, 2min after membrane rupture to the whole-cell configuration (solid line) and 15 min post rupture (dotted line). A polyclonal antibody directed towards ClC-3 was included in the pipette solution. *B*, I-V relations from the Müller cell tail currents shown in *A* at 2 minutes post rupture (closed squares) and at 15 minutes post rupture (open squares) plotted against the preceding depolarization pulses. *C*, Time course of tail currents recorded at –60 mV, elicited from voltage steps to +10 mV, of the Müller cell in *A* exposed to 100 μM Cd^{2+} for 4 minutes, partial recovery in control Ringers, and then to application of 100 μM niflumic acid. *D*, Cl_{Ca} channel tail currents expressed as percentage of current remaining 15 minutes post rupture in Müller cells dialyzed with anti-ClC-3 preadsorbed with its control peptide (ClC-3 + CP) and with anti-ClC-3 only (ClC-3). Also shown are the percentages of tail current remaining in the presence of 100 μM Cd^{2+} and 100 μM niflumic acid for cells dialyzed with anti-ClC-3 (n=3).

same cell were plotted vs. the preceding voltage step and the resultant I-V relations (Figure 5.6*B*) illustrate that there is a reduction in the tail currents over time when anti-ClC-3 was included in the pipette solution. The percentage of tail current remaining after 15 minutes was 69 ± 11% (n=4) compared to 2 minutes post rupture. To determine whether this reduction in current was due to anti-ClC-3 inhibition of Cl channels, anti-ClC-3 was preadsorbed with its control peptide (ClC-3 + CP) at a ratio of 1:3 before being dialyzed into Müller cells. When tail currents were recorded from Müller cells dialyzed with ClC-3 + CP, a small reduction in the current was still observed 15 minutes post rupture with 76 ± 1 % of peak tail current remaining (n=3). There was no significant difference between the percentage of tail current remaining 15 minutes post rupture in Müller cells exposed to dialysis of anti-ClC-3 alone or ClC-3 + CP (unpaired t test; $P<0.05$) suggesting that ClC-3 does not contribute to whole-cell Cl_{Ca} channel currents in salamander Müller cells under isotonic conditions.

Furthermore, to confirm that the current observed at 15 minutes post rupture was indeed a Ca^{2+}-activated Cl channel current, 100 μM Cd^{2+} was applied. The percentage of current remaining after the application of Cd^{2+} to a Müller cell dialyzed with anti-ClC-3 for 15 minutes was 3 ± 1% (n=3). The reversible block by Cd^{2+} suggested that the tail currents observed after 15 minutes of anti-ClC-3 dialysis were representative of a Ca^{2+}-dependent current. Subsequent application of 100 μM niflumic acid also completely blocked the tail currents. Figure 5.6*C* represents the time course of drug blockade and recovery for a Müller cell dialyzed with anti-ClC-3.

3.4 ClC-3 is localized to intracellular membranes

Acutely isolated Müller cells were treated with antibodies directed towards ClC-3 and lysosomal-associated membrane protein 1 (LAMP-1) to investigate the localization of the ClC-3 channel protein. The anti-ClC-3 antibody, displayed in green, stained throughout the entire Müller cell including the apical processes and somatic region of Müller cells (Fig. 5.7*A*). The Müller cell shown in Fig. 5.7 is a representative example of the three cells examined. Anti-LAMP-1 staining, shown in red, was also evident throughout the cell (Figure 5.7*B*). Co-localization of anti-ClC-3 and –LAMP-1 positive staining is shown in orange (Figure 5.7*C*). All areas of the Müller cell appear as orange suggesting that ClC-3 is confined LAMP-1 positive intracellular membranes, and under isotonic conditions is not transported to the plasma membrane. Omission of the primary antibodies from the protocol revealed an absence of any non-specific fluorescence which may have been due to the secondary antibody (data not shown).

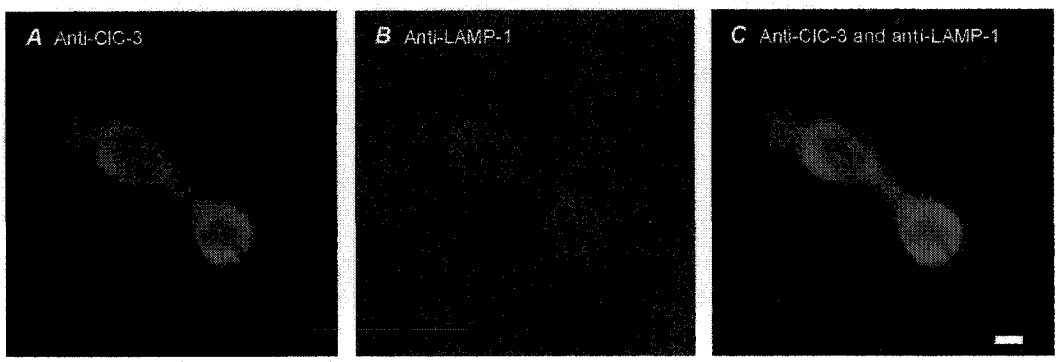

Figure 5.7. Immunoreactivity of isolated Müller cells detects intracellular expression ClC-3 channels
A, An isolated Müller cell stained with anti-ClC-3 reveals expression of ClC-3 channels (green) throughout all regions of the Müller cell including the apical processes and endfoot. *B*, The same cell shown in *A* is also immunopositive for LAMP-1 expression (red) throughout the entire Müller cell. *C*, Double-labeling of the Müller cell shown in *A* & *B* reveal that anti-ClC-3 and -LAMP-1 immunoreactivity overlap in all areas of the Müller cell (orange). Scale bar, 10 μm.

4. Discussion

4.1 Cl_{Ca} channel properties

These results suggest that a Ca^{2+}-activated Cl channel is present in freshly isolated Müller cells. Elevating intracellular Ca^{2+}, with the ionophore ionomycin, activated an outwardly rectifying Cl_{Ca} channel. The ionomycin-evoked current reversed near the predicted E_{Cl}. Analysis of the tail currents indicated that the channel was fully activated and voltage-independent in the presence of a high concentration of intracellular Ca^{2+}. Ionomycin elevates $[Ca^{2+}]_i$ independent of Ca^{2+} influx through voltage-dependent Ca channels. The increased $[Ca^{2+}]_i$ generated by the ionomycin, acting as a Ca^{2+} ionophore in the membrane, presumably enabled Ca^{2+} to saturate all of the Cl_{Ca} channel Ca^{2+}-binding sites fully activating the channel and removing any of the voltage dependence. The tail currents, measured at –60 mV, were maximal at ~400 pA of current, which was independent of the voltage step immediately preceding suggesting that Cl_{Ca} channel voltage-dependence is inferred from Ca channels.

There is evidence to suggest that Ca^{2+}-sensitivity in Cl_{Ca} channels is linked to Ca^{2+} influx through voltage-gated Ca channels since the nonspecific Ca channel blocker, Cd^{2+}, inhibited Cl_{Ca} channel activation (Barnes and Hille, 1989; Barnes and Bui, 1991). In this study of isolated salamander Müller cells, application of Cd^{2+} abolished Cl_{Ca} channel currents suggesting that Cl_{Ca} channel activation is dependent on Ca^{2+} influx through voltage-gated Ca channels. Furthermore, prolonged depolarization and rapidly repeated depolarization led to an enhancement in Cl_{Ca} channel tail currents consistent with depolarization

opening voltage-gated Ca channels, which in turn, activate Cl_{Ca} channels. In cones, the increase in Cl^- conductance resulting from elevations in $[Ca^{2+}]_i$ was found to be due to an increase in the lengthening of the time course of Cl^- tail current decay rather than an increase in the magnitude of current (Barnes and Bui, 1991). Elevations of $[Ca^{2+}]_i$ enhance Cl_{Ca} channel activation and the length of time that the channel is in its open configuration. It is likely that a similar mechanism is involved in Ca^{2+}-activation of Cl channels in Müller cells.

The direction of current flow from activation of Cl_{Ca} channels is dependent on the relationship between resting membrane potential and E_{Cl}. Experimental conditions allow E_{Cl} to be controlled by the composition of the bath and pipette solutions. In symmetrical $[Cl^-]$, E_{Cl} is 0 mV as predicted by the Nernst equation, and patch-clamp experiments control the membrane potential at which the tail currents are measured. In this study, tail currents were usually measured at -60 mV, following voltage steps to a series of potentials, while E_{Cl} was set to 0 mV. Therefore, E_{Cl} was positive to membrane potential, and an inward current resulted. The potential at which the tail currents were measured was varied to permit an estimate of the Cl^- current. A linear relationship was approximated in symmetrical $[Cl^-]$ which reversed at 0 mV. Reducing the $[Cl^-]_i$, which shifts E_{Cl} to more negative potentials, and monitoring the tail response at varying potentials, also produced a linear relationship which reversed at -40 mV.

In vivo, predicting the direction of current flow for the Müller cell Cl_{Ca} channels is not as straightforward to approximate. For example, the $[Cl^-]$ in a functioning retina, in particular, Müller cells, is not known. However, it is

universally agreed that the resting membrane potential of Müller cells is more negative, ~ -80 mV, than the resting membrane potential of retinal neurons (Sarthy, 2001). Therefore, it is likely that E_{Cl} is positive to the resting membrane potential of Müller cells, which would suggest that Cl_{Ca} channel activation results in an inward current, or an efflux of Cl^- ions. Therefore, opening of Cl_{Ca} channels located throughout the main body, i.e the somatic region, of the Müller cell membrane could cause a depolarization of the glial cell. However, the relationship between E_{Cl} and membrane potential might be different in areas of the Müller cell which are electrically isolated, such as the apical process in salamander. Without altering overall Müller cell membrane potential, the long, spine-like glial processes which project into many areas of the outer retina might "sense" voltage changes in surrounding neurons allowing a depolarizing shift in localized areas of Müller cell membrane. Under such conditions, this thesis has previously hypothesized that voltage-gated Ca channels may be activated, which may in turn lead to opening of Ca^{2+}-activated Cl channels, resulting in an outward current, i.e. an influx of Cl^- ions, and would tend to repolarize the cell.

The function of Cl_{Ca} channels, and the direction of Cl^- flux, is likely to dependent on the spatial distribution of these channels in Müller cells. The membrane potential of the body of the Müller cell is unlikely to deviate far from the high negative resting membrane potential and so E_{Cl} would likely be positive. Thus, opening of Cl_{Ca} channels in the somatic region of the Müller cell would facilitate an inward current. On the other hand, if Cl_{Ca} channels are expressed in the apical processes of the salamander Müller cell, this region of the Müller cell

membrane might experience a localized depolarization. If the depolarization is sufficient to open voltage-gated Ca channels, i.e. membrane potential of at least -30 mV, then E_{Cl} is likely to be negative to membrane potential. Ca^{2+} influx through voltage-gated Ca channels activates Cl_{Ca} channels to facilitate an outward current. Further conclusions as to the function of this novel Cl channel in Müller cells will require information about [Cl^-] in the different regions of the retina.

4.2 Cl channel localization

The molecular nature of Cl_{Ca} channels has not yet been resolved. As a result, there are few experimental tools available to investigate the expression of these channels at the RNA, DNA, or protein level. Conversely, the ClC family of Cl channels has been well characterized although the function of ClC-3 still remains controversial. There is evidence to suggest that human ClC-3 channels are regulated by Ca^{2+} (Huang et al., 2001). However, it is not yet resolved as to whether ClC-3 channels can contribute to the plasma membrane Cl^- conductance under isotonic conditions (i.e., in the absence of cell swelling) or if ClC-3 channel expression is confined to intracellular membranes. In freshly isolated salamander Müller cells, dialysis of a polyclonal antibody directed towards ClC-3 did not significantly reduce the Cl_{Ca} channel current when compared to that in Müller cells exposed to preadsorbed ClC-3 antibody + CP. The ClC-3 antibody has been previously shown to recognize an ~ 85 kDa protein from salamander retina (Wood, 2004) consistent with the reported size of murine and human ClC-3 protein (Britton et al., 2000; Wills et al., 2000). These results suggest that ClC-3 does not contribute to the Ca^{2+}-activated Cl channel current in Müller cells. A

small reduction of current with time was observed in Müller cells dialyzed with both ClC-3 alone or ClC-3 + CP. The cause of this time-dependent decrease in current is unknown but may be a rundown phenomenon. Rundown in voltage-gated Ca channels has been shown to be a result of dephosphorylation (Wu et al., 2002), and therefore, ATP and GTP are included in the pipette solution to prevent the time-dependent decrease in current. However, rundown in Cl_{Ca} channels may not be related to phosphorylation. Activation of Cl_{Ca} channels, via Ca^{2+} entry through Ca channels from the preceding test pulse, was conserved in isolated Müller cells despite the rundown phenomenon; application of Cd^{2+} completely inhibited the tail currents. The tail currents recovered upon removal of Cd^{2+} from the superfusate, and the recovered currents were sensitive to niflumic acid confirming that Cl channels mediated the currents.

Immunopositive staining for anti-ClC-3 in Müller cells colocalized with anti-LAMP-1 staining suggesting that ClC-3 was expressed on intracellular lysosomal membranes. ClC-3 Cl channels have been shown to be crucial for the acidification of intracellular vesicles (Stobrawa et al., 2001). An acidic environment is required for proper functioning of lysosomes since the enzymes contained within the lysosome are active at low pH. However, the H^+-ATPase pump that actively transports protons into the vesicle requires co-transport of Cl^- to maintain electroneutrality (Li et al., 2002). ClC-3 has been localized to other intracellular membranes such as endosomes and synaptic vesicles (Stobrawa et al., 2001), which also require acidification and Cl^- conductance to maintain function. Considering the vital role of Müller cells in preserving retinal integrity,

disruption of Müller cell functioning, by deleting the ClC-3 protein, may contribute to the retinal degeneration observed in the ClC-3 knockout mice.

In conclusion, a Cl_{Ca} channel is present on salamander Müller cell membrane. This channel has properties in common with Cl_{Ca} described in photoreceptors (Barnes and Hille, 1989; Barnes and Bui, 1991) and is distinct from Müller cell ClC-3, which was localized primarily to intracellular organelles.

Chapter 6

General Discussion and Future Work

1. Discussion

Light stimulation of the retina results in neuronal activation and increases in $[K^+]_o$ in both of the synaptic layers, the *opl* and *ipl*. Clearing of the light-induced elevation in synaptic concentrations of K^+ must be rapid and efficient to limit variations in neuronal excitability. Excess K^+ is primarily removed from the extracellular space by Müller cells. Müller cell mechanisms of buffering elevated $[K^+]_o$ occur passively, through K^+ and Cl^- uptake , and actively, through Na^+-K^+-ATPase pumps. K^+ removal also arises from a mechanism of K^+ siphoning whereby K^+ is redistributed from areas of high concentrations to regions where $[K^+]_o$ is low. Müller cells are large cells spanning the entire depth of the retina and are in contact with all types of retinal neurons. The region of the Müller cell in contact with each of the synaptic layers is small compared to the total cellular area. Light-evoked increases in $[K^+]_o$ depolarize small areas of Müller cell membrane which are adjacent to the *opl* and/or *ipl* without altering the overall membrane potential of the cell. As a result, in regions where the membrane is depolarized, excess K^+ moves along its concentration gradient into the Müller cell, and K^+ efflux occurs in regions where $[K^+]_o$ is low such as the vitreous humour which acts as a K^+ sink (reviewed by Sarthy and Ripps, 2001).

The Müller cell membrane potential is highly dependent on K^+, and there is an assumption that the synaptic elevations in $[K^+]_o$ are too small to depolarize the glial cell by any appreciable amount (Sarthy and Ripps, 2001). However, previous estimations of $[K^+]_o$, in the small, confined space of the synaptic cleft, were typically performed with relatively large K^+-sensitive electrodes, that record

net changes in K^+ activity, a highly dynamic process in retinal tissue. The vigorous K^+ uptake mechanisms of the Müller cell might prevent the initial efflux of K^+ from being measured, and thus, lead to an underestimation of the light-induced elevation of $[K^+]_o$ in the synapse (Sarthy and Ripps, 2001).

K channel distribution is highly species dependent. In fact, the morphology of Müller cells varies across species to accommodate the needs of the retina (Sarthy and Ripps, 2001). Amphibian retinas are avascular, and thus, excess K^+ cannot be directed to the layers of blood vessels between the retina and sclera. In mammalian retinas, K^+ can be deposited into the chorodial vasculature as well as the vitreous humour (Sarthy and Ripps, 2001). Frog Müller cells were found to have electronically separated and mutually independent endfoot and somatic regions (Skatchkov et al., 1999). The Skatchkov study (1999) exposed freshly isolated Müller cells to varying concentrations of $[K^+]_o$ and monitored the current responses to elevated $[K^+]_o$ in both the endfoot and somatic regions of the cell. Despite application of the same external K^+ solution, the K_{IR} channel conductance was different in each of the regions of the Müller cell membrane. A striking non-uniformity in the distribution of K^+ conductances was also found in enzymatically isolated salamander Müller cells with >90% contained in the endfoot region (Newman, 1985a). The Müller cell endfoot is at the retinal surface adjacent to the vitreous humour, where much of the light-evoked K^+ in salamander is siphoned.

This spatial distribution of voltage-gated ion channels and the unique morphological features of amphibian Müller cells may facilitate differential

changes in membrane potential by permitting electrically isolated regions of membrane. This thesis presents evidence for the presence of Ca channels, K_{Ca} channels and Cl_{Ca} channels in salamander Müller cell membranes. The traditional notion of Müller cell physiology, with membrane potential static at ~ -80 mV, would argue that voltage-dependent ion channels are inactive under normal conditions. However, this thesis hypothesizes that transient depolarizations can occur in electrically isolated regions of the Müller cell membrane, activating voltage-dependent ion channels. This raises important questions concerning Ca channels, K_{Ca} channels and Cl_{Ca} channels contributions to Müller cell physiology.

Voltage-gated Ca channels have been described on Müller cells of many species including salamander, toad, rat, rabbit, and human (Newman, 1985b; Bringmann et al., 2000c; Bringmann et al., 2000a; Xu et al., 2002; Bringmann et al., 2002; Puro et al., 1996a). In all species except rabbit, the Ca channels expressed on Müller cell membranes were high-voltage-activated, thereby requiring the cell to depolarize to at least –30 mV. Rat and human Müller cell Ca channels were determined to be an L-type, α1D subtype which is characterized by high-voltage-activation and sensitivity to dihyropyridines (Xu et al., 2002; Puro et al., 1996a). In this thesis, salamander Müller cell Ca channel currents were sensitive to a wide variety of blockers specific for three Ca channel subtypes, including dihydropyridines (L-type), ω-conotoxin GVIA (N-type), and ω-agatoxin IVA (P/Q-type). Dihydropyridine blockers inhibited ~ 50% of the Ca channel current while the Ca channel current was not enhanced by the classic L-type agonist BayK 8644. The L-type Ca channel subtypes α1C and α1D were

localized over the entire membrane with a greater propensity of channels found at the apical processes region of the Müller cell. Likewise, evidence for N-type Ca channels, α1B subtype, was most prominent at the apical processes, and these channels were also found all over the cell membrane. The N-type Ca channel blocker ω-conotoxin GVIA was an effective blocker, ~84%, of the Müller cell Ca channel current. Immunochemical staining for P/Q-type Ca channels, α1A subtype, was restricted to the apical processes. Electrophysiological evidence suggested that the Ca channel current was only slightly sensitive to ω-agatoxin IVA with ~ 13% inhibition of the current. The localization of each Ca channel subtype to the apical processes region of the salamander Müller cell is consistent with the proposed activation of an HVA Ca channel in electrically isolated regions of the cell. In salamander, the apical processes are long, spine-like glial extensions which wrap around the synaptic terminals of the photoreceptors (Sarantis and Mobbs, 1992). The close interactions between Müller cell processes and photoreceptor synapses might provide a means for localized depolarizations in which Ca channels might activate. Activation of Ca channels in salamander Müller cells, and the resulting influx of Ca^{2+}, could initiate several Ca^{2+}-dependent processes.

The voltage-dependence of K_{Ca} channels is shifted negative, requiring less depolarization to open, in the presence of elevated $[Ca^{2+}]_i$ (Hille, 2001). Activation of K_{Ca} channels via influx of Ca^{2+} through Ca channels would shift the membrane potential towards repolarization, and consequently, Ca channels become inactive. However, in this study, blocking Ca channels with 100 μM

Cd^{2+} had only a small effect on K_{Ca} channel activity, although blockade of Ca channel activity did have a pronounced effect on Cl_{Ca} channel activity in salamander Müller cells. Activation of Cl_{Ca} channels, in a region of membrane experiencing depolarization, would shift the Müller cell membrane potential towards repolarization, a similar effect as opening of K_{Ca} channels.

Ca^{2+} influx through voltage-gated Ca channels is not the only means of activating Ca^{2+}-activated ion channels. This thesis presents evidence that release of Ca^{2+} from intracellular stores, via the inclusion of IP_3 in the pipette, increased the K^+ conductance through K_{Ca} channels in salamander Müller cells. Elevation of $[Ca^{2+}]_i$, and the propagation of Ca^{2+} waves within a single Müller cell or between glia is a hallmark of Müller cells, and glia in general. The source of Ca^{2+} waves was primarily from the release from stores rather than Ca^{2+} influx through Ca channels. Metabotropic purinergic receptor activation in Müller cells has been shown to trigger elevations in $[Ca^{2+}]_i$ in a wave-like manner, in Ca^{2+}-free external Ringers (Reifel-Saltzberg et al., 2003). This suggests that Ca^{2+} influx through Ca channels is not required for the initiation or maintenance of Müller cell Ca^{2+} wave propagation.

The application of intracellular heparin and thapsigargin abolished the Ca^{2+} waves in retinal glial cells indicating that Ca^{2+} release from intracellular stores was responsible for the Ca^{2+} wave propagation (Newman and Zahs, 1997). Activation of G-protein coupled receptors, such as metabotropic glutamate and metatabotropic purinergic receptors, initiates an intracellular cascade linked to the production of IP_3. Activation of IP_3 receptors on intracellular stores permits Ca^{2+}

to be released into the cell's interior. Newman and Zahs (1997) also reported that the Ca^{2+} release in Müller cells was not accompanied by any changes in membrane potential. ATP, via activation on metabotropic purinergic receptors, has been shown to increase K_{Ca} channel currents (Bringmann et al., 2002) which could serve to stabilize the membrane potential. Elevations in $[Ca^{2+}]_i$ would likely depolarize the Müller cell membrane potential while activation of K_{Ca} channels would act to repolarize the cell.

Although it is undetermined if Cl_{Ca} channels are linked to purinergic receptor activation, it is reasonable to postulate that these channels would also be open in the presence of elevated $[Ca^{2+}]_i$. However, the effect of opening of Cl channels in Müller cells is highly dependent upon the driving force of Cl^- ions. It is hypothesized that Cl_{Ca} channels are co-localized with voltage-gated Ca channels. This thesis has shown that Ca channels are preferentially expressed in the apical processes of salamander Müller cells, and thus, Cl_{Ca} channels might also be expressed in this region of the cell. It has also been hypothesized that the apical processes of the salamander Müller cell are electrically isolated from the rest of the cell and might experience depolarization to membrane potentials above –30 mV, and thus permitting opening of voltage-gated Ca channels. The influx of Ca^{2+} activates Cl_{Ca} channels, and also moves positive charge into the cell which further depolarizes the cell. It is likely that in these regions the membrane potential is positive to E_{Cl} and therefore, when Cl_{Ca} channels open, Cl^- ions will flow into the cell to repolarize the membrane potential. The relationship between

Ca and Cl_{Ca} channels in the apical processes of the Müller cell would, therefore, tightly control the electrical properties of this region of the membrane.

Intracellular Ca^{2+} can also be increased via the activation of Müller cell metabotropic glutamate receptors. Application of glutamate or agonists for metabotropic glutamate receptors, similar to analogous studies with purinergic receptor activation, initiated Ca^{2+} wave propagation (Keirstead and Miller, 1997; Reifel-Saltzberg et al., 2003) and also suppressed K_{IR} channel conductance (Schwartz, 1993). Inhibition of K_{IR} channels limits the Müller cell's ability to effectively buffer light-evoked elevations in $[K^+]_o$. Accumulations in $[K^+]_o$ could result in sustained Müller cell membrane depolarizations and result in the prolonged activation of voltage-dependent ion channels. However, although glutamate is continually released from retinal neurons in the dark, it is likely that excess extracellular glutamate, such as occurs in retinal pathologies, would be needed to have a large effect on K_{IR} channels.

Extracellular glutamate levels in the retina are kept low primarily by the glutamate transporters expressed on Müller cells. The glutaminergic action is terminated by removal of glutamate from the synapse via high affinity transporters on Müller cells. GLAST, a glutamate transporter subtype expressed only on Müller cells, is an electrogenic uptake process which transports a single glutamate molecule, two Na^+ ions and a proton into the cell with the co-transport of one K^+ ion out (Eliasof et al., 1998). The action of the glutamate transporter is associated with an outward current mediated by Cl^- (Eliasof and Jahr, 1996). The transport of glutamate did not require the presence of Cl^- ions, but rather, an

influx of Cl^- occurs simultaneously with glutamate uptake (Eliasof and Jahr, 1996). Eliasof and Jahr (1996) suggested that the anionic conductance may be important for maintenance of electrogenic glutamate uptake. The net influx of a positive charge associated with GLAST functioning would depolarize the Müller cell and reduce the rate of glutamate transport. The influx of Cl^- that accompanies glutamate transport stabilizes the membrane potential preserving electrically dependent Müller cell process.

The properties of the outward current mediated by influx of Cl^- ions associated with glutamate transport have not been characterized. In particular, Ca^{2+} sensitivity of this anion conductance has not been assessed. Eliasof and Jahr (1996) speculated that both the glutamate transporter and a Cl channel might be part of a single molecule. Alternatively, the glutamate transporter and Cl channel might be separate, but tightly connected, molecules. The functioning of Cl_{Ca} channels has been shown to be closely coupled to Ca channel activity in this thesis work as well as in other studies (Barnes and Bui, 1991; Gruber et al., 1999). However, there have not been any reports of Cl_{Ca} channels co-localizing on the plasma membrane with any other proteins, including glutamate transporters. Furthermore, GLAST activity does not involve the transport of any Ca^{2+} ions and would be unlikely to activate a Cl_{Ca} channel. Thus, the identity of the GLAST-associated anionic conductance is unlikely to be the Cl_{Ca} channel.

Improper functioning of Müller cell glutamate transporters might contribute to the toxic effects of retinal glutamate excitotoxicity. Müller cells and the activity of GLAST were critical for the maintenance of retinal integrity

(Harada et al., 1998). Elevated extracellular glutamate levels have been linked to neurodegenerative disorders such as retinal ischemia and glaucoma (Osborne et al., 1999; McIlnay et al., 2004). In an animal model of glaucoma, which is characterized by ganglion cell death (Osborne et al., 1999), survival of ganglion cells, which are particularly sensitive to NMDA receptor overstimulation by glutamate, required the presence of functioning Müller cells (Kawasaki et al., 2000). Under ischemic conditions, extracellular K^+ and glutamate levels are increased in the retina causing depolarization in neighbouring cells including Müller cells and neurons (Maguire et al., 1998). The depolarizing effect on Müller cells compounds the problem of excess glutamate by several mechanisms. GLAST activity is electrogenic and uptake of glutamate by Müller cells is not only inhibited, but the glutamate transporter reverses to release additional glutamate (Maguire et al., 1998). Furthermore, Müller cell depolarization would also open voltage-gated channels, such as Ca channels, which permits an influx of Ca^{2+} ions and might contribute to cell death.

Ion channel expression has been shown to be altered in Müller cells from human donors suffering from proliferative vitreoretinopathy (PVR), a retinal disease which often leads to retinal detachment (Bringmann et al., 1999b). K_{IR} channel currents were strongly reduced in Müller cells from PVR patients compared to cells from healthy donors (Bringmann et al., 1999b). Decreased K_{IR} channel activity was associated with a positive, or depolarized, shift in Müller cell resting membrane potential which might permit activation of HVA Ca channels (Bringmann et al., 1999b). However, HVA Ca channel currents were smaller in

PVR retina-derived Müller cells than healthy Müller cells (Bringmann et al., 2000a). The down-regulation of HVA Ca channels may be a protective mechanism in Müller cells of a PVR retina. The positive shift of membrane potential in Müller cells from PVR retinas would tend to suggest that HVA Ca channels are more likely to be opened and $[Ca^{2+}]_i$ increased. In support of this, it has been shown that K_{Ca} channels, which are enhanced by $[Ca^{2+}]_i$, were activated in Müller cells from patient donors with PVR (Bringmann et al., 1999b).

Before Müller cells can proliferate and migrate out of the retina, a hallmark of PVR, deoxyribonucleic acid (DNA) synthesis must be increased. Mitogenic factors, such as epidermal growth factor, increase K_{Ca} channel activity via elevations Ca channel activity. The activity of K_{Ca} channels was necessary for the maintenance of elevated DNA synthesis in cultured Müller cells (Kodal et al., 2000). HVA Ca channel currents from human Müller cell cultures were enhanced after application of basic fibroblast growth factor (bFGF). Exposure of bFGF increased the number of retinal glial cells in culture in a dose-dependent manner. The proliferative effect of bFGF was blocked by nifedipine, a blocker of some HVA Ca channels, without affecting cell viability, suggesting a role for HVA Ca channels in mitogenic-induced proliferation (Puro and Mano, 1991). As proliferation continues, and diseases like PVR develop and progress, neurons might signal to the Müller cells to down-regulate HVA Ca channel activity as a protective measure. In the pure glial cultures of the Puro and Mano study (1991), Ca channel activity was not down-regulated since the neurons were not present.

In conclusion, the interactions between Müller cells and retinal neurons are important to the regulation of the retinal microenvironment. Retinal Müller glial cells span the entire depth of the retina, contacting each of the types of neurons, and exerting considerable influence within the retina. Müller cell ion channels are involved in the processes of K^+ siphoning, glutamate uptake, and signaling via Ca^{2+} waves. Underlying each of these processes is the resting membrane potential of Müller cells which is set primarily by K^+ conductance. This thesis examines the expression and properties of several ion channel types in salamander Müller cells, such as Ca channels, K_{Ca} channels, and Cl channels. Activation of one or more of these ion channels may contribute to the glia-neuron interactions that are essential for normal retinal function. The negative resting membrane potential of the Müller cell suggests that voltage-dependent ion channels would be inactive under physiological conditions. However, the morphology of the Müller cell suggests that electrically isolated regions of the cell exist. Long processes branch out from the cell body extending into the subretinal space surrounding the photoreceptors, and also project throughout the inner layers of the retinal neurons (Newman and Reichenbach, 1996). These microvilli projections are intimately associated with neurons and may be able to "sense" surrounding depolarizations without affecting the membrane potential of the Müller cell as a whole. Under these proposed conditions, voltage-dependent ion channels could be activated and would provide an additional layer of complexity to the role of Müller cells in modulating neuronal activity and retinal function.

2. Future work

This thesis confirmed that salamander Müller cells express Ca and Ca^{2+}-dependent voltage-gated ion channels, and if these channels are active under physiological conditions Müller cell physiology and function could be altered. Future research objectives would focus on examining how changes in Müller cell membrane potential regulate retinal function. Highly sensitive voltage-sensing dyes combined with two-photon microscopy have been used to probe changes in cellular membrane potentials (Kuhn et al., 2004). This imaging technique could be applied to salamander Müller cells in a retinal slice to monitor the alterations in membrane potential in various regions of the glial cell, such as the apical processes, when stimulated with light and/or elevated $[K^+]_o$. Furthermore, Ca^{2+} sensitive dyes and two-photon microscopy have shown that light-evoked increases in $[Ca^{2+}]_i$ in the individual dendritic branches of retinal starburst amacrine cells did not affect the electrical signal recorded the same amacrine cell's soma (Euler et al., 2002). A similar experiment could be performed in salamander Müller cells by imaging $[Ca^{2+}]_i$ changes in the apical processes of the Müller cell while simultaneously monitoring the membrane potential of the glial cell soma or endfoot region during light stimulus. These experiments could confirm that the apical processes of the salamander Müller cells are electrically isolated regions of the cell that might experience localized membrane depolarization sufficient to activate voltage-gated Ca channels and Ca^{2+}-dependent ion channels.

This thesis presents evidence that voltage-gated Ca channel expression in salamander Müller cells is found throughout the plasma membrane with a higher density of channels in the apical processes regions. Future research objectives would also concentrate on determining whether ion channels activated by increases in $[Ca^{2+}]_i$, such as K_{Ca} and Cl_{Ca}, are co-localized with Ca channels. In hippocampal neurons, K_{Ca} channels were selectively activated by co-localized voltage-gated Ca channels (Marrion and Tavalin, 1998). Using cell-attached-patch recordings, Marrion and Tavalin (1998) were able to show that both K_{Ca} and Ca channels were expressed in the area of membrane under the patch pipette, and that Ca channel blockers inhibited both Ca channel currents and K_{Ca} channel currents. Similar electrophysiological experiments could be used to determine if Ca channel and K_{Ca}/Cl_{Ca} channel expression is co-localized in the Müller cell membrane. Althernatively, ion channel-specific imaging might provide a less demanding experimental approach. In this thesis, the binding of fluorescent-tagged dihyrodpyridines, specific for L-type Ca channels, on Müller cells was visualized with confocal microscopy to determine cellular localization. This technique for localizing Ca channels could be combined with immunocytochemistry, using antibodies for large conductance K_{Ca} channels, and co-localized channels visualized simultaneously using confocal microscopy. The biophysical properties of Müller cell Cl_{Ca} channel currents are similar to neuronal Cl_{Ca} channels, for which the molecular identity is still unknown. Therefore, antibodies directed towards this Cl_{Ca} channel are not commercially available preventing simultaneous visualization of Ca and Cl_{Ca} channels. However, non-

specific Cl channel blockers are commercially available from Molecular Probes with fluorescent tags, and these fluorescent-labelled blockers could be applied concurrently with the fluorescent-tagged Ca channel blockers to determine co-localization of Ca and Cl channels.

The proposed future experiments will help to identify mechanisms by which voltage-dependent ion channela are activated in Müller cells. This information is essential for understanding how Müller cells regulate visual processing and retinal function.

References

Araque A, Sanzgiri RP, Parpura V, Haydon PG (1998) Calcium elevation in astrocytes causes NMDA receptor-dependent increase the frequency of miniature synaptic currents in cultured hippocampal neurons. The Journal of Neuroscience 18:6822-6829.

Barnes S, Hille B (1989) Ionic channels of the inner segment of tiger salamander cone photoreceptors. Journal of General Physiology 94:719-743.

Barnes S, Bui Q (1991) Modulation of calcium-activated chloride current via pH-induced changes of calcium channel properties in cone photoreceptors. The Journal of Neuroscience 11:4015-4023.

Bell DC, Butcher AJ, Berrow NS, Page KM, Brust PF, Nesterove A, Stauderman KA, Seabrook GR, Nurnberg B, Dolphin AC (2001) Biophysical properties, pharmacology, and modulation of human, neuronal L-type (α1D, CaV1.3) voltage-dependent calcium currents. Journal of Neurophysiology 85:816-826.

Bergles DE, Jahr CE (1998) Glial contribution to glutamate uptake at Schaffer collateral-commissural synapses in the hippocampus. The Journal of Neuroscience 18:7709-7716.

Biedermann B, Bringmann A, Reichenbach A (2002) High-affinity GABA uptake in retinal glial (Müller) cells of the guinea pig: electrophysiological characterization, immunohistochemical localization, and modeling of efficiency. Glia 39:217-228.

Biedermann B, Bringmann A, Franzer K, Faude F, Wiedermann P, Reichenbach A (2004) $GABA_A$ receptors in Müller glial cells of the human retina. Glia 46:302-310.

Boitano S, Dirksen ER, Sanderson MJ (1992) Intercellular propagation of calcium waves mediated by inositol trisphosphate. Science 258:292-295.

Bösl MR, Stein V, Hubner C, Zdebik AA, Jordt S-E, Mukhopadhyay AK, Davidoff MS, Holstein A-F, Jentsch TJ (2001) Male germ cells and photoreceptors, both dependent on close cell-cell interactions, degenerate upon ClC-2 Cl^- channel disruption. The European Molecular Biology Organization Journal 20:1289-1299.

Bringmann A, Reichenbach A (1997) Heterogeneous expression of Ca^{2+}-dependent K^+ currents by Müller glial cells. NeuroReport 8:3841-3845.

Bringmann A, Faude F, Reichenbach A (1997) Mammalian retinal glial (Müller) cells express large-conductance Ca^{2+}-activated K^+ channels that are modulated by Mg^{2+} and pH and activated by protein kinase A. Glia 19:311-323.

Bringmann A, Biedermann B, Reichenbach A (1999a) Expression of potassium channels during postnatal differentiation of rabbit Müller glial cells. European Journal of Neuroscience 11:2883-2896.

Bringmann A, Francke M, Pannicke T, Biedermann B, Faude F, Enzmann V, Wiedermann P, Reichelt W, Reichenbach A (1999b) Human Müller glial cells: Altered potassium channel activity in proliferative vitreoretinaopathy. Investigative Ophthalmology & Visual Science 40:3316-3323.

Bringmann A, Biedermann B, Schnurbusch U, Enzmann V, Faude F, Reichenbach A (2000a) Age- and disease-related changes of calcium channel-mediated currents in human Müller glial cells. Investigative Ophthalmology & Visual Science 41:2791-2796.

Bringmann A, Schopf S, Reichenbach A (2000b) Developmental regulation of calcium channel-mediated currents in retinal glial (Müller) cells. Journal of Neurophysiology 84:2975-2983.

Bringmann A, Pannicke T, Reichenbach A, Statchkov SN (2000c) Ca^{2+} channel-mediated currents in retinal glial (Müller) cells of the toad (Bufo marinus). Neuroscience Letters 281.

Bringmann A, Pannicke T, Weick M, Biedermann B, Uhlmann S, Kohen L, Wiedermann P, Reichenbach A (2002) Activation of P2Y receptors stimulates potassium and cation currents in acutely isolated human Müller (glial) cells. Glia 37:139-152.

Britton FC, Hatton WJ, Rossow CF, Duan D, Hume JR, Horowitz B (2000) Molecular distribution of volume-regulated chloride channels (ClC-2 and ClC-3) in cardiac tissues. American Journal of Physiology Heart and Circulation Physiology 279:2225-2233.

Bunge RP (1968) Glial cells and the central myelin sheath. Physiological Reviews 48:197-251.

Byzov AL, Shura-Bura TM (1986) Electical feedback mechanism in the processing of signals in the outer plexiform layer of the retina. Vision Research 26:33-44.

Candia S, Garcia ML, Latorre R (1992) Mode of action of iberiotoxin, a potent blocker of the large conductance $Ca^{(2+)}$-activated K^+ channel. Biophysical Journal 63:583-590.

Chao TI, Henke A, Reichelt W, Eberhardt W, Reinhardt-Maelicke S, Reichenbach A (1994) Three distinct types of voltage-dependent K^+ channels are expressed by Müller (glial) cells of the rabbit retina. Pflugers Archives 426:51-60.

Coetzee WA, Amarillo Y, Chiu J, Chow A, Lau D, McCormack T, Morena H, Nadal MS, Ozaita A, Poutney D, Saganich M, Vega-Saenz de Miera E, Rudy B (1999) Molecular diversity of K^+ channels. Annals of the New York Academy of Sciences 868:233-255.

Cognard C, Romey G, Galizzi JP, Fosset M, Lazdunski M (1986) Dihydropyridine-sensitive Ca2+ channels in mammalian skeletal muscle cells in culture: electrophysiological properties and interactions with Ca^{2+} channel activator (BayK8644) and inhibitor (PN 200-110). Proceedings of the National Academy of Science USA 83:1518-1522.

Cornell-Bell AH, Finkbeiner SM, Cooper MS, SJ S (1990) Glutamate induces calcium waves in cultured astocytes: long-range glial signaling. Science 247:470-473.

Crompton M (1999) The mitochrondrial permeability transition pore and its role in cell death. Biochemical Journal 341:233-249.

Cunningham SA, Awayda MS, Bubien JK, Ismailov II, Arrate MP, BK. B, Benos DJ, Fuller CM (1995) Cloning of an epithelial chloride channel from bovine trachea. Journal of Biological Chemistry 270:31016-31026.

Currie KPM, Wootton JF, RH S (1995) Activation of Ca^{2+}-dependent Cl^- currents in cultured rat sensorty neurones by flash photolysis of DM-nitrophen. Journal of Physiology 482:291-307.

Delcour AH, Lipscombe D, Tsien RW (1993) Multiple modes of N-type calcium channel activity distinguished by differences in gating kinetics. The Journal of Neuroscience 13:181-184.

Demaurex N, Distelhorst C (2003) Calcium and apoptosis. Science 300:65-67.

Distler C, Dreher Z (1996) Glial cells of the monkey retina. II. Müller cells. Visual Research 36:2381-2394.

Doyle DA, Cabral JM, Pfeutzner RA, Kuo A, Gulbis JM, Cohen SL, Chait BT, Mackinnon R (1998) The structure of the potassium channel: Molecular basis of K^+ conduction and selectivity. Science 280:69-77.

Duan D, Winter C, Cowley S, Hume JR, Horowitz B (1997) Molecular identification of a volume-regulated chloride channel. Nature 390:417-421.

Ehinger B, Zucker CL, Brunn A, Adolph A (1994) In vivo staining of oligodendroglia in the rabbit retina. Glia 10:40-48.

Eliasof S, Jahr CE (1996) Retinal glial cell glutamate transporter is coupled to an anionic conductance. Proceedings of the National Academy of Science USA 93:4153-4158.

Eliasof S, Arriza JL, Leighton BH, Kavanaugh MP, Amara SG (1998) Excitatory amino acid transporters of the salamander retina: Identification, localization, and function. The Journal of Neuroscience 18:402-411.

Enz R, Ross BJ, Cutting GR (1999) Expression of the voltage-gated chloride channel ClC-2 in rod bipolar cells of the rat retina. The Journal of Neuroscience 19:9841-9847.

Euler T, Detwiler PB, Denk W (2002) Directionally selective calcium signals in dendrites of starburst amacrine cells. Nature 418:845-852.

Faber ESL, Sah P (2003) Calcium-activated potassium channels: Multiple contributions to neuronal function. The Neuroscientist 9:181-194.

Fam SR, Gallagher CJ, Salter MW (2000) P2Y1 purinoceptor-mediated Ca^{2+} signaling and Ca^{2+} wave propagation in dorsal spinal cord astrocytes. The Journal of Neuroscience 20:2800-2808.

Fava M, Ferroni S, Nobile M (2001) Osmosensitivity of an inwardly rectifying chloride current revealed by whole-cell and perforated-patch recordings in cultured rat cortical astrocytes. FEBS Letters 492:78-83.

Fields RD, Stevens-Graham B (2002) New insights into neuron-glia communication. Science 298:556-562.

Fox DA, Poblenz AT, He L (1999) Calcium overload triggers rod photoreceptor apoptotic cell death in chemical-induced and inherited retinal degenerations. Annals of the New York Academy of Sciences 893:282-286.

Gincel D, Vardt N, Shoshan-Barmatz V (2002) Retinal voltage-dependent anion channel: Characterization and cellular localization. Investigative Ophthalmology & Visual Science 43:2097-2104.

Gray PT, Ritchie JM (1986) A voltage-gated chloride conductance in rat cultured astrocytes. Proceedings of the Royal Society of London Series B: Biological Sciences 22:267-288.

Gruber AD, Schreur KD, Ji H-L, Fuller CM, Pauli BU (1999) Molecular cloning and transmembrane structure of hClCA2 from human lung, trachea, and mammory gland. American Journal of Cell Physiology 45:C1261-C1270.

Gründer S, Thiemann A, Pusch M, Jentsch TJ (1992) Regions involved in the opening of ClC-2 chloride channel by voltage and cell volume. Nature:759-762.

Günther W, Luchow A, Cluzeaud F, Vandewalle A, Jentsch TJ (1998) ClC-5, the chloride channel mutated in Dent's disease, co-localizes with the proton pump in endocytotically active kidney cells. Proceedings of the National Academy of Science USA 95:8075-8080.

Hamberger AC, Chiang GH, Nylen ES, Scheff SW, Cotman CW (1979) Glutamate as a CNS transmitter. I. Evaluation of glucose and glutamine as precursors for the synthesis of preferentially released glutamate. Brain Research 168:513-530.

Hamill OP, Marty A, Neher E, Sakmann B, Sigworth FJ (1981) Improved patch-clamp techniques for high-resolution current recording from cells and cell-free membrane patches. Pflugers Archives 391:85-100.

Harada T, Harada C, Watanabe M, Inoue Y, Sakagawa T, Nakayama N, Sasaki S, Okuyama S, Watase K, Wada K, Tanaka K (1998) Functions of the two glutamate transporters GLAST and GLT-1 in the retina. Proceedings of the National Academy of Science USA 95:4663-4666.

Heidinger V, Hicks D, Sahel J, Dreyfus H (1999) Ability of retinal Müller glial cells to protect neurons against excitotoxicity in vitro depends upon maturation and neuron-glial interactions. Glia 25:229-239.

Henderson D, Doerr TA, Gottesman J, Miller RF (2001) Calcium channel immunoreactivity in the salamander retina. NeuroReport 12:1493-1499.

Hidalgo A, Booth GE (2000) Glia dictate pioneer axon tragectories in the Drosophila embryonic CNS. Development 127:393-402.

Hille B (2001) Ion channels of excitable membranes, 3rd Edition. Sunderland, MA: Sinauer Assoiciates Inc.

Hockerman GH, Peterson BZ, Johnson BD, Catterall WA (1997) Molecular determinants of drug binding & action on L-type calcium channels. Annual Reviews in Pharmacology and Toxicology 37.

Honda S, Yamamoto M, Saito N (1995) Immunocytochemical localization of three subtypes of GABA transporter in rat retina. Molecular Brain Research 33:319-325.

Huang P, Liu J, Di A, Robinson NC, Musch MW, Kaetzel MA, Nelsom DJ (2001) Regulation of human ClC-3 channels by mulitfunctional Ca^{2+}/calmodulin-dependent protein kinase. Journal of Biological Chemistry 276:20093-20100.

Hume DA, Perry V, Gordon S (1983) Immunohistochemical localization of a macrophage-specific antigen in developing mouse retina: Phagocytosis of dying neurons and differentiation of microglial cells to form a regular array in the plexiform layers. Journal of Cell Biology 97:253-257.

Hyde JC, Robinson N (1974) Localization of sites of GABA catabolism in the retina. Nature 248:432-443.

Jablonski MM, Iannaccone A (2000) Targeted disruption of Müller cell metabolism induces photoreceptor dysmorphogenesis. Glia 32:192-204.

Janzer RC, Raff MC (1987) Astrocytes induce blood brain barrier properties in endothelial cells. Nature 325:253-257.

Jentsch TJ, Friedrich T, Schriever A, Yamada H (1999) The CLC chloride channel family. Pflugers Archives 437:783-795.

Kainz PM, Adolph AR, Wong KY, Dowling JE (2003) Lazy eyes zebrafish mutation affects Müller glial cells, compromising photoreceptor function and causing partial blindness. Journal of Comparative Neurology 463:265-280.

Kamermans M, Fahrenfort I, Schultz K, Janseen-Bienhold U, Sjoerdsma T, Weiler R (2001) Hemichannel-mediated inhibition in the outer retina. Science 292:1178-1180.

Karwoski CJ, Lu H-K, Newman EA (1989) Spatial buffering of light-evoked potassium increases by retinal Müller (glial) cells. Science 244:578-580.

Kawasaki A, Otori Y, Barnstable CJ (2000) Müller cell protection of rat retinal ganglion cells from glutamate and nitric oxide neurotoxicity. Investigative Ophthalmology & Visual Science 41:3444-3450.

Keirstead SA, Miller RF (1997) Metabotropic glutamate receptor agonists evoke calcium waves in isolated Müller cells. Glia 21:194-203.

Klöcker N, Oliver D, Ruppersberg JP, Knaus H-G, Fakler B (2001) Developmental expression of the small-conductance Ca^{2+}-activated potassium channel SK2 in the rat retina. Molecular and Cell Neuroscience 17:514-520.

Kodal H, Weick M, Moll V, Biedermann B, Reichenbach A, Bringmann A (2000) Involvement of calcium-activated potassium channels in the regulation of DNA synthesis in cultured Müller glial cells. Investigative Ophthalmology & Visual Science 41:4262-4267.

Koschak A, Reimer D, Huber I, Grabner M, Glossmann H, Engel J, Striessnig J (2001) α1D (Cav1.3) subunits can form L-type Ca^{2+} channels activating at negative voltages. Journal of Biological Chemistry 276:22100-22106.

Koschak A, Reimer D, Walter D, Hoda J-C, Heinzle T, Grabner M, Striessnig J (2003) Cav1.4 α1F subunits can form slowly inactivating dihydropyridine-sensitive L-type Ca^{2+} channels lacking Ca^{2+}-dependent inactivation. The Journal of Neuroscience 23:6041-6049.

Kourennyi DE, Liu XD, Hart J, Mahmud F, Baldridge WH, Barnes S (2004) Reciprocal modulation of calcium dynamics in rod and cone photoreceptor synapses by nitric oxide. Journal of Neurophysiology 92:477-483.

Kuhn B, Fromherz P, Denk W (2004) High sensitivity of Stark-shift voltage-sensing dyes by one- or two-photon excitation near the red spectral edge. Biophysical Journal 87:631-639.

Kurenny DE, Moroz LL, Turner RW, Sharkey KA, Barnes S (1994) Modulation of ion channels in rod photoreceptors by nitric oxide. Neuron 13:315-324.

Kurenny DE, Thurlow GA, Turner RW, Moroz LL, Sharkey KA, S B (1995) Nitric oxide synthase in tiger salamander retina. Journal of Comparative Neurology 361:525-536.

Kurosinski P (2002) Glial cells under physiologic and pathologic conditions. Archives of Neurology 59:1524-1528.

Li X, Wang T, Zhao Z, Weinman SA (2002) The ClC-3 chloride channel promotes acidification of lysosomes in CHO-K1 and Huh-7 cells. American Journal of Cell Physiology 282:C1483-C1491.

Lin Z, Haus S, Edgerton J, Lipscombe D (1997) Identification of functionally distinct isoforms of the N-type Ca channel in rat sympathetic ganglia and brain. Neuron 18:153-166.

Mager S, Kleinberger-Doron N, Keshet GI, Davidsom N, Kanner BI, Lester HA (1996) Ion binding and permeation at the GABA transporter GAT1. The Journal of Neuroscience 16:5405-5414.

Maguire G, Simko H, Weinreb RN, Ayoub G (1998) Transport-mediated release of endogenous glutamate in the vertebrate retina. Pflugers Archives 43:481-484.

Mansvelder HD, Stoof JC, Kits KS (1996) Dihydropyridine block of omega-agatoxin IVA- & omega-conotoxin GVIA-sensitive Ca^{2+} channels in rat pituitary melanotropic cells. European Journal of Pharmacology 311:293-304.

Marrion NV, Tavalin SJ (1998) Selective activation of Ca^{2+}-activated K^+ channels by co-localized Ca^{2+} channels in hippocampal neurons. Nature 395:900-905.

Matsuda H, Saigusa A, Irisawa H (1987) Ohmic conductance through the inwardly rectifying K channel and blocking by internal Mg^{2+}. Nature 325:156-159.

McIlnay TR, Gionfriddo JR, Dubielzig RR, Powell CC, Madl JE (2004) Evaluation of glutamate loss from damaged retinal cells of dogs with primary glaucoma. American Journal of Veterinary Research 65:776-786.

McRory JE, Hamid J, Doering CL, Garcia E, Parker R, Hamming K, Chen L, Hildebrand M, Beedle AM, Feldcamp L, Zamponi GW, TP. S (2004) The CACNA1F gene encodes an L-type calcium channel with unique biophysical propterties and tissue distribution. The Journal of Neuroscience 24:1707-1718.

Mi H, Harris-Warrick RM, Deerinck TJ, Inman I, Ellisman MH, Schwarz TL (1999) Identification and localization of Ca^{2+}-activated K^+ channels in rat sciatic nerve. Glia 26:166-175.

Mintz IM, Adams ME, Bean BP (1992) P-type calcium channels in rat central & peripheral neurons. Neuron 9:85-95.

Nachman-Clewner M, St. Jules R, Townes-Anderson E (1999) L-type calcium channel in the photoreceptor ribbon synapse: localization and role in plasticity. Journal of Comparative Neurology 415:1-16.

Neher E (1992) Correction for liquid junction potentials in patch clamp experiments. Methods in Enzymology 207:123-131.

Newman EA, Frambach DA, Odette LL (1984) Control of extracellular potassium levels by retinal glial cell K^+ siphoning. Science 225:1174-1175.

Newman EA (1985a) Membrane physiology of retinal glial (Müller) cells. The Journal of Neuroscience 5:2225-2239.

Newman EA (1985b) Voltage-dependent calcium and potassium channels in retinal glial cells. Nature 317:809-811.

Newman EA (1991) Sodium-bicarbonate cotransport in retinal Müller (glial) cells of the salamander. The Journal of Neuroscience 11:3972-3983.

Newman EA (1993) Inward-rectifying potassium channels in retinal glial (Müller) cells. The Journal of Neuroscience 13:3333-3345.

Newman EA, Reichenbach A (1996) The Müller cell: a functional element of the retina. Trends in Neuroscience 19:307-312.

Newman EA, Zahs KR (1997) Calcium waves in retinal glial cells. Science 225:1174-1175.

Newman EA, Zahs KR (1998) Modulation of neuronal activity by glial cells in the retina. The Journal of Neuroscience 18:4022-4028.

Newman EA (2001) Propagaion of intercellular calcium waves in retinal astrocytes and Müller cells. The Journal of Neuroscience 21:2215-2223.

Newman EA (2003) Glial cell inhibition of neurons by release of ATP. The Journal of Neuroscience 23:1659-1666.

Newman EA (2004) Glial modulation of synaptic transmission in the retina. Glia 47:268-274.

Nilius B, Droogmans G (2003) Amazing chloride channels: an overview. Acta Physiologica Scandinavica 177:119-147.

Niu X, Qian X, Magleby KL (2004) Linker-gating ring complex as passive spring and Ca^{2+}-dependent machine for a voltage- and Ca^{2+}-activated potassium channel. Neuron 42:745-756.

Nowak L, Ascher P, Berwald-Netter Y (1987) Ionic channels in mouse astrocytes in culture. The Journal of Neuroscience 7:101-109.

Osborne NN, Ugarte M, Chao M, Chidlow G, Bae JH, Wood JP, Nash MS (1999) Neuroprotection in relation to retinal ischemia and relevance to glaucoma. Surveys in Ophthalmology 43:102-128.

Pannicke T, Fischer W, Bidermann B, Schadlich H, Grosche J, Faude F, Wiedemann P, Allgaier C, Illes P, Burnstock G, Reichenbach A (2000) $P2X_7$ receptors in Müller glial cells from the human retina. The Journal of Neuroscience 20:5965-5972.

Poitry-Yamate CL, Tsacopoulos M (1991) Glial (Müller) cells take up and phosphorylate [3H]-deoxy-D-glucose in mammalian retina. Neuroscience Letters 122:241-244.

Poitry-Yamate CL, Poitry S, Tsacopoulos M (1995) Lactate released by Müller glial cells is metabolized by photoreceptors from mammalian retina. The Journal of Neuroscience 15:5179-5191.

Puro DG, Roberge F, Chan C-C (1989) Retinal glial cell proliferation and ion channels: a possible link. Investigative Ophthalmology & Visual Science 30:521-529.

Puro DG, Mano T (1991) Modulation of calcium channels in human retinal glial cells by basic fibroblast growth factor: A possible role in retinal pathobiology. The Journal of Neuroscience 11:1873-1880.

Puro DG (1991) A calcium-activated, calcium-permeable ion channel in human retinal glial cells: modulation by basic fibroblast growth factor. Brain Research 548:329-333.

Puro DG, Hwang J-J, Kwon O-J, Chin H (1996a) Characterization of an L-type calcium channel expressed by human retinal Müller (glial) cells. Molecular Brain Research 37:41-48.

Puro DG, Yuan JP, Sucher NJ (1996b) Activation of NMDA receptor-channel in human retinal Müller glial cells inhibits inward-rectifying potassium currents. Visual Neuroscience 13:319-326.

Ramussen K-E (1974) The Muller cell: A comparative study of rod and cone retinas with and without retinal vessels. Experimental Eye Research 19:243-257.

Redburn DA, Madtes PJ (1986) Postnatal development of 3H-GABA-accumulating cells in rabbit retina. Journal of Comparative Neurology 243:41-57.

Reichenbach A, Faude F, Enzmann V, Bringmann A, Pannicke T, Francke M, Biedermann B, Kuhrt H, Stolzenburg J-U, Skatchkov SN, Heinemann U, Wiedermann P, Reichelt W (1997) The Müller (glial) cell in normal and diseased retina: A case for single-cell electrophysiology. Ophthalmic Research 29:326-340.

Reifel-Saltzberg JM, Garvey KA, Keirstead SA (2003) Pharmacological characterization of P2Y receptor subtypes on isolated tiger salamander Müller cells. Glia 42:149-159.

Rungger-Brandle E, Messerli JM, Niemeyer G, Eppenberger HM (1993) Confocal microscopy and computer-assisted image reconstruction of astrocytes in the mammalian retina. European Journal of Neuroscience 5:1093-1106.

Sarantis M, Mobbs P (1992) The spatial relationship between Müller cell processes and the photoreceptor output synapse. Brain Research 584:299-304.

Sarthy V, Ripps H (2001) The Retinal Muller Cell Structure and Function. New York: Kluwer Academic / Plenum Publishers.

Savchenko A, Barnes S, Kramer RH (1997) Cyclic-nucleotide-gated channels mediate synaptic feedback by nitric oxide. Nature 390:694-698.

Schopf S, Bringmann A, Reichenbach A (1999) Protein kinases A and C are opponents in modulating glial Ca^{2+}-activated K^+ channels. NeuroReport 10:1323-1327.

Schreibmayer W, Tripathi O, Tritthart HA (1992) Kinetic modulation of guinea-pig cardiac L-type calcium channels by fendiline and reversal of the effects of Bay K 8644. British Journal of Pharmacology 106:151-156.

Schwartz EA (1993) L-glutamate conditionally modulates the K^+ current of Müller glial cells. Neuron 10:1141-1149.

Skatchkov SN, Krusek J, Reichenbach A, Orkand RK (1999) Potassium buffering by Müller cells isolated from the center and periphery of the frog retina. Glia:171-180.

Steinmeyer K, Ortland C, Jentsch TJ (1991) Primary structure and functional expression of a developmentally regulated skeletal muscle chloride channel. Nature 354:301-304.

Stevens B (2003) Glia: much more than the neuron's side-kick. Current Biology 13:R469-R472.

Stobrawa SM, Breiderhoff T, Takamori S, Engel D, Schweizer M, Zdebik AA, Bosl MR, Ruether K, Jahn H, Draguhn A, Jahn R, Jentsch TJ (2001) Disruption of ClC-3, a chloride channel expressed on synaptic vessicles, leads to loss of the hippocampus. Neuron 29:185-196.

Stocker M (2004) Ca^{2+}-activated K^+ channels: Molecular determinants and function of the SK family. Naure Reviews Neuroscience 5:758-770.

Stone J, Itin A, Alon T, Peer J, Gnessin H, Chan-Ling T, Keshet E (1995) Development of retinal vasculature is mediated by hypoxia-induced vascular endothelial growth factor (VEGF) expression by neuroglia. The Journal of Neuroscience 15:4738-4747.

Strahonja-Packard A, Sanderson MJ (1999) Intercellular Ca^{2+} waves induce temporally and spatially distinct intracellular Ca^{2+} oscillations in glia. Glia 28:97-113.

Sucher NJ, Aizenmann E, Lipton SA (1991) N-Methyl-D-aspartate antagonists prevent kainate neurotoxicity in rat retinal ganglion cells in vitro. The Journal of Neuroscience 11:966-971.

Thiemann A, Grunder S, Pusch M, Jentsch TJ (1992) A chloride channel widely expressed in epithelial and non-epithelial cells. Nature 356:57-60.

Wakamori M, Strobeck M, Niidome T, Teramoto T, Imoto K, Mori Y (1998) Functional characterization of ion permeation pathway in the N-type Ca^{2+} channel. Journal of Neurophysiology 79:622-634.

Walz W (2002) Chloride/anion channels in glial cell membranes. Glia 40:1-10.

Wang G, Hatton WJ, Zhong J, Yamboliev I, Duan D, Hume JR (2003) Functional effects of novel anti-ClC-3 antibodies on native volume-sensitive osmolyte and anioin channels in cardiac and smooth muscle cells. American Journal of Physiology Heart and Circulation Physiology 85:1453-1463.

Watanabe T, Mio Y, Hoshino FB, Naamastsu S, Hirosawa K, Nakahara K (1994) GLUT2 expression in the rat retina: Localization at the apical end of Müller cells. Brain Research 655:128-134.

Weinreb RN, Khaw PT (2004) Primary open-angle glaucoma. The Lancet 363:1711-1721.

Welch NC, Wood S, Jollimore C, Stevens K, Kelly ME, Barnes S (2005) High-voltage-activated calcium channels in Müller cells actuely isolated from tiger salamander. Glia 49:259-274.

Weylandt K-H, Valverde MA, Nobles M, Raguz S, Amey JS, Diaz M, Nastrucci C, Higgins CF, Sardini A (2001) Human ClC-3 is not the swelling-activated chloride channel involved in cell volume regulation. Journal of Biological Chemistry 276:17461-17467.

Wilkens CM, Grabner M, Beam KG (2001) Potentiation of the cardiac L-type Ca^{2+} channel (α1C) by dihydropyridine agonist and strong depolarization occur via distinct mechanisms. Journal of General Physiology 118:495-507.

Wilkinson MF, Barnes S (1996) The dihydropyridine-sensitive calcium channel subtype in cone photoreceptors. Journal of General Physiology 107:621-630.

Williams ME, Feldman DH, McCure AF, Brenner R, Velicelebi G, Ellis SB, Harpold MM (1992) Structure and functional expression of α1, α2, and β subunits of a novel human neuronal calcium channel subtype. Neuron 8:71-84.

Wills NK, Weng T, Mo L, Hellmich HL, Yu A, Wang T, Buchheit S, Godley BF (2000) Chloride channel expression in cultured human fetal RPE cells: response to oxidative stress. Investigative Ophthalmology & Visual Science 41:4247-4255.

Witkovsky P, Yang CY (1982) Uptake and localization of 3H-2-Deoxy-D-glucose by retinal photoreceptors. Journal of Comparative Neurology 204:105-116.

Woldemussie E, Wijono M, Ruiz G (2004) Müller cell response to laser-induced increase in intraocular pressure in rats. Glia 47:109-119.

Wood S (2004) Localization of the ClC-3 Chloride Channel in the Amphibian Retina. In: Biology. Halifax: Dalhousie University.

Wu L, Bauer CS, Zhen X-g, Yan J (2002) Dual regulation of voltage-gated calcium channels by PtdIns(4,5)P2. Nature 419:947-952.

Xu H-P, Zhao J-W, Yang X-L (2002) Expression of voltage-dependent calcium channel subunits in the rat retina. Neuroscience Letters 329:297-300.

Xu W, Lipscombe D (2001) Neuronal Cav1.3 α1D L-type channels activate at relatively hyperpolarized membrane potentials and are incompletely inhibited by dihydropyridines. The Journal of Neuroscience 21:5944-5951.

Yamaguchi S, Okamura Y, Nagao T, Adachi-Akahane S (2000) Serine residue in the IIIS5-S6 linker of the L-type Ca2+ channel α1C subunit is the critical determinant of the action of dihydropyridine Ca^{2+} channel agonists. Journal of Biological Chemistry 275:41504-41511.

Yang XL, Wu SM (1996) Response sensitivity and voltage gain of the rod- and cone-horizontal cell synapses in dark- and light-adapted tiger salamander retina. Journal of Neurophysiology 76:3863-3874.